이학박사학위논문

Hydrated Protons at Solid Water–Metal Interfaces

물–금속 계면에서 수화된 양성자에 관한 연구

2017년 8월

서울대학교 대학원

화학부 물리화학전공

김 영 순

Ph. D Dissertation

Hydrated Protons at Solid Water–Metal Interfaces

Supervisor: Prof. Heon Kang

Major: Physical Chemistry

August 2017

by Youngsoon Kim

Department of Chemistry

The Graduate School

Seoul National University

Abstract

Hydrated Protons at Solid Water–Metal Interfaces

Youngsoon Kim
Department of chemistry, Physical Chemistry
The Graduate School
Seoul National University

Understanding the nature of hydrated protons at an electrolyte/electrode interface is fundamentally important to a wide range of scientific research, including heterogeneous catalysis, corrosion, and electrochemical processes in acidic environment. This thesis aims to elucidate the nature of hydrated protons at the water–metal interface in ultra-high vacuum (UHV) conditions. I studied the formation and stability of hydrated protons on a Pt surface by the coadsorption of atomic hydrogen and water layer, and examined the spatial distribution of hydrated protons at the water–Pt interface with counterions.

Chapter I introduces the simulation of the electrochemical interface under UHV, known as the UHV model study. Simulation of the electrochemical interface in UHV conditions is useful for exploring the electric double layer (EDL) outside of an electrochemical cell without an applied electrochemical potential. UHV modeling allows the study of aqueous interfaces at the molecular level. Previous UHV modeling studies have been limited to obtaining the elemental, structural, and electronic information of

surfaces. The present work demonstrates that simulation of the EDL, along with surface spectroscopic techniques, can provide valuable information about the water–metal interface at the molecular level.

The basic principle of experimental methods was discussed in Chapter II. Reflection-absorption IR spectroscopy can provide the information about the molecular structure of surface species. Cs^+ reactive ion scattering (RIS) and low energy sputtering (LES) reveal the identities of the neutral and ionic species on the surface, respectively. Kelvin probe was introduced to estimate the distance of charge separation. In addition, instruments equipped in the UHV chamber are also described.

Chapter III presents the study on the nature of hydrated protons by the coadsorption of atomic hydrogen and water layer on a Pt(111) surface. Spectroscopic evidence obtained by mass spectrometry and reflection absorption infrared spectroscopy showed that the adsorbed hydrogen atoms ionize into multiply hydrated proton species ($H_5O_2^+$, $H_7O_3^+$, and $H_9O_4^+$) on the surface, rather than into H_3O^+. Then, upon the addition of a water overlayer, the metal-bound hydrated protons spontaneously evolved into three-dimensional fully hydrated proton structures via proton transfer along the water overlayer. The stability of the hydrated protons on the Pt surface and their bulk dissolution behavior suggest the possibility that the surface hydrated protons are a key intermediate in the electrochemical interconversion between the adsorbed H atoms and H^+(aq) in water electrolysis and hydrogen evolution reactions.

In Chapter IV, the spatial distribution of hydrated protons and chloride ions is studied by the coadsorption of HCl and H_2O on a Pt surface. An amorphous solid water (ASW) film was overlaid on the ions to simulate the electrochemical interface in UHV. The experimental results showed that H^+ and Cl^- ions on the Pt surface have the thermodynamic preference to reside near the Pt surface rather than diffuse out into the ASW film. The

vertical average distance of H^+ ions from the Cl^- ions, which specifically adsorbed on the Pt surface, was estimated to be about one water layer. The migration of protons to the hydration sphere can be attributed to the stability of fully solvated structure. The distribution of H^+ and Cl^- ions near the Pt surface exhibits the consistence of the specifically adsorbed (Cl^-) and non-specifically adsorbed (H^+) ions in the EDL.

Keywords: protons, water–metal interface, platinum, hydrogen evolution reaction, electric double layer, surface analysis

Student number: 2011-20285

Contents

List of Figures and Tables

Figure 2-3. Dipolar adsorbates and its image dipole at a metal surface. (a) If the dipole is parallel to the metal surface, the image dipole opposes the original, so that $(\partial\mu/\partial Q) = 0$. (b) If the dipole is perpendicular to the surface, the dipole moment is amplified by the image dipole.

Figure 2-4. RAIRS spectra I and schematic structure II of particular water samples on Ru(0001). An intact water monolayer (a) composed of flat-lying and H-down molecules and half-dissociated (H + OH + H_2O) layer model (b) composed of flat-lying OH and H_2O molecules [16].

Figure 2-5. Schematic diagram of the Cs^+ RIS (a) and LES process (b). In the RIS process, the Cs^+ ion picks up the neutral molecules (X) adsorbed on the surface and ionic clusters (CsX^+) are formed. The positive (Y^+) and negative (Z^-) ions on the surface are detached on Cs^+ impact in the LES process. The ionic clusters (CsX^+) and sputtered ions (Y^+ and Z^-) are monitored by quadrupole mass spectrometry.

Figure 2-6. Schematic of the Kelvin probe experiment to measure the voltage from charge separation. (a) Positive and negative ions exist in the same plane. (b) Positive ion migrates along the overlayer.

Figure 2-7. Schematic diagram of the apparatus for Cs^+ RIS, LES, RAIRS, and Kelvin work function measurements, consisting of an UHV chamber.

Figure 3-1. Positive-ion LES signals (shown for $m/z \leq 85$) and RIS signals ($m/z \geq 125$) obtained from various samples. (a) H_2O (1.1 ML) was adsorbed onto preadsorbed H (0.8

MLE) Pt(111) at < 90 K. (b) The sample prepared in (a) was heated at 140 K for 100 s and at 150 K for a few seconds. (c) HCl was exposed onto H_2O 5 BL below 90 K. (d) H_2O (1.2 ML) was adsorbed on a bare Pt(111) surface (without preadsorption of H atoms), and heated in the same way as for spectrum (b). All spectra were obtained below 90 K. The Cs^+ beam energy was 28 eV.

Figure 3-2. RAIR spectra of (I) H + H_2O and (II) D + D_2O layers on Pt(111). (a) Hydrogen/Deuterium (0.75 MLE) and H_2O/D_2O (1.2 ML) was coadsorbed at 90 K, respectively. (b) The sample prepared in (a) was heated at 140 K for 100 s and heated at 150 K for a few seconds. Each inset shows hydrated proton/deuteron band in the spectrum (b), respectively.

Figure 3-3. Positive LES spectra and RIS spectra. (a) 0.75 MLE D was formed on Pt(111) and H_2O was deposited on this at < 90 K. (b) The sample was heated at 140 K for 100 s and flashed to 150 K. The LES and RIS measurements were conducted at < 90 K with Cs^+ beam energy of 28 eV.

Figure 3-4. (I) Positive LES and RIS spectra obtained at various preadsorbed Na coverage on Pt(111). Na atoms were deposited onto bare Pt surface at < 90 K for each work function change of (a) 0.4 and (b) 1.1 V. Hydrogen and water was adsorbed on each sample. The sample temperature was heated to 150 K and maintained at 90 K during measurements. Cs^+ beam energy was 28 eV.

Figure 3-5. Experimental measurements for ΔCPD value changed from the formation of hydrated protons by heating each sample to 150 K as a function of work function change

by Na, H, and H_2O adsorption. The solid line shows the simple linear fitting of data.

Figure 3-6. Variation of LES intensities for hydrated proton species [$H_5O_2^+$(■,red), $H_7O_3^+$(●,blue) and $H_9O_4^+$(▲,magenta); left ordinate scale] with increasing addition of water overlayer on preformed hydrated proton species. The initial sample was prepared by coadsorption of hydrogen (0.8 MLE) and water (1.1 ML) and heating at 150 K.

Figure 3-7. TPLES measurement of hydrated protons signal intensities on the sample prepared by hydrogen (0.8 MLE) and water (1.3 MLE) coadsorption on Pt(111) below 90 K. The black line depicts the water coverage (right ordinate scale) deduced from TPD measurement of water from the equivalent sample. The dotted vertical line marks the position of water monolayer coverage. The ramping rate was 1 K s^{-1} in both the TPLES and TPD experiments.

Figure 3-8. Series of RAIRS spectra of the sample with increasing water exposure on the MB hydrated protons preformed by coadsorption of hydrogen and water and heating to 150 K. The amount of water exposure corresponding to each spectrum is: (a) 0 ML; (b) 0.13 ML; (c) 0.26 ML; (d) 0.39 ML; (e) 0.52 ML; (f) 1.8 ML; (g) 3.0 ML. Each spectrum was obtained by adding water on previous spectrum. The sample temperature was maintained below 90 K during the water exposure.

Figure 3-9. Potential energy diagram for the Volmer reaction. The reaction energy (~0.6 eV) was estimated through a thermodynamic cycle including desorption of atomic hydrogen (+2.7 eV) [28], ionization of atomic hydrogen in the gas phase (+13.6 eV), electron transfer to water-adsorbed Pt(111) (-5.5 eV), and hydration of a gaseous proton (-11.4 eV) [32].

Figure 3-S1. TPD spectra for an adsorbed D layer on Pt(111) (a), adsorbed H_2O layer on Pt(111) (b), and coadsorbed D and H_2O layer on Pt(111) (c and d). All samples were prepared by gas adsorption at < 90 K, followed by heating at 140 K for 100 s and at 150 K briefly. The temperature ramping rate was 1 K s^{-1}.

Figure 3-S2. Experimental measurements for total work function change by Na, H, and H_2O adsorption from only Na. The solid line shows the simple linear fitting of data.

Figure 4-1. (a) Positive-ion LES , (b) negative-ion LES and (c) RIS spectra measured from the samples that were prepared under the following conditions: (I) adsorption of HCl for 0.1 ML on Pt(111) at 83 K and adsorption of H_2O for1 ML at 135 K, (II) addition of H_2O overlayer for 3 ML onto the sample (I) at 80 K. All the spectra were recorded below 90 K with Cs^+ beam energy of 32 eV.

Figure 4-2. TPLES measurements of hydrated protons (H_3O^+, $H_5O_2^+$, $H_7O_3^+$, and $H_9O_4^+$) and chloride ions ($^{35}Cl^- + {}^{37}Cl^-$) reaching the sample surface via diffusion through an ASW overlayer with 28 ML thickness. Spectra I(a) and I(b) correspond to the ion diffusion from the water/Pt interface, measured for a sample structure: H_2O (28 ML)/H^+ (0.1 ML) + Cl^- (0.1 ML)/Pt(111). H^+ and Cl^- were generated by coadsorption of HCl (0.1 ML) and water (1 ML) on Pt. Spectra II(a) and II(b) measure the ion diffusion from ASW interior by preparing a sample structure: H_2O (28 ML)/H^+ (0.1 ML) + Cl^- (0.1 ML)/H_2O (50 ML)/Pt(111). The H_2O TPD spectra for corresponding samples are shaded and the height of the TPD curves are shown in an arbitrary scale. The chloride ion intensity is the summation of $^{35}Cl^-$ and $^{37}Cl^-$. The Cl^- curves are shown as log-scaled. All spectra were recorded at a temperature ramping rate of 0.5 K s^{-1}. The sample temperature was raised

from 85 K, but the spectra are displayed for the region from 130 K. The Cs^+ beam energy for TPLES was 32 eV.

Figure 4-3. ΔCPD associated with the distributions of H^+ and Cl^- ions in ASW overlayer film with increasing exposure. (a) ΔCPD measurements for samples in which H^+ and Cl^- ions are initially formed on a Pt surface by coadsorption of HCl (0.04–0.24 ML) and H_2O (1 ML). (b) ΔCPD measurements for a sample in which H^+ and Cl^- ions are initially formed on the ASW surface by adsorption of 0.06 ML HCl (□). A sample initially only with pure water monolayer on Pt (△). A sample initially with H^+ and Cl^- ions (0.06 ML) on Pt (●), the same curve as that shown in (a). The sample temperature for the adsorption of ASW layer and CPD measurement was 83 K.

Figure 4-4. The vertical distance between H^+ and Cl^- divided by relative dielectric constant, d/ε_r, for various HCl concentration (0.04–0.12 ML). The d/ε_r values are obtained from ΔCPD in Figure 4-3(a) by converting Equation (4-1). The solid lines are the theoretical model fitted to the experimental data. ε_r values of each HCl coverage are calculated using a least-squares fit.

Figure 4-5. (a) LES intensities of hydrated protons as a function of water overlayer thickness measured for coadsorbed HCl (0.1 ML) and H_2O (1.0 ML) on Pt(111). The sample temperature was maintained at 80 K during the water adsorption and LES detection. (b) A display of the same data in the normalized intensity scale with respect to the intensity at zero thickness of water overlayer. The open circles (○) with the dotted line indicate H_3O^+ signal intensity measured for ionized HCl on a polycrystalline ice film (~50 ML). The Cs^+ beam was 32 eV.

Chapter I

Introduction

The understanding of water–metal interfaces is very important in a wide variety of scientific disciplines and technologies because water films exist on most solid surfaces under atmospheric conditions. Numerous experimental and theoretical studies have been conducted over the past decade, which have significantly improved our understanding of the structure and dynamics of water adsorption on various metal surfaces [1-3]. Despite their fundamental importance, these studies have been limited to the investigation of the interfacial reaction where water is adsorbed at the metal surface. Hydrated protons, in particular, play a crucial role in a wide variety of chemical phenomena in acidic aqueous environments [4, 5]. Consequently, understanding the nature of hydrated protons is fundamental to the investigation of many fields, including heterogeneous catalysis, corrosion, and electrochemistry. In particular, the investigation of hydrated protons is vital because of the role of proton transfer and acid–base characteristics at the water–solid interface [6].

This thesis focuses on the physical and chemical properties of hydrated protons at the metal surface, which is strongly associated with the properties of protons at the electrochemical interface. Many experiments have been performed on the stability, structure, mobility, and transport mechanism of hydrated protons on the metal surface but

many questions still remain [7-14]. Here, the nature of hydrated protons on the metal surface and in the bulk-like environment was determined. Moreover, hydrated protons with counterions were examined to study their distribution near the metal surface.

This thesis is organized as follows: In the Introduction, ultra-high vacuum (UHV) modeling is briefly summarized, especially concerning electrochemistry, and examples of simulations are given in Chapter I. Chapter II contains fundamental information on the experimental methods used in this thesis. In Chapter III, the nature of hydrated protons formed by the coadsorption of hydrogen and water is described. In Chapter IV, the investigation of the distribution of hydrated protons and counterions from the metal surface is reported.

1. Simulation of the Electrochemical Interface under Ultra-High Vacuum

When an electrode is immersed in an electrolyte solution, charge accumulation and charge separation occur at a specific interfacial region: the electric double layer (EDL) [15]. The excess charge on the electrode is compensated by an accumulation of opposing charge in the solution, which is determined by the electrode potential. The EDL at electrode/electrolyte interface controls the rates, direction, and even the nature of electrochemical reactions [15, 16]. A simplified model of the EDL is shown in Figure 1-1 [17]. This model consists of two planes: the inner Helmholtz layer (IHP) and the outer Helmholtz layer (OHP). The IHP layer consists of specifically adsorbed ions and adsorbed water molecules. The OHP passes through the center of the hydrated ions, which are non-specifically adsorbed ions. However, this picture of the EDL is based on thermodynamic information rather than microscopic structural information because it is difficult to experimentally probe the structure of the EDL in an electrochemical environment.

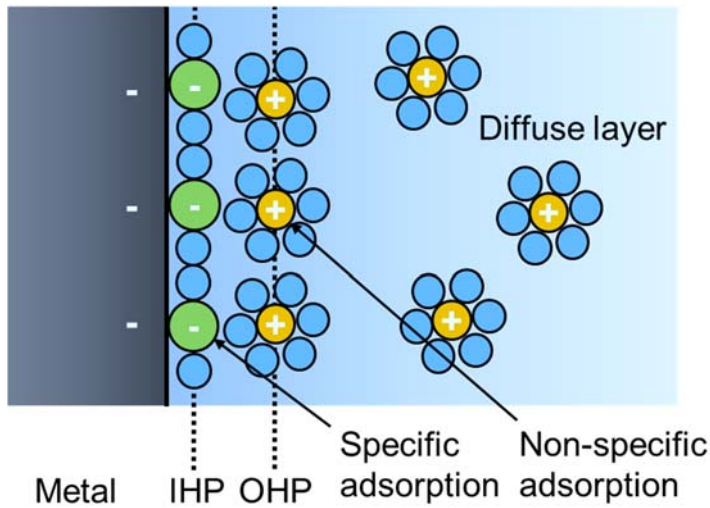

Figure 1-1. Schematic model of the electric double layer. In the inner Helmholtz layer, anions are specifically adsorbed on the metal surface without solvation. In the outer Helmholtz layer, solvated cations, known as non-specifically adsorbed ions, are present.

1.1. Comparing UHV Modeling to Electrochemical Measurements

The simulation of the electrochemical interface in UHV conditions is one way to explore the EDL outside of an electrochemical cell without an applied electrochemical potential [18-21]. UHV modeling allows the study of aqueous interfaces at the molecular scale. To form the model double layer, known quantities of water and other species are coadsorbed at the metal surface. These species are chosen so that they react to produce species relevant to the electrical double layer. One advantage of UHV modeling is that the surface coverage of adsorbates at the interface is adjustable, whereas it is a dependent variable affected by the electrolyte and electrode composition in electrochemical experiments. This simplifies the UHV model experiment compared to the complex electrochemical system, which has many variables. Surface spectroscopic techniques are used to determine the

electrochemical identity of the species in the EDL. After removing the bulk electrolyte, surface analytical techniques can be used to investigate the electrochemical interface; in contrast, the number of spectroscopic techniques for the solid-liquid interface is extremely limited. Therefore, the structure and composition of the double layer at the electrochemical interface are of interest in UHV modeling.

The electrode potential is one of the most important quantities in an electrochemical cell. It is normally compared to the work function of the electrode surface under UHV conditions [22, 23]. A potential drop develops at the interface because of adsorption, and this can be converted to the electrochemical potential compared to the normal hydrogen electrode (NHE). A comparison of the work function and the electrode potential provides a better understanding of the fundamental processes in the immediate vicinity of the electrode. In the case of specific adsorption, adsorbates on the electrode induce the polarization of charge on the electrode surface and give rise to a local potential minimum in the IHP. Under UHV conditions, chemisorbed species are assumed to be analogous to those specifically adsorbed at the electrochemical interface. Chemical charge transfer between the electrode and specifically adsorbed species can induce the charging of the electrode surface. For example, alkali metals or halogen atoms, which are electropositive and electronegative adsorbates, respectively, can be observed to determine the influence of electric fields on the adsorption of the electrolyte [18, 20, 22, 24-26]. These results show that the work function is changed by the formation of a dipole layer. However, this voltage is not externally variable and is controlled by the adsorbates. The differences and similarities between the electrochemical and UHV measurements are shown in Table 1.

	Electrochemical method	UHV modeling method
Surface species	Surface species are difficult to identify.	Surface species can be identified by spectroscopy.
	Surface coverage of adsorbates is a dependent variable of the system.	Surface coverage of adsorbates can be controlled.
Solution species	Direct control of electrolyte composition.	Very limited availability of electrolytes for use at UHV.
Voltage across interface	Easy control of the electrode potential, which produces a potential drop across the electrode/electrolyte interface.	The potential drop, to a certain extent, is related to the work function, which is a dependent variable of the system.

Table 1-1. Difference and similarities between electrochemical and UHV measurements.

1.2. Objections to the UHV Models and Improvements

An important question is whether it is possible to produce equivalent interfaces from these two very different approaches. Firstly, the low temperature used in UHV modeling is not consistent with the electrochemical environment. In UHV experiments, a cryogenic temperature must be maintained to retain a water layer on the metal substrate. This results in the low diffusivity of water (self-diffusion rates ~1 monolayer per second (ML/s) at T = 150 K) [27], which is the weak point of the UHV simulations.

An outstanding feature of electrochemical experiments is the ability to control the electrode potential, thereby producing a potential drop across the electrode/electrolyte interface. In the UHV experiment, one can change the potential of a metal surface by changing the work function [21, 28], as mentioned above. However, the change in the

surface work function does not necessarily produce a potential drop across the interface in the aqueous phase. Thus, recently, the ice film capacitor method has been developed to overcome this limitation. In this method, low-energy ions are deposited onto molecular films [29-34]. To prepare the ice film capacitor, water molecules are deposited on a cold substrate, forming an ice film. Then, the ice film is electrically charged by depositing Cs^+ ions on the ice surface from a low-energy ion beam (on the order of 10 eV); the Cs^+ ions have a thermodynamic affinity to float on the surface. This film can be considered equivalent to a parallel-plate capacitor with Cs^+ ion on the ice film and electrons induced at the metal surface by image charge. The ice film capacitor provides a large potential drop across the interface, and the potential drop can be controlled by the amount of Cs^+ ion on the ice surface.

Electrolyte ions are immobile in an ice film, unlike the environment of the diffuse layer. As far as the dielectric response of the medium is concerned, the dipolar dielectric relaxation of water molecules can occur in an ice film at temperatures greater than 130 K. For the transport of electrochemically active species, recent studies have shown that H^+ can migrate efficiently through an ice film. Therefore, H^+ ions are desirable in a UHV system to investigate the electrochemistry.

2. Water at Metal Surfaces

2.1. Intact Water Structures on the Metal Surfaces

Molecules of H_2O, the most commonly used solvent, are the main species at the electrolyte–electrode interface. The fundamental behavior of H_2O at interfaces must be studied to obtain a better understanding of the double layer, and studies have been recently carried out on a number of metal surfaces [1, 3, 35, 36]. H_2O molecules adsorbed at the metal

surfaces have a remarkably rich variety of structures. The current knowledge concerning these metal surfaces will be introduced in this chapter.

Individual water molecules adsorb on the top sites of close-packed transition metal surfaces bonding through the $1b_1$ molecular orbital with a roughly parallel alignment to the surface [37-39]. The binding energy of isolated water molecules is in the range of 0.1–0.5 eV [37, 38]. The isolated water molecules interact via water-water hydrogen bonds (~0.25 eV), forming a 2D honeycomb network structure, which obeys 2D ice rules [40] or forms 3D clusters depending on the binding energy of the water molecules and lattice parameters of the metal. The representative wetting surfaces are Pt, Ru, and Pd, and examples of non-wetting surfaces include Cu, Ag, and Au [2, 3, 35, 36].

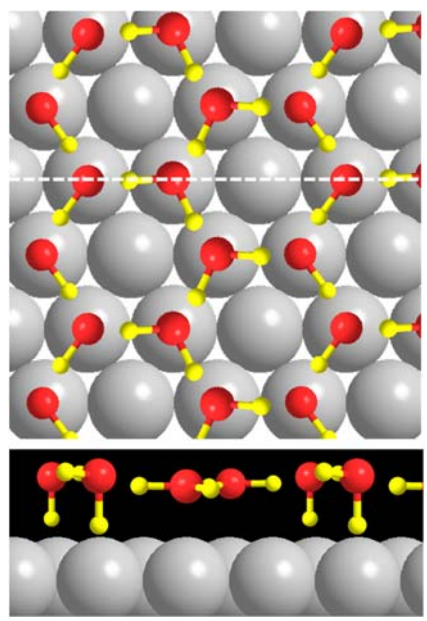

Figure 1-2. Structural models composed of flat layer and H-down molecules connected through an extended hydrogen-bonded network. The O atoms are in a $(\sqrt{3} \times \sqrt{3})R30°$ arrangement relative to the Ru(0001) surface, which is typical example of close-packed metal surface.

In earlier research of low-energy electron diffraction (LEED) experiments [1, 41], the water wetting layer was observed as a (√3 × √3)R30° structure on several metal surfaces. This structure was suggested because the 2D honeycomb network structure forms an ice-like bilayer because the lattice parameters of the metal are similar to those of the I_h(0001) ice surface. In this buckled bilayer, the lower part of the layer strongly interacts with the metal surface via the O atom, whereas water molecules in the upper part are connected to the lower part though H-bonding and do not interact with the metal surface. The water orientation of the upper part of the layer has been intensively studied to clarify whether uncoordinated OH is in either the H-up (pointing toward the vacuum) or H-down (toward to the metal surface) orientation [42]. The results for some metal surfaces (Ru, Pt, etc.) show that uncoordinated OH points toward the metal surface (H-down), and these H-down molecules exist on the almost same plane as water molecules in the lower part. This indicates that the water layer is a non-buckled structure comprising H-down and flat water 2model is only true for some metals, and water layers on metal structures can have various structures, which are determined by the balance between the metal–water and water–water interactions.

Instead of a 2D water monolayer, 3D ice clusters form when the metal has weak interactions with the water molecules, or there are significant differences in the lattice parameters compared to the I_h(0001) ice surface. These non-wetting surfaces show a variety of complex structures that cannot be generalized into a specific structure. Detailed structural information of each metal surface have been obtained by experimental measurements such as thermal desorption spectroscopy (TPS) [43, 44], X-ray photoelectron spectroscopy (XPS) [45, 46], X-ray absorption spectroscopy (XAS) [47], reflection absorption IR spectroscopy (RAIRS) [42, 48-52], high-resolution electron energy loss spectroscopy (HREELS) [53, 54], low energy electron diffraction (LEED) [55,

56], He atom scattering (HAS) [57], work function measurements, and scanning tunneling microscopy (STM) [58-60]. Density functional theory (DFT) calculations are also crucial for the determination of the model structure, aiding in the interpretation of experimental data [61, 62]. Therefore, reliable model of water structures can be achieved only when experimental observations from several techniques are combined with theoretical simulations.

2.2. Water Monolayer Structure on Pt(111)

According to early LEED studies, water on Pt(111) is a perfect example of an ice-like bilayer with a simple commensurate ($\sqrt{3} \times \sqrt{3}$)R30° structure (R3 structure), as shown in Figure 1-3(a). Further investigations using non-invasive HAS [57] and low-current LEED [43] measurements have concluded that the ($\sqrt{3} \times \sqrt{3}$)R30° structure is attributed to electron induced dissociation or the formation of mixed OH/H_2O structures. The diffraction results show that water molecules form a large unit cell, ($\sqrt{37} \times \sqrt{37}$)R25.3° (R37 structure), at coverages less than 1 ML [43]. This structure is reconstructed into the ($\sqrt{39} \times \sqrt{39}$)R16° (R39 structure) phase on the completion of the first layer. The R37 structure is slightly expanded (3.6%) compared to a bulk ice bilayer, while the R39 structure is compressed (4.4%).

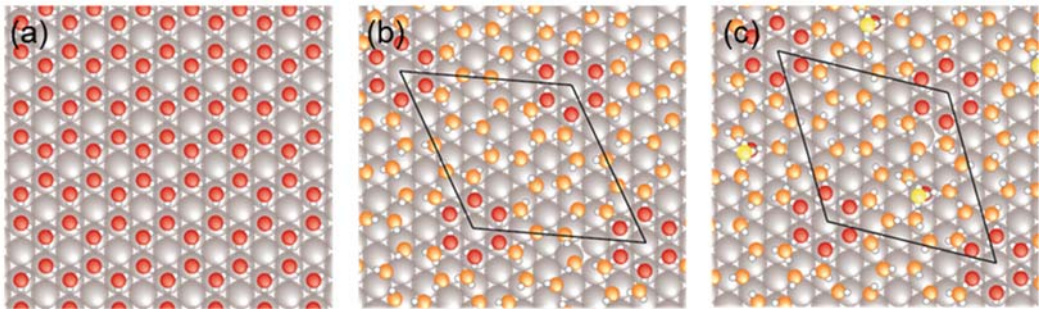

Figure 1-3. Water exhibits three different monolayer structures on Pt(111) [63]. (a) The (√3 × √3)R30° structure is an ideal model on Pt(111). (b) The (√37 × √37)R25.3° structure is energetically most favorable. (b) The (√39 × √39)R16.1° structure forms when a full wetting layer is achieved. The bright spots on top of the Moiré structure are due to a single second layer water molecule per unit cell.

Further XAS and XPS measurements have provided structural information concerning the orientation of uncoordinated OH groups [42]. The experimental results were compared to the DFT calculations for a commensurate H-up and H-down R3 structures, and this comparison led to the conclusion that uncoordinated OH points toward the metal (H-down), which is screened by the metal electrons [42]. This configuration maximizes the water-metal interactions by optimizing hydrogen-bonded network of water molecules.

A better insight in the 2D water monolayer on Pt(111) was obtained from high-resolution STM images of the water layer [60, 64]. DFT calculation of the R37 structure [65], shown in Figure 1-3(b), indicate that the wetting layer consists of a flat arrangement of water hexagons surrounded by pentagons and heptagons, and this suggested model is the most stable structure compared to other possible commensurate structures, such as the ice-like bilayer. The driving force to form this unique structure may be the formation of the hexagons adsorbed at the top site on Pt(111) with a flat orientation. This maximizes the interactions between the water and the metal surface. The R39 commensurate structure

shown in Figure 1-3(c) has also been assigned as the relaxed configuration of a water molecule added on top of the R37 structure. RAIR spectra identified the free OH stretching band, which is red-shifted by more than 1000 cm^{-1}, by simulating the vibrational modes. This result is consistent with the proposed model obtained from the STM images.

3. Acid-Base Chemistry in UHV Models

The acid-base reactions at the water/metal interface play an important role in helping us understand the ionic species, mainly H_3O^+ and OH^-, that are present in the EDL. The reactions of adsorbed water and other molecules are intimately related to proton transfer reactions at interfaces, including the hydrogen-evolution and oxygen-reduction reactions. The H_3O^+ and OH^- molecules are also connected to the pH of the double layer, and it important to understand acid-base chemistry at the molecular level in UHV, which is not well defined in electrochemistry.

The migration of protons occurs via proton hopping, which guarantees high mobility [66]. This supports the Brønsted acid-base equilibrium, even at the low temperatures used under UHV conditions. Previous efforts to introduce hydronium to the UHV surface have involved the coadsorption of water and strong acids, such as HF and HCl, on Pt(111) [67, 68]. The coadsorption of HF and water on the Pt surface have been investigated, and the formation of H_3O^+ and F^- was determined by HREELS experiment. It is known that anhydrous HF adsorbs on Pt(111) without dissociation. The experimental results show that HF molecules react with water at the interface to form ionic species. Moreover, thermal programmed desorption (TPD) experiments have shown that ionic species produced by the reaction have full primary solvation and weak surface interactions. The H_3O^+ and F^- ions could be considered non-specifically adsorbed state at the water/metal interface, which is defined as solvated species in the OHP. On the other hand, chloride from

HCl is regarded as “specifically adsorbed” on the surface. Although the coadsorption of HCl and H_2O on Pt(111) produces H_3O^+ and Cl^-, the structure at the interface is dominated by the Pt-Cl^- interactions as a function of HCl coverage. The solvation effects of chloride were not observed in the TPD experiments. Hydronium and counterions formed by strong acid and water reaction on the metal surface demonstrate the interaction between solvent and representative counterions in the EDL. In Chapter IV, the investigation, using contact potential difference (CPD) measurements, into the coadsorption of HCl and water on Pt(111) demonstrates how specifically adsorbed chloride ions and non-specifically adsorbed protons are distributed at the molecular level, and this is an alternative approach to those used previously.

In the case of a H_2SO_4 solution in an electrochemical environment, the experimental results were compared to the reaction of H_2O and SO_3 on Pt(111) [69]. In situ and UHV experiments showed the products to be H_3O^+ and HSO_4^- at specific potential ranges and temperatures. The existence of HSO_4^- changed the molecular orientation of H_3O^+ from C_3-axis perpendicular to parallel to the surface. The number of the coordination water molecules per HSO_4^- was also clarified by the comparison of two experimental methods.

Water adsorption with electropositive species, such as Na, K, and Cs, form the base adsorbed layers by the production of hydroxide [70, 71]. The dissociation of H_2O above a certain coverage of electropositive species may be qualitatively understandable in electrochemistry because the alkali metals reduce the work function of the metal, and these reactions can be achieved by satisfying the minimum work function value. Nevertheless, it is difficult to understand the macroscopic work function quantitatively compared to the local electrostatic potential.

The acidity of H_2O on Ru(0001) was investigated by the adsorption of NH_3, as a probe molecule, on a water monolayer. RIS, LES, RAIRS, and TPD experiments provide evidence of protons transfer from H_2O to NH_3, which induced the formation of ammonium ions [72, 73]. The acidic water corresponds to H-down oriented water molecules in two-dimensional network structures. Interestingly, the partially dissociated structure, (H + OH + H_2O) on Ru(0001), was not responsible for the acidity of the water layer, demonstrating the acid-base characteristic of adsorbed water on the metal surface at the molecular level.

Protons at the EDL are involved in one of the most elementary electrochemical reactions, and the representative reaction is a complete description of the hydrogen evolution reaction, which requires the understanding of H^+ formation and transport at the interface. This subject has been approached using UHV studies to obtain fundamental knowledge that is not well defined in the electrochemical environment. The electrochemical reaction was later identified unambiguously in UHV by coadsorbing H and H_2O on Pt(111) and Cu(110) and isotopically substituting H_{ad} by D_{ad} [9]. Hydronium ions were also observed under UHV, and H and H_2O were coadsorbed on Pt(100) and Pt(110) [10, 11]. The nature of the adsorbed hydronium species has been investigated recently by Masel and coworkers who obtained EELS spectra compatible with hydrated hydronium ions. This study is developed in the present thesis in Chapter III.

Previous UHV modeling studies have been limited to obtaining elemental, structural and electronic information of surfaces. The present work demonstrates that simulation of the EDL can provide valuable information at the water–metal interface at the molecular level by surface spectroscopic techniques. This study will widen the scope of spectroscopic chemical properties at interfaces and even in the bulk-like environment.

References

1. Thiel, P. A.; Madey, T. E. The Interaction of Water with Solid Surfaces Fundamental Aspects. *Surf. Sci. Rep.* **1987**, *7*, 211-385.
2. Henderson, M. A. The interaction of water with solid surfaces: fundamental aspects revisited. *Surf. Sci. Rep.* **2002**, *46*, 5-308.
3. Hodgson, A.; Haq, S. Water adsorption and the wetting of metal surfaces. *Surf. Sci. Rep.* **2009**, *64*, 381-451.
4. Eigen, M. Proton Transfer Acid-Base Catalysis + Enzymatic Hydrolysis .I. Elementary Processes. *Angew. Chem. Int. Ed.* **1964**, *3*, 1-19.
5. Trasatti, S. Work Function, Electronegativity, and Electrochemical Behavior of Metals .3. Electrolytic Hydrogen Evolution in Acid Solutions. *J. Electroanal. Chem.* **1972**, *39*, 163-184.
6. Tanaka, K. I.; Ozaki, A. Acid-Base Properties and Catalytic Activity of Solid Surfaces. *J. Catal.* **1967**, *8*, 1-7.
7. Wagner, F. T. Simulation of the Electrical Double-Layer in Ultrahgh Vacuum. In *Structure of Electrified Interfaces*; Ross, J. L. P. N., Ed.; VCH Publishers: New York, 1993.
8. Wagner, F. T.; Moylan, T. E. Generation of Surface Hydronium from Water and Hydrogen Coadsorbed on Pt(111). *Surf. Sci.* **1988**, *206*, 187-202.
9. Lackey, D.; Schott, J.; Sass, J. K.; Woo, S. I.; Wagner, F. T. Surface-Science Simulation Study of the Electrochemical Charge-Transfer Reaction $(H)_{ad} + (H_2O)_{ad} \rightarrow (H_3O^+)_{ad} + e^-_{metal}$ on Pt(111) and Cu(110). *Chem. Phys. Lett.* **1991**, *184*, 277-281.

10. Kizhakevariam, N.; Stuve, E. M. Coadsorption of Water and Hydrogen on Pt(100) - Formation of Adsorbed Hydronium Ions. *Surf. Sci.* **1992**, *275*, 223-236.

11. Chen, N.; Blowers, P.; Masel, R. I. Formation of hydronium and water-hydronium complexes during coadsorption of hydrogen and water on (2x1)Pt(110). *Surf. Sci.* **1999**, *419*, 150-157.

12. Shingaya, Y.; Ito, M. Coordination number and molecular orientation of hydronium cation bisulfate anion adlayers on Pt(111). *Surf. Sci.* **1996**, *368*, 318-323.

13. Pan, M.; Pozun, Z. D.; Yu, W. Y.; Henkelman, G.; Mullins, C. B. Structure Revealing H/D Exchange with Co-Adsorbed Hydrogen and Water on Gold. *J. Phys. Chem. Lett.* **2012**, *3*, 1894-1899.

14. Cao, Z.; Kumar, R.; Peng, Y. X.; Voth, G. A. Hydrated Proton Structure and Diffusion at Platinum Surfaces. *J. Phys. Chem. C* **2015**, *119*, 14675-14682.

15. Parsons, R. Electrical Double-Layer - Recent Experimental and Theoretical Developments. *Chem. Rev.* **1990**, *90*, 813-826.

16. Weaver, M. J.; Gao, X. P. In-Situ Electrochemical Surface Science. *Annu. Rev. Phys. Chem.* **1993**, *44*, 459-494.

17. Bockris, J. O. M.; Khan, S. U. M. *Surface Electrochemistry A Molecular Level Approach*; Springer US, 1993.

18. Sass, J. K.; Kretzschmar, K.; Holloway, S. Water-Adsorption on Metal-Surfaces - an Electrochemical Viewpoint. *Vacuum* **1981**, *31*, 483-486.

19. Sass, J. K.; Lackey, D.; Schott, J. Electrochemical Hydration and Reaction Processes on Metal-Surfaces Studied by Gas-Phase Adsorption. *Electrochim. Acta* **1991**, *36*, 1879-1882.

20. Sass, J. K.; Lackey, D.; Schott, J.; Straehler, B. Electrochemical Double-Layer Simulations by Halogen, Alkali and Hydrogen Coadsorption with Water on Metal-Surfaces. *Surf. Sci.* **1991**, *247*, 239-247.

21. Trasatti, S. Surface Science and Electrochemistry - Concepts and Problems. *Surf. Sci.* **1995**, *335*, 1-9.

22. Bonzel, H. P.; Pirug, G.; Ritke, C. Adsorption of H2o on Alkali-Metal-Covered Pt(111) and Ru(001) - a Systematic Comparison. *Langmuir* **1991**, *7*, 3006-3011.

23. Pirug, G.; Bonzel, H. P. UHV simulation of the electrochemical double layer: adsorption of HClO4/H2O on Au(111). *Surf. Sci.* **1998**, *405*, 87-103.

24. Stuve, E. M.; Bange, K.; Sass, J. K. In *Trends in Interfacial Electrochemistry*; Silva, A. F., Ed.; Springer Netherlands, 1986; pp 255-280.

25. Nakamura, M.; Song, M. B.; Ito, M. Hydrogen bonding between a water molecule and electronegative additives (O or Cl^-) on a Pt(111) surface. *Chem. Phys. Lett.* **2000**, *320*, 381-386.

26. Soriaga, M. P. Ultra-High Vacuum Techniques in the Study of Single-Crystal Electrode Surfaces. *Prog. Surf. Sci.* **1992**, *39*, 325-443.

27. Smith, R. S.; Kay, B. D. The existence of supercooled liquid water at 150 K. *Nature* **1999**, *398*, 788-791.

28. Tsiplakides, D.; Vayenas, C. G. Electrode work function and absolute potential scale in solid-state electrochemistry. *J. Electrochem. Soc.* **2001**, *148*, E189-E202.

29. Cyriac, J.; Pradeep, T.; Kang, H.; Souda, R.; Cooks, R. G. Low-Energy Ionic Collisions at Molecular Solids. *Chem. Rev.* **2012**, *112*, 5356-5411.

30. Tsekouras, A. A.; Iedema, M. J.; Ellison, G. B.; Cowin, J. P. Soft-landed ions: a route to ionic solution studies. *Int. J. Mass Spectrom.* **1998**, *174*, 219-230.

31. Wu, K.; Iedema, M. J.; Cowin, J. P. Ion penetration of the water-oil interface. *Science* **1999**, *286*, 2482-2485.

32. Bell, R. C.; Wu, K.; Iedema, M. J.; Schenter, G. K.; Cowin, J. P. The Oil-Water Interface: Mapping the Solvation Potential. *J. Am. Chem. Soc.* **2009**, *131*, 1037-1042.

33. Miller, S. A.; Luo, H.; Pachuta, S. J.; Cooks, R. G. Soft-landing of polyatomic ions at fluorinated self-assembled monolayer surfaces. *Science* **1997**, *275*, 1447-1450.

34. Shin, S.; Kim, Y.; Moon, E.-S.; Lee, D. H.; Kang, H.; Kang, H. Generation of strong electric fields in an ice film capacitor. *J. Chem. Phys.* **2013**, *139*, 074201.

35. Carrasco, J.; Hodgson, A.; Michaelides, A. A molecular perspective of water at metal interfaces. *Nat. Mater.* **2012**, *11*, 667-674.

36. McBride, F.; Hodgson, A. Water and its partially dissociated fragments at metal surfaces. *Int. Rev. Phys. Chem.* **2017**, *36*, 1-38.

37. Michaelides, A.; Ranea, V. A.; de Andres, P. L.; King, D. A. General model for water monomer adsorption on close-packed transition and noble metal surfaces. *Phys. Rev. Lett.* **2003**, *90*, 216102.

38. Carrasco, J.; Michaelides, A.; Scheffler, M. Insight from first principles into the nature of the bonding between water molecules and 4d metal surfaces. *J. Chem. Phys.* **2009**, *130*, 184707.

39. Schiros, T.; Takahashi, O.; Andersson, K. J.; Ostrom, H.; Pettersson, L. G. M.; Nilsson, A.; Ogasawara, H. The role of substrate electrons in the wetting of a metal surface. *J. Chem. Phys.* **2010**, *132*, 094701.

40. Cerda, J.; Michaelides, A.; Bocquet, M. L.; Feibelman, P. J.; Mitsui, T.; Rose, M.; Fomin, E.; Salmeron, M. Novel water overlayer growth on Pd(111) characterized

with scanning tunneling microscopy and density functional theory. *Phys. Rev. Lett.* **2004**, *93*, 116101.

41. Doering, D. L.; Madey, T. E. The Adsorption of Water on Clean and Oxygen-Dosed Ru(001). *Surf. Sci.* **1982**, *123*, 305-337.

42. Ogasawara, H.; Brena, B.; Nordlund, D.; Nyberg, M.; Pelmenschikov, A.; Pettersson, L. G. M.; Nilsson, A. Structure and bonding of water on Pt(111). *Phys. Rev. Lett.* **2002**, *89*, 276102.

43. Haq, S.; Harnett, J.; Hodgson, A. Growth of thin crystalline ice films on Pt(111). *Surf. Sci.* **2002**, *505*, 171-182.

44. Hinch, B. J.; Dubois, L. H. Stable and Metastable Phases of Water Adsorbed on Cu(111). *J. Chem. Phys.* **1992**, *96*, 3262-3268.

45. Andersson, K.; Nikitin, A.; Pettersson, L. G. M.; Nilsson, A.; Ogasawara, H. Water dissociation on Ru(001): An activated process. *Phys. Rev. Lett.* **2004**, *93*, 196101.

46. Andersson, K.; Gomez, A.; Glover, C.; Nordlund, D.; Ostrom, H.; Schiros, T.; Takahashi, O.; Ogasawara, H.; Pettersson, L. G. M.; Nilsson, A. Molecularly intact and dissociative adsorption of water on clean Cu(110): A comparison with the water/Ru(001) system. *Surf. Sci.* **2005**, *585*, L183-L189.

47. Cavalleri, M.; Ogasawara, H.; Pettersson, L. G. M.; Nilsson, A. The interpretation of X-ray absorption spectra of water and ice. *Chem. Phys. Lett.* **2002**, *364*, 363-370.

48. Nakamura, M.; Shingaya, Y.; Ito, M. The vibrational spectra of water cluster molecules on Pt(111) surface at 20 K. *Chem. Phys. Lett.* **1999**, *309*, 123-128.

49. Nakamura, M.; Ito, M. Monomer and Tetramer Water Clusters Adsorbed on Ru(0001). *Chem. Phys. Lett.* **2000**, *325*, 293-298.

50. Nakamura, M.; Ito, M. Ring hexamer like cluster molecules of water formed on a Ni(111) surface. *Chem. Phys. Lett.* **2004**, *384*, 256-261.

51. Nakamura, M.; Ito, M. Coadsorption of water dimer and ring-hexamer clusters on M(111) (M = Cu, Ni, Pt) and Ru(001) surfaces at 25 K as studied by infrared reflection absorption spectroscopy. *Chem. Phys. Lett.* **2005**, *404*, 346-350.

52. Beniya, A.; Yamamoto, S.; Mukai, K.; Yamashita, Y.; Yoshinobu, J. The first layer of water on Rh(111): Microscopic structure and desorption kinetics. *J. Chem. Phys.* **2006**, *125*, 054717.

53. Andersson, S.; Nyberg, C.; Tengstal, C. G. Adsorption of Water Monomers on Cu(100) and Pd(100) at Low-Temperatures. *Chem. Phys. Lett.* **1984**, *104*, 305-310.

54. Hock, M.; Seip, U.; Bassignana, I.; Wagemann, K.; Kuppers, J. Coadsorption of Oxygen and Water at Ni(110) Surfaces. *Surf. Sci.* **1986**, *177*, L978-L982.

55. Faradzhev, N. S.; Kostov, K. L.; Feulner, P.; Madey, T. E.; Menzel, D. Stability of water monolayers on Ru(0001): Thermal and electronically induced dissociation. *Chem. Phys. Lett.* **2005**, *415*, 165-171.

56. Held, G.; Menzel, D. The Structure of the p($\sqrt{3} \times \sqrt{3}$)R30° Bilayer of D_2O on Ru(001). *Surf. Sci.* **1994**, *316*, 92-102.

57. Glebov, A.; Graham, A. P.; Menzel, A.; Toennies, J. P.; Senet, P. A helium atom scattering study of the structure and phonon dynamics of the ice surface. *J. Chem. Phys.* **2000**, *112*, 11011-11022.

58. Tatarkhanov, M.; Ogletree, D. F.; Rose, F.; Mitsui, T.; Fomin, E.; Maier, S.; Rose, M.; Cerda, J. I.; Salmeron, M. Metal- and Hydrogen-Bonding Competition during Water Adsorption on Pd(111) and Ru(0001). *J. Am. Chem. Soc.* **2009**, *131*, 18425-18434.

59. Maier, S.; Lechner, B. A. J.; Somorjai, G. A.; Salmeron, M. Growth and Structure of the First Layers of Ice on Ru(0001) and Pt(111). *J. Am. Chem. Soc.* **2016**, *138*, 3145-3151.

60. Nie, S.; Feibelman, P. J.; Bartelt, N. C.; Thurmer, K. Pentagons and Heptagons in the First Water Layer on Pt(111). *Phys. Rev. Lett.* **2010**, *105*.

61. Michaelides, A.; Hu, P. Catalytic water formation on platinum: A first-principles study. *J. Am. Chem. Soc.* **2001**, *123*, 4235-4242.

62. Hamada, I.; Meng, S. Water Wetting on Representative Metal Surfaces: Improved Description from Van der Waals Density Functionals. *Chem. Phys. Lett.* **2012**, *521*, 161-166.

63. Lechner, B. A. J.; Kim, Y.; Feibelman, P. J.; Henkelman, G.; Kang, H.; Salmeron, M. Solvation and Reaction of Ammonia in Molecularly Thin Water Films. *J. Phys. Chem. C* **2015**, *119*, 23052-23058.

64. Standop, S.; Morgenstern, M.; Michely, T.; Busse, C. H2O on Pt(111): structure and stability of the first wetting layer. *J. Phys. Condens. Matter* **2012**, *24*, 124103.

65. Feibelman, P. J.; Bartelt, N. C.; Nie, S.; Thurmer, K. Interpretation of high-resolution images of the best-bound wetting layers on Pt(111). *J. Chem. Phys.* **2010**, *133*, 154703.

66. Eigen, M.; De Maeyer, L. In *The Structure of Electrolytic Solutions*; Hamer, W., Ed.; Wiley: New York, 1959; pp 64-85.

67. Wagner, F. T.; Moylan, T. E. Identification of Surface Hydronium - Coadsorption of Hydrogen-Fluoride and Water on Platinum (111). *Surf. Sci.* **1987**, *182*, 125-149.

68. Wagner, F. T.; Moylan, T. E. Hydrogen-Chloride Adsorption and Coadsorption with Hydrogen or Water on Platinum(111). *Surf. Sci.* **1989**, *216*, 361-385.

69. Ito, M. Structures of water at electrified interfaces: Microscopic understanding of electrode potential in electric double layers on electrode surfaces. *Surf. Sci. Rep.* **2008**, *63*, 329-389.

70. Kiskinova, M.; Pirug, G.; Bonzel, H. P. Adsorption and Decomposition of H_2O on a K-Covered Pt(111) Surface. *Surf. Sci.* **1985**, *150*, 319-338.

71. Baumann, P.; Pirug, G.; Reuter, D.; Bonzel, H. P. Uhv Adsorption Studies of K/H_2O on Pt(111) and O/Ch3cooh on Cu(110) - Orientation and Intermediates. *Surf. Sci.* **1995**, *335*, 186-196.

72. Kim, Y.; Moon, E. S.; Shin, S.; Kang, H. Acidic Water Monolayer on Ruthenium(0001). *Angew. Chem. Int. Ed.* **2012**, *51*, 12806-12809.

73. Kim, Y.; Shin, S.; Moon, E. S.; Kang, H. Spectroscopic Monitoring of the Acidity of Water Films on Ru(0001): Orientation-Specific Acidity of Adsorbed Water. *Chem. Euro. J.* **2014**, *20*, 3376-3383.

Chapter II

Methods

1. Reflection Absorption FT-IR Spectroscopy (RAIRS)

Vibrational spectroscopy is one of the mostly available and useful methods that can provide information about the molecular structure. Reflection absorption infrared spectroscopy (RAIRS) has been used to study thin films and adsorbed molecules on the metal substrate [1, 2]. This technique measures changes in the reflectance spectrum from the substrate and gives information about the molecular structure of surface species. One of the advantages of this technique is that a component of only the transition dipole component perpendicular to the surface is detected by the surface selection rule. The selection rules also provide information about the orientation of molecules adsorbed on the metal surface. Other advantages of the technique include its high sensitivity for adsorbates and correspondence to the information obtained from other vibrational spectroscopies [3-6]. A significant disadvantage, however, is its difficulty for unambiguously assigning the molecular structure from the band frequencies alone, without other additional information [7]. Despite such a drawback, RAIRS can provide valuable insight into understanding of adsorbate structures.

A RAIR spectrum of thin films shows complex features arising from multiple

reflections at the film/vacuum and film/metal substrate interface. When the film thickness, d, is much smaller than the wavelength, λ, the Fresnel equation can be used to analyze the RAIRS spectra. Before analyzing the thin film system, a two-phase system is initially considered with a plane boundary. The following solution of the wave function describes the propagation of plane waves: $E\ (r,t)\ =\ E^{\circ}exp[i(\omega t - K\cdot r)]$, where E° is the amplitude of the electric field vector, $\omega\ =\ 2\pi\nu$ is the angular frequency, K is the wave vector, and r refers to the coordination. The Fresnel reflection coefficient in the two-phase system is defined as $r = E_r/E_i$. The boundary condition for the electric field and magnetic field for parallel and perpendicular polarized radiation can be solved using the Maxwell equation. The Fresnel coefficients of the interface between two phase are obtained as [8]

$$r^{p}{}_{12}\ =\ \frac{(\tilde{n}_1\mu_2)cos\theta_1\ -\ (\tilde{n}_2\mu_1)cos\theta_2}{(\tilde{n}_1\mu_2)cos\theta_1\ +\ (\tilde{n}_2\mu_1)cos\theta_2} \tag{2-1}$$

$$r^{s}{}_{12}\ =\ \frac{(\tilde{n}_1\mu_1)cos\theta_1\ -\ (\tilde{n}_2\mu_2)cos\theta_2}{(\tilde{n}_1\mu_1)cos\theta_1\ +\ (\tilde{n}_2\mu_2)cos\theta_2} \tag{2-2}$$

where $\tilde{n}$ is the complex refractive index, μ is the magnetic permeability, θ_1 is the incident angle of the electric field with respect to the surface normal, and θ_2 is the angle between the refracted beam in the ice and surface normal.

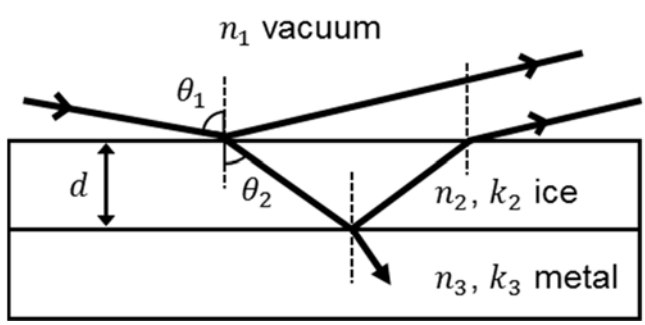

Figure 2-1. Schematic three-phase system consisting of vacuum, ice film, and metal.

The three-phase system [9, 10] consists of vacuum, the absorbing film, and the metal substrate, as shown in Figure 2-1. For this system, the equivalent Fresnel coefficients are

$$r^p{}_{123} = \frac{r^p{}_{12} + r^p{}_{23} exp(-2i\beta)}{1 + r^p{}_{12} r^p{}_{23} exp(-2i\beta)} \tag{2-3}$$

$$r^s{}_{123} = \frac{r^s{}_{12} + r^s{}_{23} \exp(-2i\beta)}{1 + r^s{}_{12} r^s{}_{23} \exp(-2i\beta)} \tag{2-4}$$

where β, the phase change of the beam during one traversal of the adsorbing film with thickness d, is given by $\beta = 2\pi(d/\lambda)\tilde{n}_2 cos\theta_2$. The reflectance of this system can be calculated as $R = |r_{123}|^2$. The reflectance can be expressed as absorbance in order to compare with experimental data

$$A = -log\left(\frac{R^s + R^p}{R_0{}^s + R_0{}^p}\right) \tag{2-5}$$

where A is an absorbance unit, R_0 is the reflectance of the vacuum–metal interface ($d = 0$), and the total reflectance is expressed as $R = R^s + R^p$ (Fresnel continued research) [10-12]. Therefore, this indicates that the Fresnel reflection coefficient obtained from the refractive index provides information about absorbance in RAIRS.

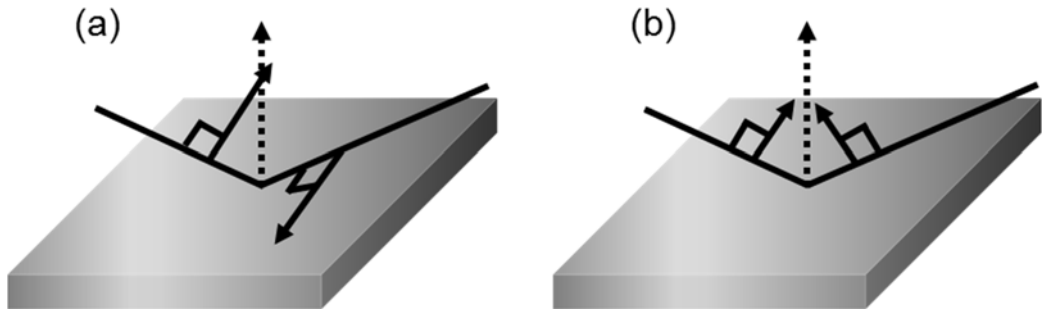

Figure 2-2. Schematic representation of the electric field vectors of the incident and reflected radiation with (a) δ = 180º (destructive interference) and (b) δ = 90º (constructive interference) [14].

For very thin films ($d \ll \lambda$), a linear approximation can be applied to the Fresnel reflection coefficient of the three-phase model. This provides the normalized reflectance change, $\Delta R/R_0$, for s-polarized light as,

$$\left(\frac{\Delta R}{R_0}\right)_s = 0 \tag{2-6}$$

where $\Delta R = R - R_0$. This indicates that s-polarized radiation is not adsorbed by a thin film. This can be attributed to a phase change, δ, of 180º, and the incident and reflected rays interfering destructively. The phase change of p-polarized light is determined by the incident angle. The schematic features are shown in Figure 2-2. The absorbance of p-polarized light increases with the incident angle. To reach the maximum absorbance, the experiment is performed at grazing reflected angle [13].

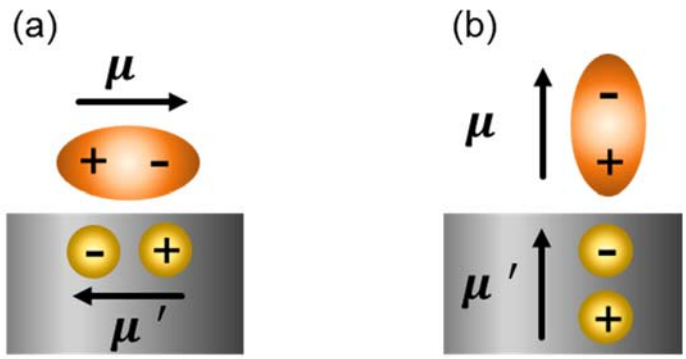

Figure 2-3. Dipolar adsorbates and its image dipole at a metal surface. (a) If the dipole is parallel to the metal surface, the image dipole opposes the original, so that $(\partial\mu/\partial Q) = 0$. (b) If the dipole is perpendicular to the surface, the dipole moment is amplified by the image dipole.

The RAIR spectrum only shows surface species with a dipole moment derivative $\partial\mu/\partial Q$ in the direction perpendicular to the surface [15]. This is the surface selection rule for RAIRS, which does not apply to other vibrational spectroscopy methods. It can be explained by image dipole being induced at the surface of a metal and the net dipole moment always being zero when adsorbates are parallel to the surface. On the other hand, the image dipole of molecules perpendicular to the substrate changes the net dipole moment, as schematically shown in Figure 2-3.

For example, Figure 2-4I shows the RAIR spectra of intact monolayer and mixed H + OH + H_2O layer on Ru(0001) and Figure 2-4II shows the component of each layer. An intact water monolayer consisting of H-down and flat-lying configuration of molecular H_2O exhibits the bands of OH stretching, bending, and librational modes, as seen in Figure 2-4I(a), whereas the vibrational mode of a mixed OH/H_2O layer, shown in Figure 2-4I(b), was not observed because of the all flat-lying orientation with respect to the metal surface.

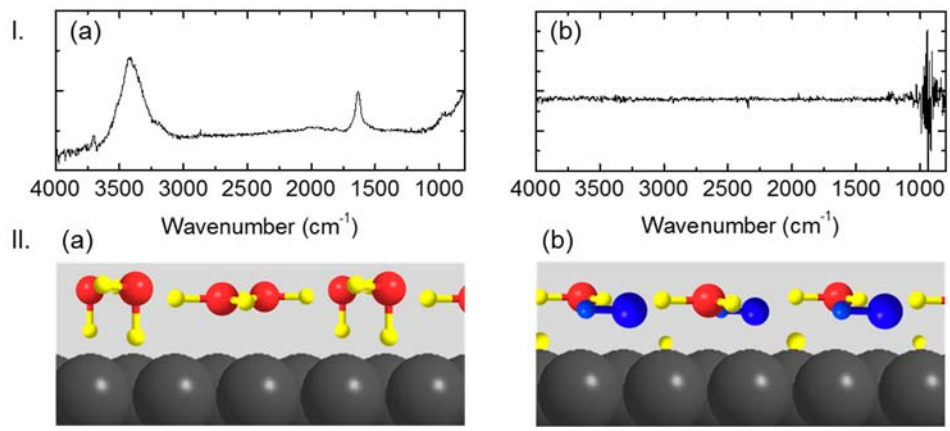

Figure 2-4. RAIRS spectra I and schematic structure II of particular water samples on Ru(0001). An intact water monolayer (a) composed of flat-lying and H-down molecules and half-dissociated (H + OH + H_2O) layer model (b) composed of flat-lying OH and H_2O molecules [16].

Recently, RAIRS has been applied for the identification of water clusters, monolayers, and multilayers on the metal surface [4, 17-22]. Moreover, RAIRS experiments of coadsorbates adsorbed with water show the interesting insights obtained from surface reactions [16, 23-27]. Vibrational frequencies and intensities can provide physical and chemical information about adsorbates and allow us to monitor the surface reactions of water and adsorbates. The information obtained by RAIRS will be more powerful when the local structure is supported by STM imaging or theoretical calculations.

2. Cs^+ Reactive Ion Scattering (RIS) and Low-Energy Sputtering (LES)

Control of the incident ion energy offers an attractive means to examine the dynamics of scattering. Depending on the kinetic energy, ion scattering methods are classified as

hyperthermal ion scattering (1–100 eV), low-energy ion scattering spectroscopy (LEIS, 500 eV–10 keV), medium-energy ion scattering (MEIS, 100–200 keV), or high-energy ion scattering (HEIS, 1–10 MeV). For hyperthermal energy (< 100 eV), penetration and implantation do not occur by ion impact, but the chemical bond of adsorbates on the surface can be broken during the collision process. This implies that hyperthermal energy scattering is the ideal surface-sensitive measurement to probe physical and chemical properties. Furthermore, hyperthermal scattering phenomena are quite different from those occurring at high energy (> 1 keV). The collision process for high energy is generally considered to comprise binary collisions (BCs) between a projectile and target atoms of the surface. On the other hand, a projectile ion in hyperthermal scattering moves very slowly, and surface atoms can respond collectively during the collision. This induces prominent multiple scattering events of hyperthermal energy from the surface. Recently, hyperthermal energy Cs^+ ion scattering has been developed by Kang and coworkers [28]. During the collision of Cs^+ with a surface at low energy, adsorbates (ions and molecules) are detached from the surface by reactive ion scattering (RIS) and associated low-energy sputtering (LES) processes. These processes have been examined for various surfaces [29-40]. The basic principle of these two processes will be presented below.

In the RIS process, a Cs^+ ion projectile picks up a neutral molecule (X) from the surface, leading to the formation of an ion complex (CsX^+), shown in Figure 2-5(a). The CsX^+ complex can be detected by quadrupole mass spectrometry (QMS) with the filament switched off and identified by the mass. A typical RIS experiment shows that all the surface molecules are scattered without fragmentation of the molecules. The peak intensity ratio for CsX^+/Cs^+ is typically of the order of 10^{-4} for chemisorbed molecules and 0.1–1 for physisorbed molecules.

The mechanism of the RIS process has been investigated by Kang and coworkers

using experiments and simulation [34, 41]. In early Cs^+-RIS experiments with chemisorbed species, the mechanism of RIS was proposed as a two-step one: collision-induced desorption (CID) of adsorbates and Cs^+ molecule association. However, the high RIS yield for physisorbed molecules cannot be explained by a two-step mechanism. On the basis of molecular dynamics simulations, the RIS process has proved to be a one-step abstraction mechanism: the Eley-Rideal (ER) mechanism. In this mechanism, the impinging Cs^+ ion bounces off the substrate surface, rather than colliding directly with the adsorbate, to lose a part of the initial kinetic energy to the surface. The outgoing Cs^+ induces desorption of the adsorbate by ion-dipole attraction, and a Cs^+-molecule cluster is formed. The velocity of the impinging Cs^+ should be slow enough to accommodate for the adsorbate's inertia, so that adsorbates of low mass can be efficiently abstracted The lower velocity of the outgoing trajectory enhances the RIS efficiency. Moreover, a heavier projectile can transfer more energy to the target surface. This is corroborated by experimental observations that Cs^+ is the most effective projectile in forming RIS products among various alkali metal ions [42].

The LES process simultaneously occurs with the RIS process when the Cs^+ projectile collides with the surface at low energy (< 100 eV). When Cs^+ ions collide with the surface at a low incident energy, its momentum can be transferred to the adsorbates, which are neutral molecules and positive (Y^+) and negative ions (Z^-). These species are ejected from the surface and detected by QMS with the ionizer filament switched off. Thus, LES signals reveal the identities of ionic species on the surface. As the kinetic energy of the colliding ion is sufficiently low, the secondary ion formation that occurs with > 1 keV ion-surface collision is suppressed. This indicates that the emitted ions are ions preexisting at the surface before the collision.

In summary, hyperthermal energy Cs^+ ion impact can be applied to surface analysis. Neutral molecules are detected by Cs^+-molecule clusters via RIS and preexisting ions are

sputtered by the LES process. Both are sensitive to the first monolayer of a surface because the low-energy ion impact ejects atoms and molecules exclusively from the top layer [31, 34, 43]. LES signals and RIS signals are simultaneously recorded in one spectrum. As the RIS signals appear at > 133 amu, which is the molar mass of Cs, LES and RIS signals are well distinguished in the spectrum. This can be a universal technique to resolve surface characteristics.

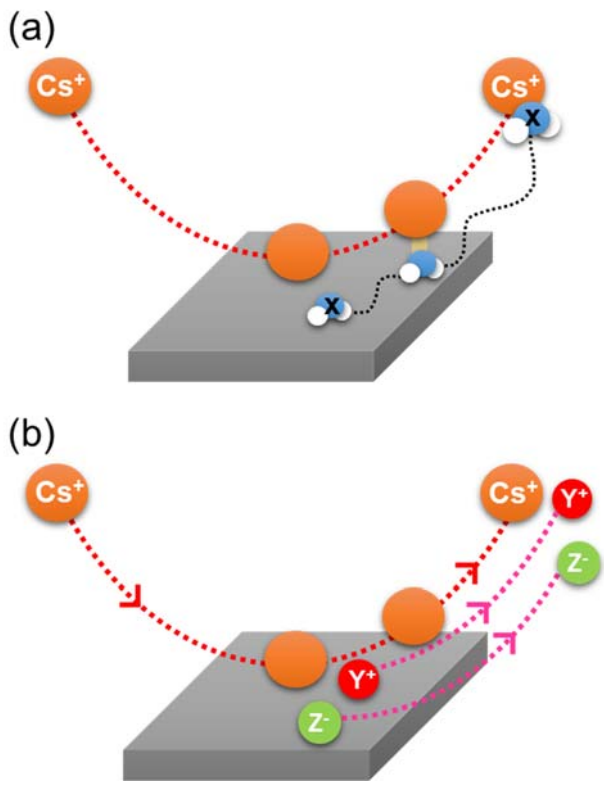

Figure 2-5. Schematic diagram of the Cs^+ RIS (a) and LES process (b). In the RIS process, the Cs^+ ion picks up the neutral molecules (X) adsorbed on the surface and ionic clusters (CsX^+) are formed. The positive (Y^+) and negative (Z^-) ions on the surface are detached on Cs^+ impact in the LES process. The ionic clusters (CsX^+) and sputtered ions (Y^+ and Z^-) are monitored by quadrupole mass spectrometry.

3. Kelvin Work Function Measurement

The Kelvin probe (KP) technique measures the contact potential difference (CPD) between the probe and the sample.

$$\text{CPD} = \Phi(probe) - \Phi(sample) \tag{2-7}$$

In principle, electrons in a lower work function metal can flow to a higher work function metal through a connecting wire between the two substrates. When the electronic states of two metals are balanced in this process, electron transfer stops, and the CPD is obtained at this state. In the Kelvin probe instrument, two metal substrates are electrically connected via an external backing potential V_b. The reference electrode in the Kelvin probe oscillates relative to the sample surface and changes proportionally with the capacitance. The CPD can be measured by the vanishing current when V_b is equal to – CPD. In detail, the current signal, $i = dQ/dt = \Delta V\,(dC/dt)$, of the KP instrument is dependent on the oscillation amplitude d_1, mean spacing d_0, and probe oscillation frequency ω. If the distance changes with a sinusoidal variation $d = d_0 + d_1 sin(\omega t + \varphi)$, according to the KP oscillation, the current is

$$i = -\varepsilon\varepsilon_0 \cdot A \cdot \Delta V \cdot \frac{d_1 \cos(\omega t + \varphi)}{[d_0 + d_1 \sin(\omega t + \varphi)]^2} \tag{2-8}$$

where A is the parallel plate capacitor of the area, φ is an arbitrary phase, and ΔV is the sum of V_b and CPD. This indicates that the current and its amplitude are proportional to ΔV. The current is zero when $\Delta V = 0$, which is V_b = – CPD. Therefore, CPD can be measured from the current signal.

The application of the Kelvin work function technique for studying condensed molecular films and their dielectric response has been reported previously [44, 45]. The technique can be applied to measure the voltage induced by charge separation, as well [46].

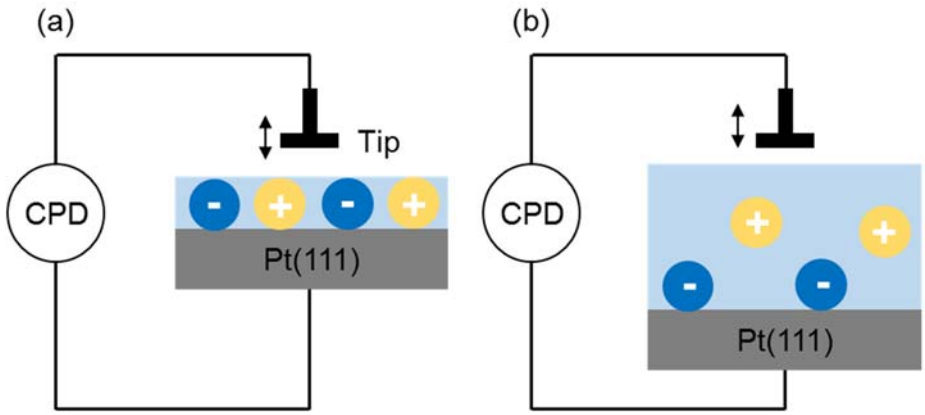

Figure 2-6. Schematic of the Kelvin probe experiment to measure the voltage from charge separation. (a) Positive and negative ions exist in the same plane. (b) Positive ion migrates along the overlayer.

A simple example is shown schematically in Figure 2-6. Figure 2-6(a) shows the positive charges and negative charges adsorbed on the metal surface. If the positive charge migrates along the H-bonding of water overlayers shown in Figure 2-6(b), a positive voltage can develop between these two separate charges. The difference in the CPD before and after the adsorption of the water overlayer can be measured and defined as $V_{migration}$.

$$\Delta\text{CPD} = -\left[V(film)_{final} - V(film)_{initial}\right] = V_{migration} \quad (2\text{-}9)$$

$V_{migration}$ can be expressed by a parallel-plate simple capacitor model [47].

$$\Delta\text{CPD} = V_{migration} = \left(\frac{\sigma}{\epsilon_r \epsilon_0}\right) d \quad (2\text{-}10)$$

Here σ is the density of positive or negative ions per unit surface area, which is determined by the amount of HCl coverage, d is the distance between two sheets of oppositely charged ions, ε_r is the relative dielectric constant of the medium, and ε_0 is the vacuum permittivity. Since ions are distributed over a certain depth, the vertical distance of charge separation

can be defined as

$$d = \langle d_{q+} \rangle - \langle d_{q-} \rangle \quad (2\text{-}11)$$

where $\langle d_{q+} \rangle$ and $\langle d_{q-} \rangle$ are average vertical distances of positive and negative charges from the metal surface, respectively. Therefore, the experimental method using the KP instrument is expected to estimate the distance of charge separation.

4. Instruments

The experiments were carried out in an UHV chamber equipped with instrumentation for Cs^+ reactive ion scattering, low-energy sputtering, reflection-absorption infrared spectroscopy, Kelvin work function measurements, and temperature-programmed desorption measurements (Figure 2-7). The chamber was deliberately designed to have a small internal volume to allow fast pump-downs. The base pressure of the UHV chamber was maintained below 3×10^{-10} Torr by a turbomolecular pump (TMP, Leybold, model Turbovac 361; 360 L s^{-1}) and rotary vane pump (Edwards, model E2M18). The pressure of the chamber was monitored by an ion gauge (Granville–Phillips).

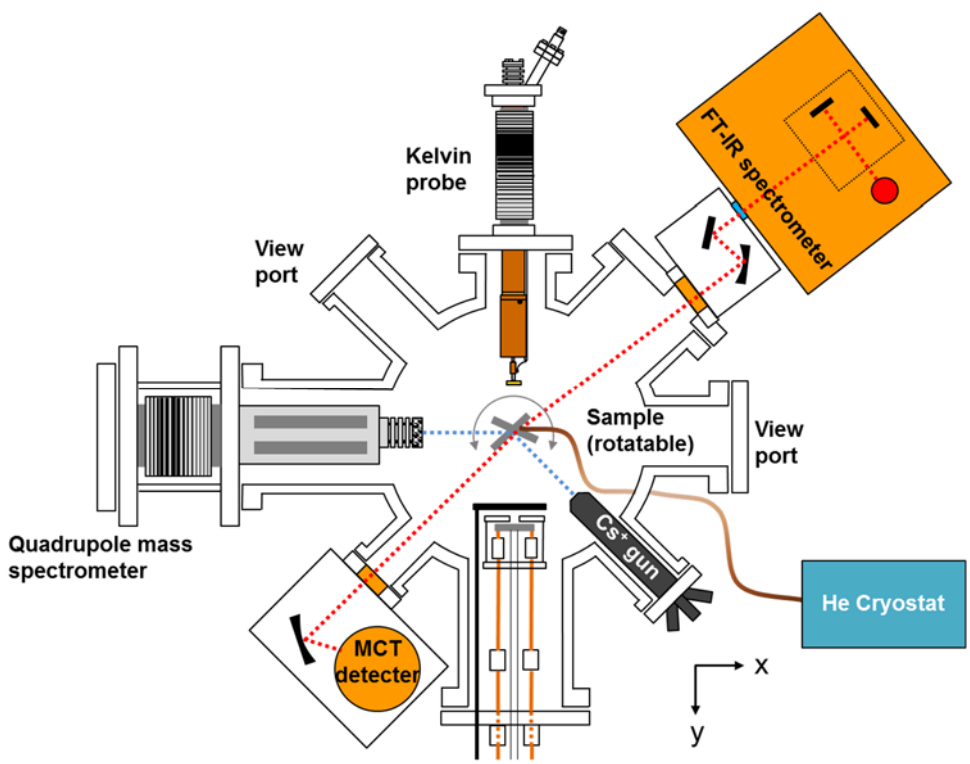

Figure 2-7. Schematic diagram of the apparatus for Cs^+ RIS, LES, RAIRS, and Kelvin work function measurements, consisting of an UHV chamber.

The substrate was a single-crystal disk-shaped Pt(111) surface with one polished side (9 mm in diameter and 1.3 mm in thickness). The sample was mounted on a Cu block holder using Ta wires (0.5 mm). The sample manipulator provided accommodation for a sample stage in xyz direction and a single-axis 360º rotational stage. The manipulator allows the sample to be precisely located for each analysis position. The sample temperature was varied by resistive heating and liquid nitrogen cooling. Resistive heating was performed by passing an electric current through a heating filament. The current through the filaments was provided by a DC power supply (Kepco, model ATE36-30M19). The current to control the temperature was applied by a programmable temperature controller (Eurotherm, model 2404) based on proportional-integral-derivative (PID) logic so that the temperature could be maintained at a constant value or changed at a constant rate. An in-house-prepared dewar in thermal contact with the sample holder stored LN_2, and the lowest temperature achieved was 83 K. The temperature controller provided the current temperature in real time through an N-type thermocouple attached to the sample. The sample temperature was maintained in the range of 83–1300 K. The sample surface was cleaned by Ar^+ sputtering, heated to 800 K in an O_2 environment, and flashed to 1200 K, allowing the measurement of a clean surface. The sample quality was confirmed by RIS and TPD.

Surface analysis of the hyperthermal ion scattering, RIS, and LES, was performed by a low-energy Cs^+ ion gun and a quadrupole mass spectrometer (QMS, manufactured by Extrel). The Cs^+ ion gun (Kimball Physics) with a surface ionization source produces Cs^+ beam with an energy of 1–100 eV. The Cs^+ beam flux was maintained below 1 nA cm^{-1} to avoid Cs^+ charging on the surface and damage by ion impact. The products of RIS and LES were analyzed by a QMS with its ionizer filament switched off, in which the masses of neutral and ionic constituents (X and Y^+) on the surface were identified. The angle between

the QMS and the ion gun was fixed at 135º, and the QMS was movable along the *x*-axis using a linear translator.

The chamber was equipped with a commercial FTIR spectrometer (Perkin-Elmer Spectrum 100) for RAIRS studies. The infrared beam exiting the interferometer was directed to an external port of the FTIR instrument and focused onto the metal substrate inside the UHV chamber through the optical mirror and ZnSe window. The reflected beam on the metal surface was detected by a mercury–cadmium–telluride (MCT) detector, installed on the other side of UHV chamber to the FTIR instrument. The RAIRS experiments employed a grazing reflection geometry at an angle of 84º. The detailed beam path is shown in the Figure 2-7 by a dashed line.

For work function measurements, a Kelvin probe (McAllister Technical Services KP6500) was mounted to the chamber with a linear translator that moves along the *y*-axis. A Na-atom dispenser (homebuilt) was used to control the work function of Pt(111). A DC power supply was used to heat the dispenser, and the temperature of the source was monitored by a thermocouple spot-welded to the dispenser.

References

1. Chabal, Y. J. Surface Infrared-Spectroscopy. *Surf. Sci. Rep.* **1988**, *8*, 211-357.
2. Trenary, M. Reflection absorption infrared spectroscopy and the structure of molecular adsorbates on metal surfaces. *Annu. Rev. Phys. Chem.* **2000**, *51*, 381-403.
3. Nakamura, M.; Shingaya, Y.; Ito, M. The vibrational spectra of water cluster molecules on Pt(111) surface at 20 K. *Chem. Phys. Lett.* **1999**, *309*, 123-128.
4. Nakamura, M.; Ito, M. Monomer and Tetramer Water Clusters Adsorbed on Ru(0001). *Chem. Phys. Lett.* **2000**, *325*, 293-298.
5. Nakamura, M.; Ito, M. Ring hexamer like cluster molecules of water formed on a Ni(111) surface. *Chem. Phys. Lett.* **2004**, *384*, 256-261.
6. Sumiyoshi, S.; Kobayashi, Y.; Souda, K.; Takehara, Y.; Nakamura, H. Hepatobiliary and pancreatic: Insulinoma metastases with focal hepatic steatosis. *J. Gastroenterol. Hepatol.* **2005**, *20*, 650-650.
7. Slater, D. A.; Hollins, P.; Chesters, M. A.; Pritchard, J.; Martin, D. H.; Surman, M.; Shaw, D. A.; Munro, I. H. Reflection Absorption Infrared-Spectroscopy at the Daresbury Srs. *Rev. Sci. Instrum.* **1992**, *63*, 1547-1550.
8. Yamamoto, K.; Masui, A.; Ishida, H. Kramers-Kronig Analysis of Infrared Reflection Spectra with Perpendicular Polarization. *Appl. Opt.* **1994**, *33*, 6285-6293.
9. Mcintyre, J. D.; Aspnes, D. E. Differential Reflection Spectroscopy of Very Thin Surface Films. *Surf. Sci.* **1971**, *24*, 417-434.
10. Mate, B.; Medialdea, A.; Moreno, M. A.; Escribano, R.; Herrero, V. J.

Experimental studies of amorphous and polycrystalline ice films using FT-RAIRS. *J. Phys. Chem. B* **2003**, *107*, 11098-11108.

11. Gozhenko, V. V.; Pinchuk, A. O. On the choice of the phase constant of the Fresnel transmission coefficient of a slab. *J. Opt.* **2012**, *14*, 035705.
12. Cholette, F.; Zubkov, T.; Smith, R. S.; Dohnalek, Z.; Kay, B. D.; Ayotte, P. Infrared Spectroscopy and Optical Constants of Porous Amorphous Solid Water. *J. Phys. Chem. B* **2009**, *113*, 4131-4140.
13. A.M. Bradshaw, E. S. Infrared Reflection-Absorption Spectroscopy of Adsorbed Molecules. In *Spectroscopy of Surfaces*; R.J.H. Clark, R. E. H., John Wiley & Sons, Ed., 1988; pp 413–483.
14. Bhargava, R.; Fernandez, D. C.; Schaeberle, M. D.; Levin, I. W. Theory and application of gain ranging to Fourier transform infrared spectroscopic Imaging. *Appl. Spectrosc.* **2001**, *55*, 1580-1589.
15. Pearce, H. A.; Sheppard, N. Possible Importance of a Metal-Surface Selection Rule in Interpretation of Infrared-Spectra of Molecules Adsorbed on Particulate Metals - Infrared-Spectra from Ethylene Chemisorbed on Silica-Supported Metal-Catalysts. *Surf. Sci.* **1976**, *59*, 205-217.
16. Kim, Y.; Shin, S.; Moon, E. S.; Kang, H. Spectroscopic Monitoring of the Acidity of Water Films on Ru(0001): Orientation-Specific Acidity of Adsorbed Water. *Chem. Euro. J.* **2014**, *20*, 3376-3383.
17. Haq, S.; Harnett, J.; Hodgson, A. Growth of thin crystalline ice films on Pt(111). *Surf. Sci.* **2002**, *505*, 171-182.
18. Clay, C.; Haq, S.; Hodgson, A. Hydrogen bonding in mixed OH+H2O overlayers on Pt(111). *Phys. Rev. Lett.* **2004**, *92*, 046102.
19. Beniya, A.; Yamamoto, S.; Mukai, K.; Yamashita, Y.; Yoshinobu, J. The first layer

of water on Rh(111): Microscopic structure and desorption kinetics. *J. Chem. Phys.* **2006**, *125*, 054717.

20. Feibelman, P. J.; Kimmel, G. A.; Smith, R. S.; Petrik, N. G.; Zubkov, T.; Kay, B. D. A unique vibrational signature of rotated water monolayers on Pt(111): Predicted and observed. *J. Chem. Phys.* **2011**, *134*, 8.
21. Ito, M. Structures of water at electrified interfaces: Microscopic understanding of electrode potential in electric double layers on electrode surfaces. *Surf. Sci. Rep.* **2008**, *63*, 329-389.
22. Denzler, D. N.; Hess, C.; Dudek, R.; Wagner, S.; Frischkorn, C.; Wolf, M.; Ertl, G. Interfacial structure of water on Ru(001) investigated by vibrational spectroscopy. *Chem. Phys. Lett.* **2003**, *376*, 618-624.
23. Ogasawara, H.; Horimoto, N.; Kawai, M. Ammonia adsorption by hydrogen bond on ice and its solvation. *J. Chem. Phys.* **2000**, *112*, 8229-8232.
24. Takaoka, T.; Inamura, M.; Yanagimachi, S.; Kusunoki, I.; Komeda, T. Ammonia adsorption on and diffusion into thin ice films grown on Pt(111). *J. Chem. Phys.* **2004**, *121*, 4331-4338.
25. Kim, Y.; Moon, E. S.; Shin, S.; Kang, H. Acidic Water Monolayer on Ruthenium(0001). *Angew. Chem. Int. Ed.* **2012**, *51*, 12806-12809.
26. Kim, Y.; Shin, S.; Kang, H. Zundel-like and Eigen-like Hydrated Protons on a Platinum Surface. *Angew. Chem. Int. Ed.* **2015**, *54*, 7626-7630.
27. Lechner, B. A. J.; Kim, Y.; Feibelman, P. J.; Henkelman, G.; Kang, H.; Salmeron, M. Solvation and Reaction of Ammonia in Molecularly Thin Water Films. *J. Phys. Chem. C* **2015**, *119*, 23052-23058.
28. Lee, C. W.; Lee, P. R.; Lahaye, R. J. W. E.; Kang, H. Effect of adsorbate mass on an Eley-Rideal reaction. Reactive scattering of Cs^+ from noble gases and N-2

adsorbed on Ru(0001) surfaces at hyperthermal energy. *Phys. Chem. Chem. Phys.* **2009**, *11*, 2268-2271.

29. Park, S. C.; Maeng, K. W.; Pradeep, T.; Kang, H. Reactive ion scattering from pure and mixed HCl, NH_3 and D_2O surfaces. *Nucl. Instr. Meth. Phys. Res.* **2001**, *182*, 193-199.

30. Park, S. C.; Maeng, K. W.; Pradeep, T.; Kang, H. Unique chemistry at ice surfaces: Incomplete proton transfer in the H_3O^+-NH_3 system. *Angew. Chem. Int. Ed.* **2001**, *40*, 1497-1500.

31. Hahn, J. R.; Lee, C. W.; Han, S. J.; Lahaye, R. J. W. E.; Kang, H. Low-energy Cs^+ scattering from water on Pt(111): A kinetic energy analysis of the Cs+ - Water clusters. *J. Phys. Chem. A* **2002**, *106*, 9827-9831.

32. Park, S. C.; Maeng, K. W.; Kang, H. Organic chemistry on cold molecular films: Kinetic stabilization of S(N)1 and S(N)2 intermediates in the reactions of ethanol and 2-methylpropan-2-ol with hydrogen bromide. *Chem. Euro. J.* **2003**, *9*, 1706-1713.

33. Jung, K. H.; Park, S. C.; Kim, J. H.; Kang, H. Vertical diffusion of water molecules near the surface of ice. *J. Chem. Phys.* **2004**, *121*, 2758-2764.

34. Lahaye, R. J. W. E.; Kang, H. Reactive rideal ion surface scattering as an Eley-Rideal process: A molecular dynamics study into the abstraction reaction mechanism by low energy Cs+ from Pt(111). *ChemPhysChem* **2004**, *5*, 697-705.

35. Kang, H. Chemistry of ice surfaces. Elementary reaction steps on ice studied by reactive ion scattering. *Acc. Chem. Res.* **2005**, *38*, 893-900.

36. Kim, J. H.; Kim, Y. K.; Kang, H. Interaction of NaF, NaCl, and NaBr with amorphous ice films. Salt dissolution and ion separation at the ice surface. *J. Phys. Chem. C* **2007**, *111*, 8030-8036.

37. Moon, E. S.; Lee, C. W.; Kim, J. K.; Park, S. C.; Kang, H. UV-induced protonation of molecules adsorbed on ice surfaces at low temperature. *J. Chem. Phys.* **2008**, *128*, 191101

38. Lee, C. W.; Kim, J. K.; Moon, E. S.; Minh, Y. C.; Kang, H. Formation of Glycine on Ultraviolet-Irradiated Interstellar Ice-Analog Films and Implications for Interstellar Amino Acids. *Astrophys. J.* **2009**, *697*, 428-435.

39. Kang, H. Reactive Ion Scattering of Low Energy Cs^+ from Surfaces. A Technique for Surface Molecular Analysis. *Bull. Korean Chem. Soc.* **2011**, *32*, 389-398.

40. Moon, E.-s.; Kim, Y.; Shin, S.; Kang, H. Asymmetric Transport Efficiencies of Positive and Negative Ion Defects in Amorphous Ice. *Phys. Rev. Lett.* **2012**, *108*, 226103.

41. Lahaye, R. J. W. E.; Kang, H. Reactive ion scattering study of physisorbed adsorbates: experiment and theory. *Curr. Appl. Phys.* **2003**, *3*, 25-29.

42. Yang, M. C.; Lee, H. W.; Kang, H. Secondary-Ion Mass-Spectrometry without Secondary-Ion Emission - Recombinative Scattering of Hyperthermal Cs^+ Ions from a Si(111) Surface-Adsorbed with Water. *J. Chem. Phys.* **1995**, *103*, 5149-5152.

43. Rabalais, J. W. Principles and Applications of Ion Scattering Spectrometry. Wiley-Interscience: New Jersey, 2003.

44. Wu, K.; Iedema, M. J.; Cowin, J. P. Ion penetration of the water-oil interface. *Science* **1999**, *286*, 2482-2485.

45. Horowitz, Y.; Asscher, M. Low energy charged particles interacting with amorphous solid water layers. *J. Chem. Phys.* **2012**, *136*.

46. Lee, D. H.; Bang, J.; Kang, H. Surface Charge Layer of Amorphous Solid Water with Adsorbed Acid or Base: Asymmetric Depth Distributions of H^+ and OH^- Ions. *J. Phys. Chem. C* **2016**, *120*, 12051-12058.

47. Tsekouras, A. A.; Iedema, M. J.; Cowin, J. P. Amorphous water-ice relaxations measured with soft-landed ions. *Phys. Rev. Lett.* **1998**, *80*, 5798-5801.

Chapter III

Stabilization of Hydrated Protons on Platinum Surface

Abstract

The nature of hydrated protons at an electrolyte/electrode interface are intimately related to fundamental understanding of electrochemical processes in the acidic environment. Proton transfer between an electrode and solvated protons is a key process in hydrogen evolution reaction, which is one of the most extensively studied electrode reactions. Stability of hydrated protons on the electrode surface remains a central issue in this reaction, which is deeply related to the nature of the ionization of H atom and its reverse neutralization process. In this study, a variety of surface spectroscopic tools was used to examine the coadsorption process of atomic hydrogen in water layer in ultra-high vacuum (UHV) condition. Spectroscopic evidences obtained by mass spectrometry and reflection-absorption infrared spectroscopy (RAIRS) consistently shows that adsorbed hydrogen can first ionize into metal-bound (MB) hydrated proton species ($H_5O_2^+$, $H_7O_3^+$, and $H_9O_4^+$), rather than H_3O^+ on the Pt surface. Then, the surface hydrated protons evolve into to a fully hydrated proton structure via proton transfer along additional water overlayer. The stability

of hydrated protons on Pt surface and their bulk dissolution behavior suggest the possibility that surface hydrated protons are a key intermediate in electrochemical interconversion between adsorbed H atoms and H^+(aq) in water electrolysis and hydrogen evolution reactions.

1. Introduction

Hydrogen evolution reaction (HER) is one of the most studied electrochemical reactions related to the electrolysis of water and the standard hydrogen electrode. A key electrochemical step of HER in acidic solution is the conversion between H^+ ion in solution and atomic hydrogen adsorbed on the electrode surface in so-called Volmer reaction Equation (3-1).

$$H_{ad} + H_2O \leftrightarrow H_3O^+ + e^-_{metal} \quad (3\text{-}1)$$

Despite extensive studies, the charge transfer mechanism of this reaction is not well understood. It is disputable whether the ionization of H atom and reverse process of H_3O^+ neutralization occur right on the electrode surface or through electron tunneling in solution phase [1, 2]. A central question to this issue is the stability of hydrated protons adsorbed on the electrode surface. Yet, the nature of hydrated protons at an electrode/electrolyte interface has remained veiled mainly because of experimental difficulties in clearly identifying hydrated proton structures at the buried interface with currently available spectroscopic techniques.

The hydrated protons on metal surfaces have been explored by using surface science approach in UHV condition by preparing simplified model systems of electrode/electrolyte interfaces [2-13]. Using high-resolution electron energy loss spectroscopy (HREELS), Wagner and coworkers [2, 5, 6] reported that coadsorption of hydrogen and water on a Pt(111) surface and heating the surface at 150 K produced adsorbate species with a vibrational band at ~1150 cm^{-1}, and interpreted it as a signature of hydronium (H_3O^+) ions. Subsequently, the same feature was also observed on a Pt(100) surface [7], and by reflection–absorption infrared spectroscopy (RAIRS) as well [9]. Theoretical calculations of gas-phase protonated water clusters suggested that the ~1150

cm^{-1} feature is more likely due to protonated water clusters rather than hydronium ions [8]. Protonated water clusters have been suggested as an intermediate for the hydrogen/deuterium (H/D) exchange between coadsorbed water and hydrogen on Au(111) [13]. On the other hand, there is continuing doubt regarding the existence of hydrated protons on a Pt surface. Furthermore, many features of hydrated protons still remain veiled, such as their molecular structure and conversion to bulk hydrated forms, as well as possible link with HER mechanism in an electrochemical environment. The present paper addresses these questions by conducting experiments to prepare surface hydrated protons under various conditions and characterize them with spectroscopic methods.

2. Experimental Section

The experiment was carried out in a UHV surface analysis chamber [14, 15] equipped with instrumentation for Cs^+ reactive ion scattering (RIS), low energy sputtering (LES), temperature-programmed desorption (TPD), reflection-absorption infrared spectroscopy (RAIRS), and surface work function measurement described in section II. The analyzed samples were prepared on a clean Pt(111) single-crystal surface by dosing various gases through variable leak valves with or without a tube doser. Atomic H (D) coverage of 0.7–0.8 monolayer equivalent (MLE) was adsorbed on a Pt(111) substrate surface at a temperature of 80–90 K by dosing H_2 (D_2) gas through a tube doser. A saturation coverage of hydrogen yields an atomic H_{ad}:Pt ratio of 1:1, which is defined as 1 MLE = 1.5×10^{15} atoms cm^{-2} equivalent to the metal atom density on Pt(111) [16, 17]. After hydrogen adsorption on Pt(111), water was adsorbed below 90 K by back-filling the chamber with H_2O vapor at a partial pressure of 1×10^{-8} Torr. The coverage of H_2O was estimated from TPD measurements [18, 19] and reported in units of water monolayer on Pt(111) (i.e., 1 ML = 1.2×10^{15} molecules cm^{-2}). Na atoms were deposited onto the surface by using a

commercial alkali metal dispenser (SAES Getters). A full monolayer coverage of Na on Pt(111) corresponds to 0.59 MLE according to LEED measurement [20]. The surface coverage (θ) of Na was estimated by TPD experiment [20, 21]. The work function change ($\Delta\Phi$) of surface associated with Na adsorption was measured with a Kelvin work function probe [22]. A $\Delta\Phi$-θ(Na) calibration curve was established through these measurements, and $\Delta\Phi$ and θ(Na) will often be used interconvertible in this paper.

LES and RIS methods were used for analyzing chemical species on the sample surface [14, 15]. In these experiments, a Cs^+ beam from low-energy ion gun (Kimball Physics) collides with the surface at a low incident energy (28 eV, unless mentioned otherwise), and the scattered ions are detected by a quadrupole mass spectrometer (Extrel) with its ionizer filament switched off. The Cs^+ impact at this energy do not cause secondary ionization of water molecules. The probing depth is estimated to be 1 ML. In RIS, neutral species (X) on the surface are picked up by the scattering Cs^+ projectiles to form Cs^+-neutral clusters (CsX^+). In LES, preexisting ionic species (Y^+) on the surface are ejected by the Cs^+ impact. Thus, RIS and LES signals reveal the identities of neutral (X) and ionic species (Y^+), respectively, on the surface [14, 15].

RAIRS experiment was performed in a grazing angle (84˚) reflection geometry and at a spectral resolution of 4 cm^{-1} in the range of 800–4000 cm^{-1} using a commercial FTIR instrument (PerkinElmer, Spectrum 100) equipped with a mercury-cadmium telluride detector. The incident IR beam was linearly p-polarized using a wire grid polarizer (Edmund optics).

A Kelvin probe monitored the work function change of a sample by measuring contact potential difference (CPD) between the Au-coated metal probe and the sample, *i.e.*, CPD = Φ(probe) – Φ(sample). The change in CPD (ΔCPD) before and after heating to react hydrogen and water gives information about the voltage developed by production of

hydrated protons. This ΔCPD value represented the amount of surface hydrated protons as a function of $\Delta\Phi$ by Na adsorption.

3. Results and Discussion

3.1. Spectroscopic Evidence of Hydrated Protons on Pt(111)

Surface species formed by coadsorption of hydrogen and water on a Pt surface were examined using low-energy sputtering (LES) and reactive ion scattering (RIS). The sample was prepared with H atoms of 0.8 MLE coverage introduced by H_2 gas exposure and then adsorbed H_2O molecules of 1.1 ML coverage at < 90 K. Figure 3-1(a) shows the mass spectrum of LES and RIS signals measured on the surface. An RIS signal of $Cs(H_2O)^+$ appears at *m/z* = 151 owing to the pickup of water molecules by a Cs^+ projectile. No LES signal was detected from this surface. A small peak at *m/z* = 39 is the scattering signal of impurity K^+ ions contained in the Cs^+ beam.

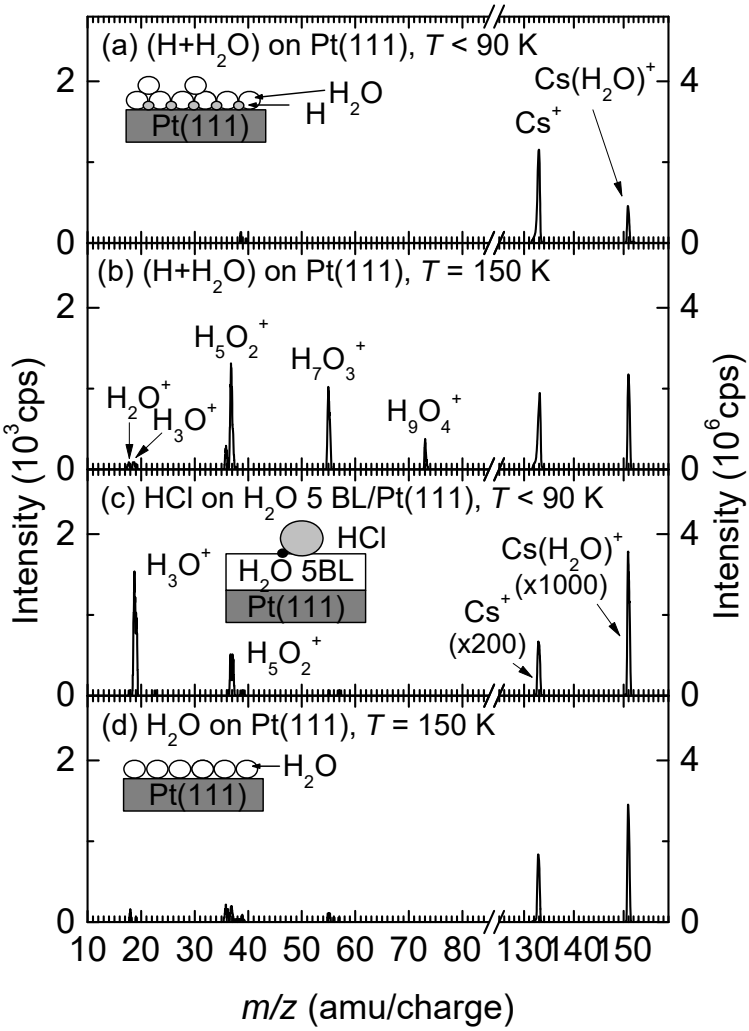

Figure 3-1. Positive-ion LES signals (shown for $m/z \leq 85$) and RIS signals ($m/z \geq 125$) obtained from various samples. (a) H_2O (1.1 ML) was adsorbed onto preadsorbed H (0.8 MLE) Pt(111) at < 90 K. (b) The sample prepared in (a) was heated at 140 K for 100 s and at 150 K for a few seconds. (c) HCl was exposed onto H_2O 5 BL below 90 K. (d) H_2O (1.2 ML) was adsorbed on a bare Pt(111) surface (without preadsorption of H atoms), and heated in the same way as for spectrum (b). All spectra were obtained below 90 K. The Cs^+ beam energy was 28 eV.

When the H and H_2O coadsorbed surface was heated at 150 K, LES signals appeared at m/z = 37 ($H_5O_2^+$) and 55 ($H_7O_3^+$), along with a small intensity peak at m/z = 73 ($H_9O_4^+$) as shown in Figure 3-1(b). These signals indicate that hydrated protons are produced on the surface, and they exist in multiply hydrated structures [$H^+(H_2O)_2$, $H^+(H_2O)_3$ and $H^+(H_2O)_4$]. Interestingly, H_3O^+ (m/z = 19) signal was absent from the surface or very weak compared to the signals of multiply hydrated protons. Moreover, small LES signals are seen at m/z = 18 and 36, corresponding to H_2O^+ and $H_4O_2^+$. H_2O^+ intensity is even similar to H_3O^+, which is very unusual for ionization of condensed water.

Figure 3-1(c) shows that hydrated protons generated by HCl ionization on amorphous solid water layer are hydronium ions in the majority population, and monohydrate hydronium ions. The nearly absent H_3O^+ signal in Figure 3-1(b) indicates the hydrated protons have a quite different nature compared to those generated by acid ionization on water films. The strong intensities of $H_5O_2^+$ and $H_7O_3^+$ signals suggest that planar hydration structures are preferred in water monolayer which has two-dimensional H-bonded network structure on the Pt surface. On the other hand, the hydration of proton formed by HCl ionization on an ASW surface occurs in three-dimensional water structure, and it may be affected by the presence of Cl^- ions. Under these conditions, LES measurements have been reported to exhibit preferential H_3O^+ emission over the ejection of larger clusters [23].

The weak signals in the spectrum corresponding to H_2O^+, H_3O^+, and $H_4O_2^+$ may be produced by fragmentation of larger protonated water clusters such as $H_5O_2^+$ and $H_7O_3^+$ during the Cs^+ impact, rather than by the presence of H_2O^+, H_3O^+ and $H_4O_2^+$ species on the surface. It is unlikely that H_2O^+ exists on the metal surface because the ionization energy of H_2O is too high (12.6 eV) to occur on a Pt surface. The unimolecular dissociation reaction in the gas phase may take place from energized hydrated proton species via such

reactions.

$$(H_5O_2^+)^* \rightarrow (H_3O^+)^* + H_2O \rightarrow H_2O^+ + H + H_2O \quad (3\text{-}2)$$

$$(H_7O_3^+)^* \rightarrow (H_5O_2^+)^* + H_2O \rightarrow H_4O_2^+ + H + H_2O \quad (3\text{-}3)$$

Here, $(H_7O_3^+)^*$, $(H_5O_2^+)^*$ and $(H_3O^+)^*$ denote the energized species in the gas phase. The intensities of H_3O^+ and H_2O^+ signals produced by Equation (3-2) will depend on the lifetime of $(H_3O^+)^*$ insi de the mass spectrometer. An $H_4O_2^+$ peak generated by Equation (3-3) exists in higher abundance than H_3O^+ and H_2O^+ because large parent ion, $H_7O_3^+$, is easier to decompose than smaller one.

The control experiments were performed to examine if hydrated proton species were formed when only H_2O was present on a Pt(111) surface without preadsorbed H atoms. Figure 3-1(d) shows a spectrum from a H_2O monolayer surface on Pt(111) heated at 150 K. $H_5O_2^+$ and $H_7O_3^+$ signals appeared, but with very small intensities compared to those on the H + H_2O coadsorbed Pt surface. Because a small amount of H impurity may exist on the Pt surface with H_2O adsorbate, it is unclear whether these ions were formed solely from H_2O monolayer or not. When H was adsorbed for a coverage of < 0.1 ML on Pt, LES spectrum showed the same impurity signals. Therefore, the comparative experiments clearly show that the formation of multiply hydrated protons was facilitated when both H atoms and water molecules are present.

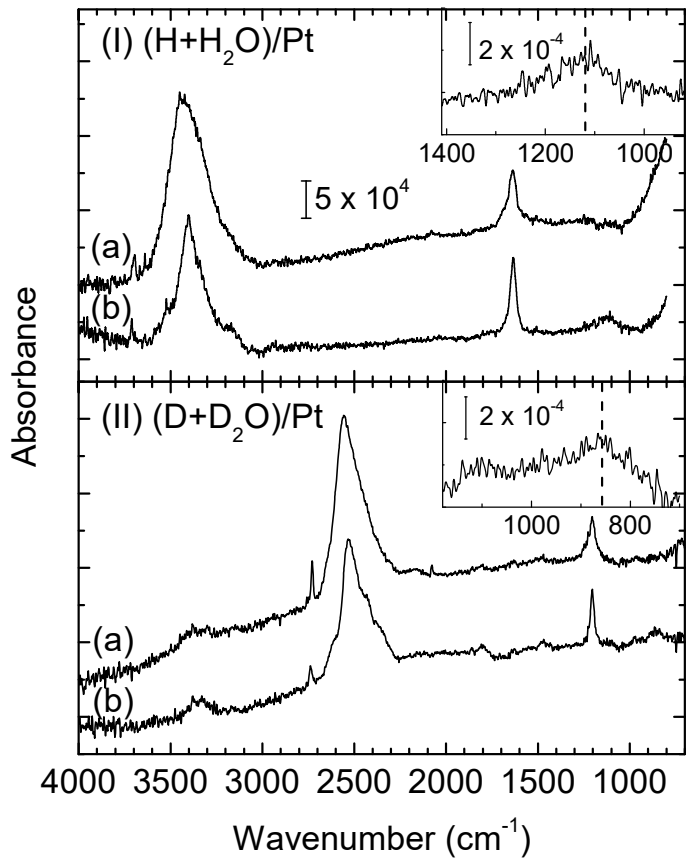

Figure 3-2. RAIR spectra of (I) H + H_2O and (II) D + D_2O layers on Pt(111). (a) Hydrogen/Deuterium (0.75 MLE) and H_2O/D_2O (1.2 ML) was coadsorbed at 90 K, respectively. (b) The sample prepared in (a) was heated at 140 K for 100 s and heated at 150 K for a few seconds. Each inset shows hydrated proton/deuteron band in the spectrum (b), respectively.

Figure 3-2 shows RAIR spectra of Pt(111) substrate where H/D atoms were adsorbed for 0.75 MLE coverage, and then H_2O/D_2O monolayers were adsorbed, respectively. Spectrum (a) was measured after sample preparation at 90 K, and it shows

bands at 3700 cm^{-1}/2730 cm^{-1} (free O-H/O-D stretching), 3400 cm^{-1}/2550 cm^{-1} (hydrogen-bonded O-H/O-D stretching), 1640 cm^{-1}/1200 cm^{-1} (scissoring), and 900 cm^{-1}/750 cm^{-1} (librational mode; not well resolved of the H_2O band and the D_2O band in the cut-off region). After heating the sample at 150 K, a new band appears at ~ 1130 cm^{-1} in Spectrum I-(b). This isotope band at 850 cm^{-1} in Spectrum II-(b) are also observed in D + D_2O sample. These bands do not appear when only pure water monolayer was adsorbed on Pt(111). In a close match with the HREELS and RAIRS features reported in previous studies, a vibrational band at ~1150 cm^{-1}/~850 cm^{-1} was assigned as symmetric bending mode of "hydronium" ions on the Pt surface by the charge-transfer reaction, $H_{ads} + H_2O_{ads} \rightarrow H_3O^+_{ads} + e^-_{ads}$ [5, 6, 9]. Accordingly, the bands at ~1130 cm^{-1} and ~850 cm are in agreement with the ionized hydrogen and deuterium assigned in previous HREELS and RAIRS results. However, the observation shown in Figure 3-1 confirms that they exist mostly as multiply hydrated protons, which are $H_5O_2^+$, $H_7O_3^+$ and $H_9O_4^+$, rather than H_3O^+.

3.2. Structure of Hydrated Protons Bounded on Pt

According to theoretical studies [24], the most prevalent structure of hydrated protons in bulk liquid water is a triply coordinated hydronium ion, $H_3O^+(H_2O)_3$, often called an Eigen cation. In the case of water monolayer, two-dimensional hydrogen bonding network hinders the formation of $H_3O(H_2O)_3^+$ as bulk state or restrains the geometry which cannot be adapted in monolayer. This might lead to the formation of metal bound (MB)-$H_7O_3^+$ and $H_9O_4^+$ formed in monolayer being regarded as two-dimensional Eigen structure. Recently these MB-$H_7O_3^+$ and MB-$H_9O_4^+$ structures were also obtained using the DFT calculation [25]. $H_7O_3^+$ and $H_9O_4^+$ signals in Figure 3-1 can be attributed that both MB-$H_9O_4^+$ and MB-$H_7O_3^+$ structures may coexist in the monolayer as a result of their rapid interconversion via proton transfer. It is well known that proton hopping along the hydrogen-bonded water

chain has a very small energy barrier [26, 27]. The LES signal of $H_5O_2^+$ appearing on the surface with small water coverage (not shown) may be produced from isolated $H_5O_2^+$ units on the surface. At high coverage of water, $H_5O_2^+$ signal may arise from collision-induced dehydration of larger protonated clusters on the surface during Cs^+ impact. The observed LES intensity distribution, $H_5O_2^+ > H_7O_3^+ > H_9O_4^+$, may reflect the tendency that sputtering efficiency of adsorbates decreases with increasing molecular weight as well as their surface populations.

3.3. Amount of Hydrated Protons Formed on Pt

To estimate the portion of surface hydrogen atoms converted into hydrated proton species, D atoms were coadsorbed with H_2O on Pt(111). H/D ratio was observed in both LES and RIS spectrum. Figure 3-3(a) shows a LES and RIS spectrum of this sample. The spectrum shows only a $Cs(H_2O)^+$ signal with absent LES ions, which shows that only H_2O are present on the surface and hydrated proton species do not form. When the sample was heated at 150 K in Figure 3-3(b), a $Cs(HDO)^+$ signal newly appeared with 20 % intensity of a $Cs(H_2O)^+$ signal, indicating the occurrence of the H/D exchange reaction of water molecules. LES spectrum shows $H_5O_2^+$ and $H_7O_3^+$ signals along with their D-substituted isotopologues. The intensity ratio for $H_5O_2^+$: $H_4DO_2^+$: $H_3D_2O_2^+$ is 0.60 : 0.29 : 0.11, and the $H_7O_3^+$: $H_6DO_3^+$: $H_5D_2O_3^+$ ratio is 0.58 : 0.25 : 0.16. These ratios indicate the H/D abundance ratio in the hydrated proton species was 0.91 : 0.09, which is identical to the H/D ratio in water molecules. The same H/D ratio was observed for desorbing water molecules as well in TPD experiments (Supporting Information). When hydrated protons are not formed, H/D exchange is not observed for surface water molecules. These results indicate efficient proton (deuteron) exchange reaction occurs between the hydrated proton and water, for which hydrated proton acts as the catalyst. The observed H/D ratios, however,

indicate that only part of surface D atoms was utilized for the H/D exchange reaction. The HDO/H_2O abundance ratio of 20 % corresponds to 0.13 ML of D atoms. This value indicates the partial coverage of surface hydrogen atoms participated in the exchange. The amount of hydrated protons formed on Pt will be smaller than 0.13 ML of surface hydrogen atoms.

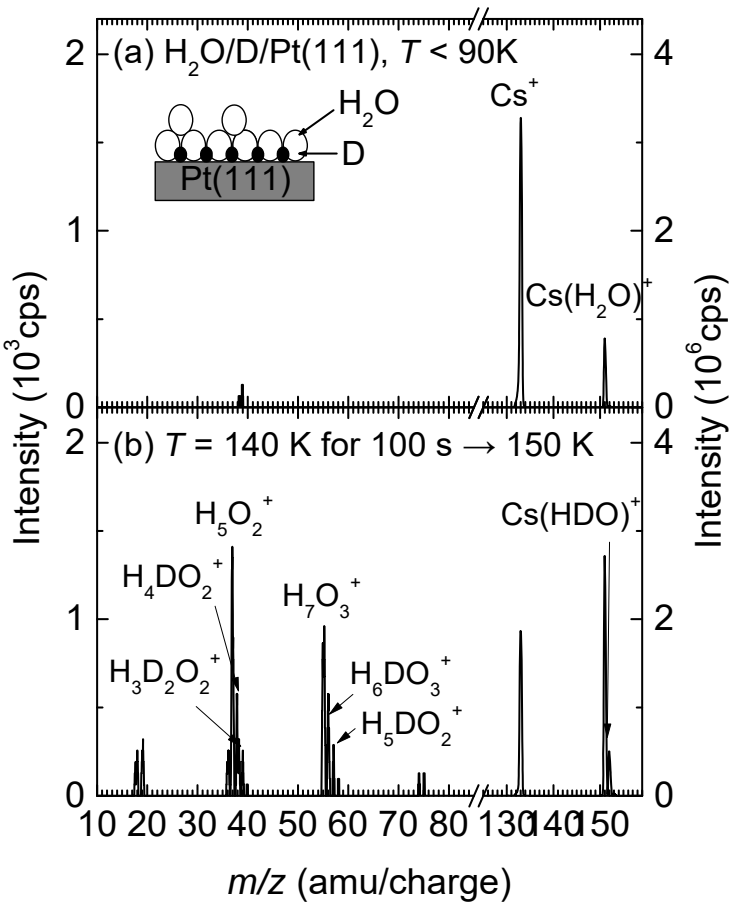

Figure 3-3. Positive LES spectra and RIS spectra. (a) 0.75 MLE D was formed on Pt(111) and H_2O was deposited on this at < 90 K. (b) The sample was heated at 140 K for 100 s and flashed to 150 K. The LES and RIS measurements were conducted at < 90 K with Cs^+ beam energy of 28 eV.

3.4. Energetics of the Formation of Hydrated Protons on Pt

In a previous work [6], hydrated protons were formed on a Pt surface, which has a high work function, but not on a Cu surface. It was explained that work function related to the energy of electron transfer is a key value of the stability of hydrated protons on the metal surface [7, 28]. When a hydrogen and a water react to form a hydrated proton on the surface and an electron is transferred to the metal,

$$H_{ads} + (H_2O)_{n,ads} \rightarrow H(H_2O)^{+}_{n,ads} + e^{-}_{metal} \quad (3\text{-}4)$$

thermochemistry of the reaction will be downhill if the electron affinity of hydrated proton is lower than the metal work function. Here, it is assumed that the difference in adsorption energies of adsorbates is negligible. To study the relation between the formation of hydrated protons and metal work function, electropositive atom, Na, was adsorbed on Pt(111). Na atom, which is the smallest alkali metal, is available to control work function with small adsorption of accurate coverage on Pt(111) without reaction site blocking [20, 22]. Figure 3-4 shows the LES and RIS spectra obtained from coasdosprtion of H and water preadsorbed Na on Pt surface. The Na coverage and the work function of Na adsorbed on Pt surface was measured by TPD and CPD experiment, respectively. Since Na can dissociate water layer on Pt(111) above critical coverage and produce NaOH species [22], the coverage of Na was maintained below 0.1 MLE and the $Cs(NaOH)^{+}$ signal was observed in order to remove the effect of water dissociation. When Na induced change of $\Delta\Phi$ = –0.4 eV, shown in Figure 3-4(a), multiply hydrated protons signals retained the original intensity distribution observed in Figure 3-1(b) with lower intensities compared to bare Pt surface. When $\Delta\Phi$ = –1.1 eV (Figure 3-4b), however, hydrated proton signals completely disappear from the sample. The absence of hydrated proton signals was also confirmed with higher Cs^{+} beam energy.

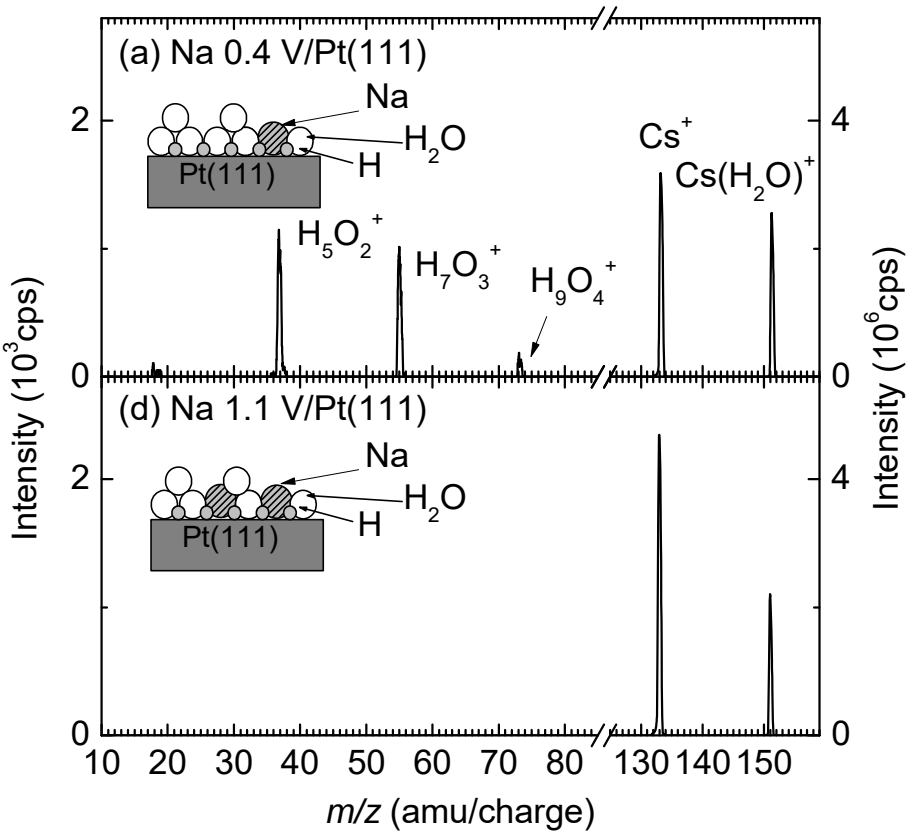

Figure 3-4. (I) Positive LES and RIS spectra obtained at various preadsorbed Na coverage on Pt(111). Na atoms were deposited onto bare Pt surface at < 90 K for each work function change of (a) 0.4 and (b) 1.1 V. Hydrogen and water was adsorbed on each sample. The sample temperature was heated to 150 K and maintained at 90 K during measurements. Cs^+ beam energy was 28 eV.

Figure 3-5 displays the change of ΔCPD before and after heating process as function of decreased work function by Na, H and H_2O adsorption. The work function change before heating linearly decreases with Na coverage as shown in Supporting Information (Figure 3-S2). When Na atom was not adsorbed on Pt, average ΔCPD value was ~0.3 eV. The positive value of ΔCPD represents the formation of a positive charge,

and this can be correlated with the formation of hydrated protons on the Pt surface. The ΔCPD value steadily decreased and reached a negative region. The work function represents an exothermic energy of electron transfer from outside to inside of the metal. The decrease of work function affects total thermodynamic energy for this reaction and it leads to produce less hydrated protons because of lower equilibrium constant. According to linear fitting of the data, hydrated protons were not formed when work function change is about -0.8 eV. The negative value of ΔCPD can be attributed to water desorption or dissociation during the heating process although Na is less than critical coverage of water dissociation.

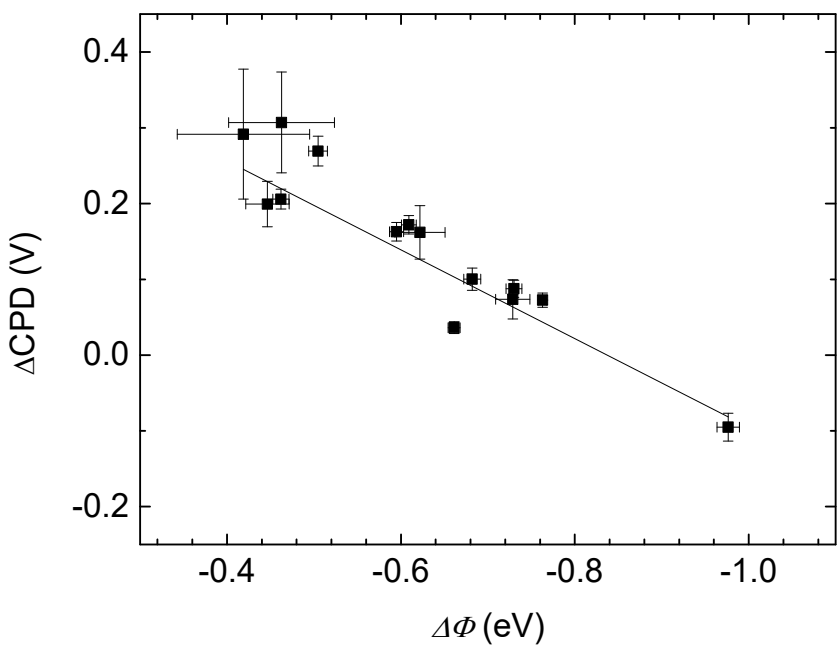

Figure 3-5. Experimental measurements for ΔCPD value changed from the formation of hydrated protons by heating each sample to 150 K as a function of work function change by Na, H, and H_2O adsorption. The solid line shows the simple linear fitting of data.

The above observations show that surface work function is a critical parameter for the stability of hydrated protons [7, 28]. The electron affinity of hydrated proton is estimated to be $EA(H_3O^+)$ ~ 6.11 eV and EA(multiply hydrated H^+) ~ 4.86 eV [28], and Φ ~ 6.0 eV for a pristine Pt(111) surface [29] and Φ ~ 5.5 eV for a water-covered Pt(111) surface. If certain uncertainties are admitted in these estimates, these numbers reasonably justify the observation that multiply hydrated protons are stabilized on the water adsorbed Pt(111) surface (Φ ~ 5.5 eV), but H_3O^+ is not. The multiply hydrated protons can be destabilized when a work function change is above ~ -1.14 eV according to electron affinity of hydrated protons. The smaller value measured in Figure 3-5 (~ -0.8 eV) can be attributed to the uncertain side effect of Na adosprtion on the surface. Despite of uncertainty, it is reasonably interpreted that stabliity of multiple hydrated protons are mainly affected by the work function value of the metal. It is also consistent with the previous report that hydrated protons do not form on a Cu surface (Φ ~ 4.5 eV) [6]. It is worthy to mention that although macroscopic Φ values are compared for the surfaces, there can be substantial variation in microscopic Φ values at specific surface sites [30].

3.5. The Transition from Metal Surface to Bulk

The effect of water overlayer was studied on MB hydrated protons. Figure 3-6 shows the intensity variation of different hydrated proton signals in LES experiment upon the progressive increase of water overlayer coverage on the MB hydrated protons, which are preformed in water monolayer on Pt(111). As hydrated protons were covered by increasing amounts of water overlayer, total intensities of hydrated protons decreased because LES is sensitive to the outmost surface layer. Regarding specific ion behaviors, the $H_5O_2^+$ and $H_7O_3^+$ intensities generally decreased with increasing water coverage, except for the small increase of $H_7O_3^+$ at the initial stage. In contrast, the intensity of $H_9O_4^+$ solely increased up

to ~0.3 ML of water overlayer and then decreases at higher coverage. The absolute intensity of $H_9O_4^+$ is smaller than other species, which can be attributed to the LES scattering sensitivity dependence on molecular weight. Because the water overlayer provides a bulk-like environment, the increase of the $H_9O_4^+$ intensity with increasing water overlayer indicates that two-dimensional MB hydration structures ($H_5O_2^+$, $H_7O_3^+$, and $H_9O_4^+$) evolve into three-dimensional structures that contribute to the $H_9O_4^+$ signal.

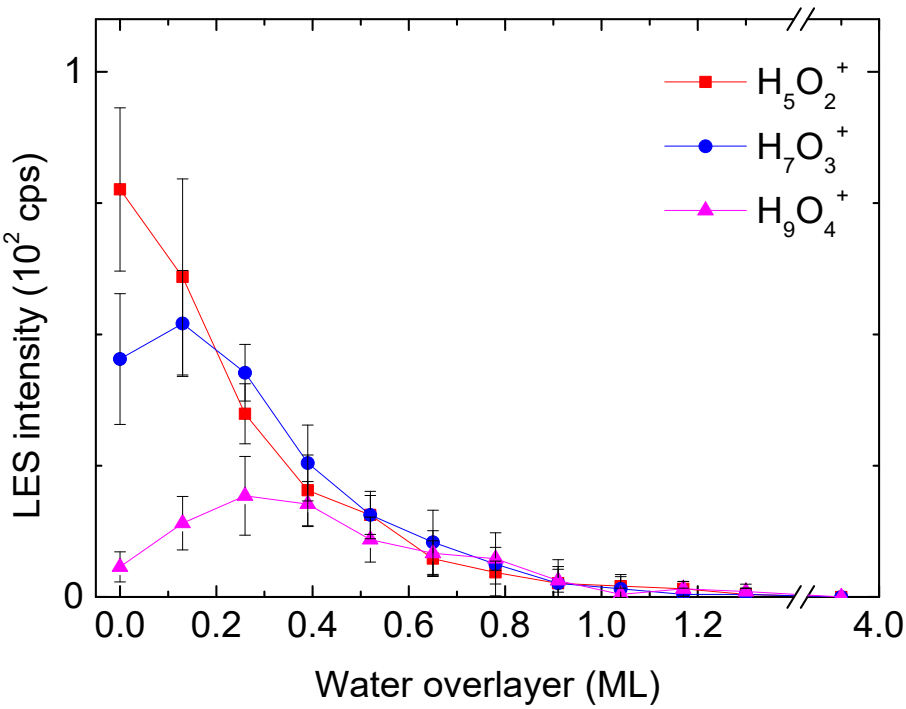

Figure 3-6. Variation of LES intensities for hydrated proton species [$H_5O_2^+$(■,red), $H_7O_3^+$(●,blue) and $H_9O_4^+$(▲,magenta); left ordinate scale] with increasing addition of water overlayer on preformed hydrated proton species. The initial sample was prepared by coadsorption of hydrogen (0.8 MLE) and water (1.1 ML) and heating at 150 K.

The unique behavior of $H_9O_4^+$ signal in the presence of water overlayer is observed in temperature-programmed LES (TPLES) experiment as well, as shown in Figure 3-7. In this experiment, the sample was prepared by coadsorption of hydrogen (0.8 MLE) and water (1.3 ML) on Pt(111) at < 90 K. By gradually heating this sample to a temperature below the onset of water desorption (< 145 K), TPLES measurement monitored the effect of temperature on the formation of hydrated protons. The continuous heating above the water desorption temperature allowed the experiment to monitor the hydrated protons during decrease in water surface coverage. Figure 3-7 shows TPLES intensity curves of $H_5O_2^+$, $H_7O_3^+$ and $H_9O_4^+$ signals. Variation in water surface coverage during a temperature scan is also plotted, which was obtained by integrating the temperature programmed desorption (TPD) curve of water that was measured from a separately prepared sample. Multiply hydrated protons ($H_5O_2^+$, $H_7O_3^+$ and $H_9O_4^+$) started to appear gradually at a temperature above ~125 K, which indicates that thermal energy facilitates the ionization of adsorbed hydrogen atoms, most likely via rearrangement of adsorbates. The population of $H_5O_2^+$ and $H_7O_3^+$ abruptly increased up to ~152 K, at which temperature only full monolayer remained, and then decreased with the desorption of water monolayer. The brief dip of $H_5O_2^+$ and $H_7O_3^+$ signals at 145–148 K can be attributed to the growth of $H_9O_4^+$ population. Only the $H_5O_2^+$ signal persists above ~165 K, which may be attributed to Zundel-like $H_5O_2^+$ species on the surface with small water coverage. The $H_9O_4^+$ intensity showed its maximum in the region of 145–148 K, where a water multilayer existed, and disappeared with desorption of the multilayer. These observations clearly indicate that correlations exist between the water multilayer and the $H_9O_4^+$ signal, and between the water monolayer and the $H_5O_2^+$ and $H_7O_3^+$ signals, further supporting that MB hydrated proton structures develop into three-dimensional hydration structures in the water multilayer.

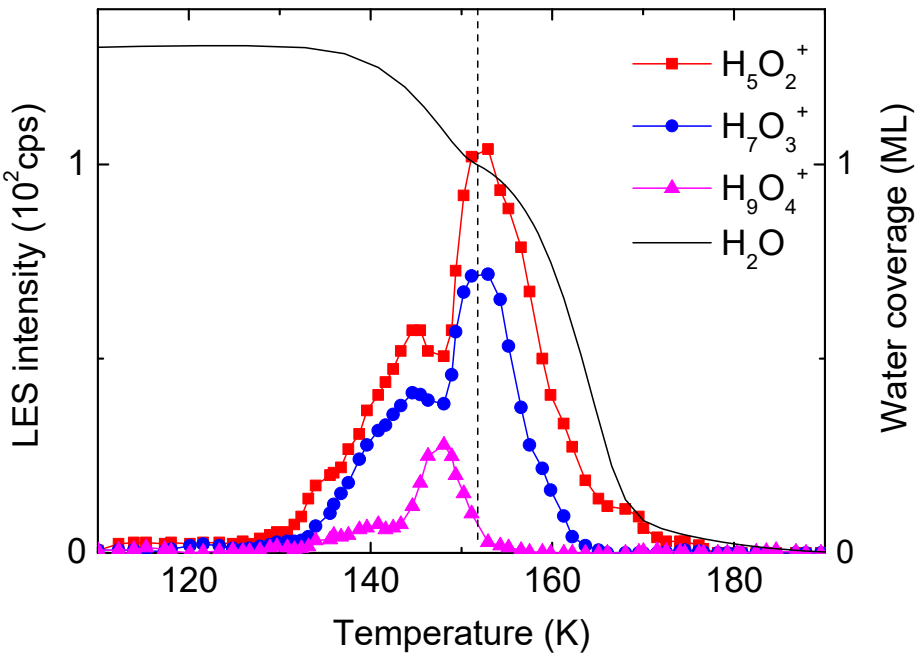

Figure 3-7. TPLES measurement of hydrated protons signal intensities on the sample prepared by hydrogen (0.8 MLE) and water (1.3 MLE) coadsorption on Pt(111) below 90 K. The black line depicts the water coverage (right ordinate scale) deduced from TPD measurement of water from the equivalent sample. The dotted vertical line marks the position of water monolayer coverage. The ramping rate was 1 K s^{-1} in both the TPLES and TPD experiments.

DFT calculations investigated the transformation of MB hydrated protons into three-dimensional structures in the water multilayer [25]. This shows that the proton transfer to the second layer can occur easily and the hydronium on Pt surface is fully hydrogen bonded with water to form the $H_9O_4^+$ structure. The deformation of metal-adsorbed hydronium ions to $H_9O_4^+$ ions to the upper layer is in agreement with the LES results, in which the relative intensity of $H_9O_4^+$ increases as the water overlayer develops.

Figure 3-8 shows the changes in the vibrational band of MB hydrated protons with the addition of a water overlayer, observed by RAIRS. In spectrum (a), a band appeared at ~1130 cm^{-1} after heating of coadsorbed H and H_2O layer in RAIRS is in agreement with the ionized hydrogen assigned in previous HREELS and RAIRS results [5, 6, 9]. As mentioned in previous section, the observation shown in Figure 3-1 confirms that charge transfer does occur on the Pt surface, and resulting species are $H_5O_2^+$, $H_7O_3^+$ and $H_9O_4^+$ rather than H_3O^+. With a small extent of water coverage, the vibrational band of hydrated protons on a Pt surface blue-shifted as shown in spectrum (b)–(g). This vibrational band reached at ~1260 cm^{-1} in spectrum (g) and did not change upon further addition of water. The band at ~1260 cm^{-1} are known as hydronium ion in bulk solid water [31]. This indicates that water overlayer transforms MB hydrated proton structures (two-dimensional structures) to fully solvated three-dimensional structures, which produce the $H_9O_4^+$ signal in LES and the ~1260 cm^{-1} band in RAIRS, via vertical proton migration into the upper layer. The band shift also verified that this fully solvated $H_9O_4^+$ is different from MB-$H_9O_4^+$ structure.

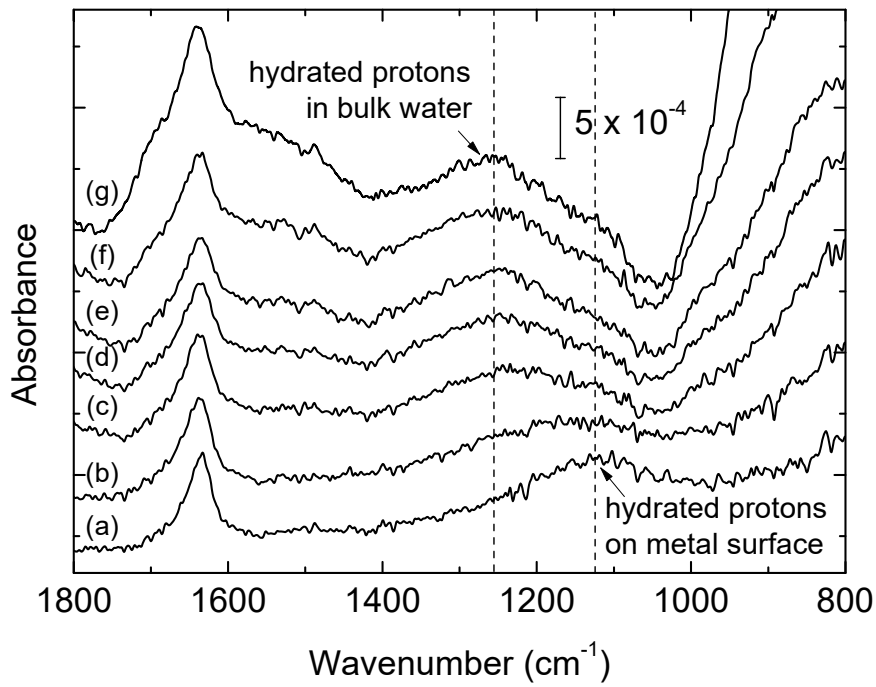

Figure 3-8. Series of RAIRS spectra of the sample with increasing water exposure on the MB hydrated protons preformed by coadsorption of hydrogen and water and heating to 150 K. The amount of water exposure corresponding to each spectrum is: (a) 0 ML; (b) 0.13 ML; (c) 0.26 ML; (d) 0.39 ML; (e) 0.52 ML; (f) 1.8 ML; (g) 3.0 ML. Each spectrum was obtained by adding water on previous spectrum. The sample temperature was maintained below 90 K during the water exposure.

3.6. Implication for HER on Pt Electrode Surface

The stability of multiply hydrated protons on the water-covered Pt surfaces suggests the possibility that they form on a Pt electrode surface as well during the Volmer reaction (Equation 3-1), which is the electrochemical interconversion between adsorbed hydrogens and solvated protons in aqueous phase. These surface hydrated protons may be intermediate

states of the Volmer reaction. As illustrated in Figure 3-9, the first step of the reaction is the ionization of an adsorbed hydrogen atom to a multiply hydrated proton that is specifically adsorbed on the electrode surface, which occurs via electron transfer from the adsorbed atom to metal surface. Then, the surface hydrated proton becomes fully solvated as it moves from the electrode surface to the bulk solution. The hydrated proton migration occurs via succesive proton hopping events (Grotthuss mechanism) along the hydrogen bond of interfacial water molecules. The bulk dissolution of hydrated protons is energetically downhill in the UHV experiment, according to the present work. The reaction energy (~0.6 eV), which is estimated through a thermodynamic cycle, is correlated with the threshold (~0.8 eV) measured in Figure 3-4. Analogous process at electrode/electrolyte interface is therefore expected to occur spontaneously.

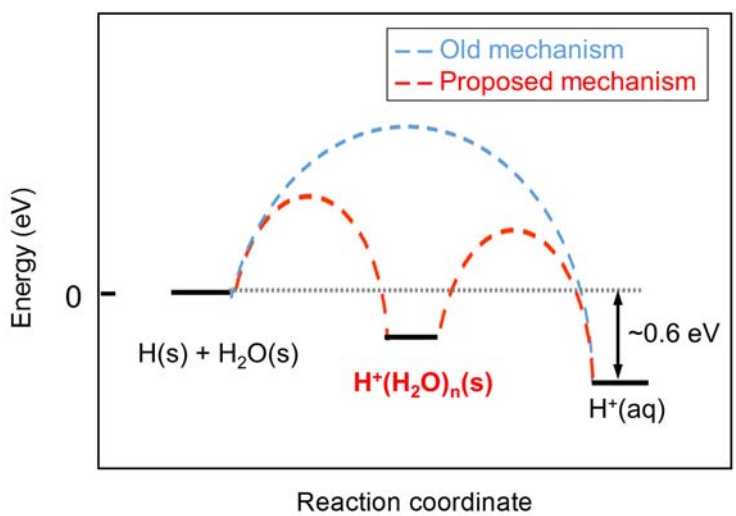

Figure 3-9. Potential energy diagram for the Volmer reaction. The reaction energy (~0.6 eV) was estimated through a thermodynamic cycle including desorption of atomic hydrogen (+2.7 eV) [28], ionization of atomic hydrogen in the gas phase (+13.6 eV), electron transfer to water-adsorbed Pt(111) (-5.5 eV), and hydration of a gaseous proton (-11.4 eV) [32].

Electron transfer between adsorbed hydrogen atom and metal, the first step of the reaction, will occur instantaneously (~10^{-15} s) once an appropriate arrangement in the surrounding water geometry can be made. On the other hand, the second step involving proton transfer will occur with a certain time delay because the proton transfer from the electrode surface to solution requires further hydration structure rearrangement, albeit it occurs via a Grotthuss mechanism. Therfore, there will be a certain time delay between first and second step. Owing to these dynamic characteristics, the surface hydrated protons are considered as an intermediate of the mechanism of Volmer reaction. This interpretation contrasts with an old view in which the conversion from adsorbed hydrogen to H^+(aq) may occur in a single step. In the proposed mechnism, specific adsorption of a hydrated proton, H^+(aq) ↔ H^+(s), induces negative charge on the electrode surface, and this process will draw most of the underpotential deposition current of H^+(aq) observed in cyclic voltammetry experiments [33]. On the other hand, the conversion of H^+(s) to H(s) on the surface will draw only a relatively small amount of additional electrode current. For comparison, according to the previous mechanism, the voltammetric current was considered to be due to the electron transfer from the electrode surface to H^+(aq). These two mechanisms may not be distinguishable in ordinary voltammetry experiments. Theoretical methods have been employed to understand the molecular mechanism of the Volmer reaction [34-36]. Future theoretical studies of the reaction mechanism including surface hydrated protons would be interesting.

4. Conclusion

The LES and RAIRS analyses of coadsorbed hydrogen and water layer on a Pt(111) surface showed a clear evidence that the adsorbed hydrogen atoms are ionized to hydrated protons on the surface. The hydrated protons exist preferentially as multiply hydrated species

($H_5O_2^+$, $H_7O_3^+$, and $H_9O_4^+$) rather than as H_3O^+, according to the mass spectrometric detection of LES signals. Hydration number of protonated water cluster and the work function of metal surface are critical parameters that determine the stability of hydrated protons on the surface. The CPD experiment provided a work function threshold for the formation of hydrated protons on the Pt surface. The additional water overlayer on surface hydrated protons converts them to fully hydrated proton structures. This change is evidenced by the stronger intensity of LES signal of $H_9O_4^+$ on water multilayer films and shift of the IR absorption band of hydrated protons from ~1130 cm^{-1} to ~1260 cm^{-1}. The "nonspecifically adsorbed" $H_9O_4^+$ structure resembles the Eigen cation in bulk water and is different from metal-bound $H_9O_4^+$ structure. The proton migration distance for this conversion is about one water layer according to the CPD measurement, indicating the residence of nonspecifically adsorbed hydrated protons in the outer Helmholtz layer region.

The above-mentioned observations suggest the possibility that surface hydrated protons form on a Pt electrode surface in electrochemical environment at appropriate potential ranges. As such, the specifically adsorbed hydrated protons may act as kinetic intermediates in the conversion between adsorbed H atom and H^+(aq) in Volmer reaction, and possibly in other electrochemical reactions of hydrogens. There has been a long debate on the relevance of "synthetic double layer" prepared in UHV to real electrochemical interfaces [2]. The present work demonstrates that the recent progress in surface preparation and characterization techniques may indeed make useful contribution to fundamental understanding of the electrode surface processes in the molecular picture.

References

1. Schmickler, W. *Interfacial Electrochemistry*; Oxford: New York, 1996.
2. Wagner, F. *Structure of Electrified Interfaces*; VCH: New York, 1993.
3. Thiel, P. A.; Madey, T. E. The Interaction of Water with Solid-Surfaces: Fundamental Aspects. *Surf. Sci. Rep.* **1987**, *7*, 211-385.
4. Hodgson, A.; Haq, S. Water adsorption and the wetting of metal surfaces. *Surf. Sci. Rep.* **2009**, *64*, 381-451.
5. Wagner, F. T.; Moylan, T. E. Generation of Surface Hydronium from Water and Hydrogen Coadsorbed on Pt(111). *Surf. Sci.* **1988**, *206*, 187-202.
6. Lackey, D.; Schott, J.; Sass, J. K.; Woo, S. I.; Wagner, F. T. Surface-Science Simulation Study of the Electrochemical Charge-Transfer Reaction $(H)_{ad} + (H_2O)_{ad} \rightarrow (H_3O^+)_{ad} + e^-_{metal}$ on Pt(111) and Cu(110). *Chem. Phys. Lett.* **1991**, *184*, 277-281.
7. Kizhakevariam, N.; Stuve, E. M. Coadsorption of Water and Hydrogen on Pt(100) - Formation of Adsorbed Hydronium Ions. *Surf. Sci.* **1992**, *275*, 223-236.
8. Chen, N.; Blowers, P.; Masel, R. I. Formation of hydronium and water-hydronium complexes during coadsorption of hydrogen and water on (2x1)Pt(110). *Surf. Sci.* **1999**, *419*, 150-157.
9. Shingaya, Y.; Ito, M. Coordination number and molecular orientation of hydronium cation bisulfate anion adlayers on Pt(111). *Surf. Sci.* **1996**, *368*, 318-323.
10. van der Niet, M. J. T. C.; Dominicus, I.; Koper, M. T. M.; Juurlink, L. B. F. Hydrophobic interactions between water and pre-adsorbed D on the stepped Pt(533) surface. *Phys. Chem. Chem. Phys.* **2008**, *10*, 7169-7179.
11. den Dunnen, A.; van der Niet, M. J. T. C.; Koper, M. T. M.; Juurlink, L. B. F.

Interaction between H2O and Preadsorbed D on the Stepped Pt(553) Surface. *J. Phys. Chem. C* **2012**, *116*, 18706-18712.

12. Olivera, P. P.; Ferral, A.; Patrito, E. M. Theoretical investigation of hydrated hydronium ions on Ag(111). *J. Phys. Chem. B* **2001**, *105*, 7227-7238.
13. Pan, M.; Pozun, Z. D.; Yu, W. Y.; Henkelman, G.; Mullins, C. B. Structure Revealing H/D Exchange with Co-Adsorbed Hydrogen and Water on Gold. *J. Phys. Chem. Lett.* **2012**, *3*, 1894-1899.
14. Kang, H. Chemistry of ice surfaces. Elementary reaction steps on ice studied by reactive ion scattering. *Acc. Chem. Res.* **2005**, *38*, 893-900.
15. Kang, H. Reactive Ion Scattering of Low Energy Cs+ from Surfaces. A Technique for Surface Molecular Analysis. *Bull. Korean Chem. Soc.* **2011**, *32*, 389-398.
16. Badescu, S. C.; Jacobi, K.; Wang, Y.; Bedurftig, K.; Ertl, G.; Salo, P.; Ala-Nissila, T.; Ying, S. C. Vibrational states of a H monolayer on the Pt(111) surface. *Phys. Rev. B* **2003**, *68*, 205401.
17. Poelsema, B.; Lenz, K.; Comsa, G. The dissociative adsorption of hydrogen on defect-'free' Pt(111). *J. Phys. Cond. Matt.* **2010**, *22*, 304006.
18. Haq, S.; Harnett, J.; Hodgson, A. Growth of thin crystalline ice films on Pt(111). *Surf. Sci.* **2002**, *505*, 171-182.
19. Gland, J. L.; Kollin, E. B. Ammonia Adsorption on the Pt(111)and Pt(S)-6(111)X(111) Surfaces. *Surf. Sci.* **1981**, *104*, 478-490.
20. Cousty, J.; Riwan, R. Structures of Na and Cs Layers Adsorbed on Pt(111). *Surf. Sci.* **1988**, *204*, 45-56.
21. More, S.; Seitsonen, A. P.; Berndt, W.; Bradshaw, A. M. Ordered phases of Na adsorbed on Pt(111): Experiment and theory. *Phys. Rev. B* **2001**, *63*.
22. Bonzel, H. P.; Pirug, G.; Ritke, C. Adsorption of H2o on Alkali-Metal-Covered

Pt(111) and Ru(001) - a Systematic Comparison. *Langmuir* **1991**, *7*, 3006-3011.

23. Lee, C. W.; Lee, P. R.; Kang, H. Protons at ice surfaces. *Angew. Chem. Int. Ed.* **2006**, *45*, 5529-5533.

24. Voth, G. A. Computer simulation of proton solvation and transport in aqueous and biomolecular systems. *Acc. Chem. Res.* **2006**, *39*, 143-150.

25. Kim, Y.; Noh, C. N.; Jung, Y.-J.; Kang, H. The Nature of Hydrated Protons on Platinum Surface. *To be submitted*.

26. Kobayashi, C.; Saito, S. J.; Ohmine, I. Mechanism of fast proton transfer in ice: Potential energy surface and reaction coordinate analyses. *J. Chem. Phys.* **2000**, *113*, 9090-9100.

27. Cao, Z.; Kumar, R.; Peng, Y. X.; Voth, G. A. Hydrated Proton Structure and Diffusion at Platinum Surfaces. *J. Phys. Chem. C* **2015**, *119*, 14675-14682.

28. Masel, R. I. *Principles of adsorption and reaction on solid surfaces*; Wiley: New York, 1996.

29. Salmeron, M.; Ferrer, S.; Jazzar, M.; Somorjai, G. A. Photoelectron-Spectroscopy Study of the Electronic-Structure of Au and Ag Overlayers on Pt(100), Pt(111), and Pt(997) Surfaces. *Phys. Rev. B* **1983**, *28*, 6758-6765.

30. Sinsarp, A.; Yamada, Y.; Sasaki, M.; Yamamoto, S. Microscopic study on the work function reduction induced by Cs-adsorption. *Jpn. J. Appl. Phys.* **2003**, *42*, 4882-4886.

31. Parent, P.; Lasne, J.; Marcotte, G.; Laffon, C. HCl adsorption on ice at low temperature: a combined X-ray absorption, photoemission and infrared study. *Phys. Chem. Chem. Phys.* **2011**, *13*, 7111-7117.

32. Zhan, C. G.; Dixon, D. A. Absolute hydration free energy of the proton from first-principles electronic structure calculations. *J. Phys. Chem. A* **2001**, *105*, 11534-

11540.

33. Koper, M. T. M. Blank voltammetry of hexagonal surfaces of Pt-group metal electrodes: Comparison to density functional theory calculations and ultra-high vacuum experiments on water dissociation. *Electrochim. Acta* **2011**, *56*, 10645-10651.

34. Ohwaki, T.; Yamashita, K. A DFT study of electric field effects on proton transfer reactions at H+(H2O)(2)/Pt(111) and Ag(111). *J. Electroanal. Chem.* **2001**, *504*, 71-77.

35. Wilhelm, F.; Schmickler, W.; Nazmutdinov, R. R.; Spohr, E. A model for proton transfer to metal electrodes. *J. Phys. Chem. C* **2008**, *112*, 10814-10826.

36. Pecina, O.; Schmickler, W. A model for electrochemical proton-transfer reactions. *Chem. Phys.* **1998**, *228*, 265-277.

Supporting Information

Figure 3-S1 shows the result of TPD measurements for hydrogen and water from three samples: D/Pt(111), H_2O/Pt(111), and (D + H_2O)/Pt(111). In these samples, the coverage of deuterium was 0.75 MLE and that of water was 1.2 ML after adsorption of the corresponding gases at < 90 K. The samples were heated at 140 K for 100 s and flash-annealed at 150 K, which reduced the deuterium coverage to 0.7 MLE and the water coverage to 0.8 ML. The TPD spectra from D/Pt(111) (Figure 3-S1a) and H_2O/Pt(111) samples (Figure 3-S1b) showed single-peak desorption spectra, in agreement with the previous reports.[1] A small HD signal in Figure S1a originated from H or H_2O impurities on the surface. On the surface with coadsorbed H_2O and D, hydrogen TPD experiment detected the desorption of D_2, HD, and H_2 (Figure 3-S1c), and water TPD experiment detected the desorption of H_2O and HDO (Figure 3-S1d). These signals indicated the occurrence of H/D exchange reactions between adsorbed H_2O and D. The H/D exchange products had relatively very small or negligible populations in the TPD spectra shown in Figures 3-S1a and b. The H:D ratio in the water desorption flux was estimated to be 0.91:0.09 from the integrated peak areas. This ratio was the same as that for observed hydrated protons and water molecules on the surface in LES and RIS experiments. The H content in D_2, HD, and H_2 desorption fluxes in Figure 3-S1c was increased by 15% from that for Figure 3-S1(a). The result indicated that this amount of surface D atoms underwent H/D exchange reaction with water.

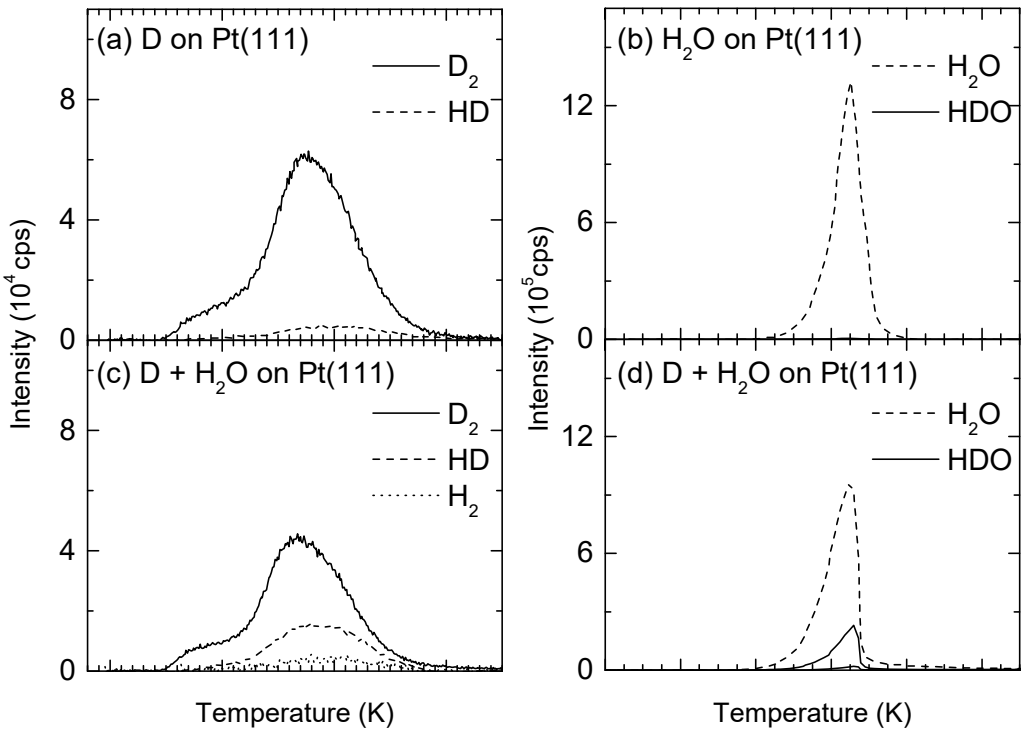

Figure 3-S1. TPD spectra for an adsorbed D layer on Pt(111) (a), adsorbed H_2O layer on Pt(111) (b), and coadsorbed D and H_2O layer on Pt(111) (c and d). All samples were prepared by gas adsorption at < 90 K, followed by heating at 140 K for 100 s and at 150 K briefly. The temperature ramping rate was 1 K s^{-1}.

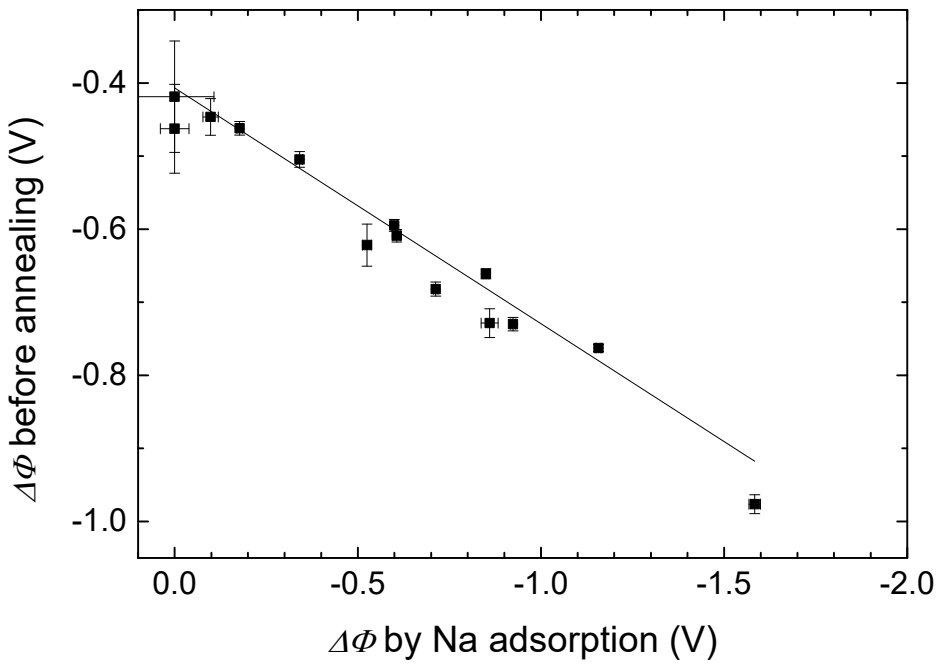

Figure 3-S2. Experimental measurements for total work function change by Na, H, and H_2O adsorption from only Na. The solid line shows the simple linear fitting of data.

Chapter IV

Spatial Distribution of Hydrated Protons and Chloride Ions at the Solid Water/Pt Interface

Abstract

The behaviors of H^+ and Cl^- ions were studied at the interface of a solid water layer and a Pt surface. H^+ and Cl^- ions were prepared on a Pt(111) surface by coadsorption of HCl and H_2O, and an amorphous solid water (ASW) film was overlaid on the ions to simulate the electrochemical interface in ultra-high vacuum (UHV) environment. The spatial distributions of H^+ and Cl^- ions at the interface of an ASW film and a Pt metal were examined by using low-energy sputtering (LES) and a Kelvin work function probe. The experimental results showed that H^+ and Cl^- ions have thermodynamic tendency to reside near the metal surface rather than diffuse out into the ASW film. The average vertical distance of H^+ ions from that of Cl^- ions, which specifically adsorbed on the Pt surface, was estimated to be about on water layer. The migration of protons from the metal surface to the hydration sphere can be attributed to the stability of fully solvated structure. The distribution of H^+ and Cl^- ions near the Pt surface is reminiscent of the electrical double

layer (EDL) structure consisting of specifically adsorbed (Cl^-) and non-specifically adsorbed (H^+) ions. The spacing of single water monolayer between H^+ and Cl^- may be related to the location of outer Helmholtz plane in EDL.

1. Introduction

It has long been conceived that studies of adsorbed molecular layers on metal surfaces in an UHV environment might eventually improve our understanding of the phenomena at electrode surfaces in solutions [1-3]. As a simplified model of an electrochemical interface, a "synthetic double layer" has been prepared by coadsorption of water and electrochemically relevant species on metals under UHV and surface-sensitive spectroscopic techniques have been applied to investigate the adsorbate–metal or adsorbate–water interactions in such model systems [2, 3]. Early experimental work based on this approach has employed partial or full monolayer coverage of adsorbed water on metal surfaces to examine the effect of the adsorbed water layer [4-9]. However, such conditions are too simplified for the simulation of the diverse aspects of a real electrochemical interface, where some ions are located in diverse environments from partial solvation in specifically adsorbed on the electrode surface, while others are fully solvated in the bulk solution phase. The UHV experiment might simulate the fully solvated environment of the solution phase by growing a multilayer film of water on a cold metal substrate. However, the molecular mobility is very low in solid water at low temperature; the self-diffusion speed is approximately one molecular distance per second at 150 K [10, 11]. This questions the feasibility of using solid water films for synthetic double layer under UHV because the low molecular mobility hampers the effective solvation of ions and diffusion for the occurrence of a reaction, not to mention the conduction of charge through the water film, which is required to an establish electrostatic equilibrium of the interface.

Recently, studies of proton transport in crystalline ice (CI) or amorphous solid water (ASW) samples showed that an excess proton (H^+) is quite mobile in these samples at low temperature [11-24]. Excess protons can migrate across a distance of ~25 layers in ASW at 90 K via an efficient hopping relay mechanism [25]. The migration distance can

be extended at higher temperature (> 130 K) due to the reorientation of water [12-14, 18, 21]. Also, it was reported that protons have a thermodynamic affinity to the surface of water and thus migrate spontaneously from the interior of ice to its surface upon heating of the sample [11, 19, 22, 23]. These unique properties of protons suggest that some of the obstacles of the synthetic double layer mentioned above might be overcome using protons in solid water. Based on their high mobility, even at low temperature, protons can make effectively carry charge in solid water films grown under UHV and induce acid–base reactions at the surface [11, 26]. In the present work, the properties of H^+ and Cl^- ions were studied at the interface of an ASW film and Pt metal. The H^+ and Cl^- ions were produced by coadsorption of HCl and H_2O on a Pt(111) substrate, and an ASW film was overlaid on the ions to simulate the solution phase of an electrochemical interface. The spatial distribution of these ions at the water/metal interface was investigated as a model system for specifically adsorbed (Cl^-) and non-specifically adsorbed (H^+) ions in the electric double layer (EDL).

2. Experimental Section

The experiments were conducted in a UHV surface analysis chamber [27, 28] equipped with instrumentation for Cs^+ reactive ion scattering (RIS), low-energy sputtering (LES), temperature-programmed desorption (TPD), and surface work function measurement. The HCl was adsorbed on a Pt(111) substrate surface at a temperature below 90 K using a tube doser. After the HCl adsorption on Pt(111), the water layer was adsorbed on the surface at a desired temperature between 80 K and 135 K by back-filling the chamber with H_2O vapor at a partial pressure of 1×10^{-8} Torr. The coverages of HCl and H_2O were estimated from the TPD measurements [29, 30] and reported in units of water monolayer on Pt(111) (1 ML of water = 1.2×10^{15} molecules cm^{-2}).

The RIS and LES methods were used to analyze the chemical species on the sample surface [27, 28]. In these experiments, a Cs^+ beam from a low-energy ion gun (Kimball Physics) collided with the surface at an incidence energy of 32 eV, unless otherwise noted. The scattered ions were detected by a quadrupole mass spectrometer (Extrel) with its ionizer filament switched off. The Cs^+ impact at this energy did not cause the secondary ionization of water molecules. In RIS, neutral species (X) on the surface are picked up by the scattering Cs^+ projectiles to form Cs^+-neutral clusters (CsX^+). In LES, preexisting ionic species (Y^+) on the surface are ejected by the Cs^+ impact. The probing depth of LES and RIS methods is one molecular layer from the outmost surface at this incident energy [31-33]. Thus, the RIS and LES signals reveal the identity of neutral (X) and ionic species (Y^+), respectively, on the surface.

A Kelvin work function probe measured the contact potential difference (CPD) between the Au-coated metal probe and sample, i.e., CPD = Φ(probe) – Φ(sample), where Φ is the work function. The CPD was measured before and after the adsorption of the water overlayer. The difference of two CPD measurements, ΔCPD, corresponds to the voltage of the water film that contains H^+ and Cl^- ions. These ions are initially produced on the Pt surface and migrate through the water overlayer; they have characteristic depth distributions in the film. The average depths of ions is related to ΔCPD as follows [24]. If it is assumed that H^+ and Cl^- ions form stratified layers, the voltage (V_s) due to the charge separation can be expressed by Equation (4-1) in a parallel-plate capacitor model [34].

$$V_s = \frac{\sigma d}{\varepsilon_r \varepsilon_0} \tag{4-1}$$

Here, σ is the density of positive or negative ions per unit surface area, which is determined by the amount of HCl coverage, d is the distance between two sheets of oppositely charged ions, ε_r is the relative dielectric constant of the medium, and ε_0 is the

vacuum permittivity. The vertical charge-separation distance is the difference of the average depths of positive and negative ions, $d = \langle d_{q+} \rangle - \langle d_{q-} \rangle$. The ΔCPD is contributed by both V_s and the voltage due to the small net orientation of the water dipoles in the film.

3. Results

Surface ionic species formed by coadsorption of HCl and water on a Pt surface were examined using low-energy sputtering (LES) and reactive ion scattering (RIS). The HCl was adsorbed on Pt(111) at 90 K by introducing HCl gas into the chamber using a tube doser. It is known that HCl gas is dissociatively adsorbed on the Pt surface when $\theta_{HCl} \leq 0.3$ ML in units of the coverage of the water monolayer [30]. The H_2O monolayer was then adsorbed onto the HCl/Pt surface by H_2O vapor deposition at 135 K, a condition that is known to form a well-ordered water monolayer on a Pt(111) surface. Figure 4-1I shows the mass spectra of LES and RIS signals obtained on the Pt surface. Hydrated proton signals appear at *m/z* = 19 (H_3O^+), 37 ($H_5O_2^+$), 55 ($H_7O_3^+$), and 73 ($H_9O_4^+$) in the positive-ion LES spectrum I(a). The Cl^- ions were observed at *m/z* = 35 and 37 in the negative-ion LES spectrum I(b). These LES signals indicate that HCl molecules ionized to H^+ and Cl^- and that H^+ is efficiently hydrated by adsorbed water molecules. The RIS signals of CsH_2O^+ and $Cs(H_2O)_2^+$ at *m/z* = 151 and *m/z* = 169, respectively, in spectrum I(c) confirm the presence of H_2O molecules on the surface. The *m/z* = 169 signal might originate from $Cs(H_2O)_2^+$ and $Cs(H^{35}Cl)^+$, but the absence of a $Cs(H^{37}Cl)^+$ signal at *m/z* = 171 shows that molecular HCl does not exist on the surface.

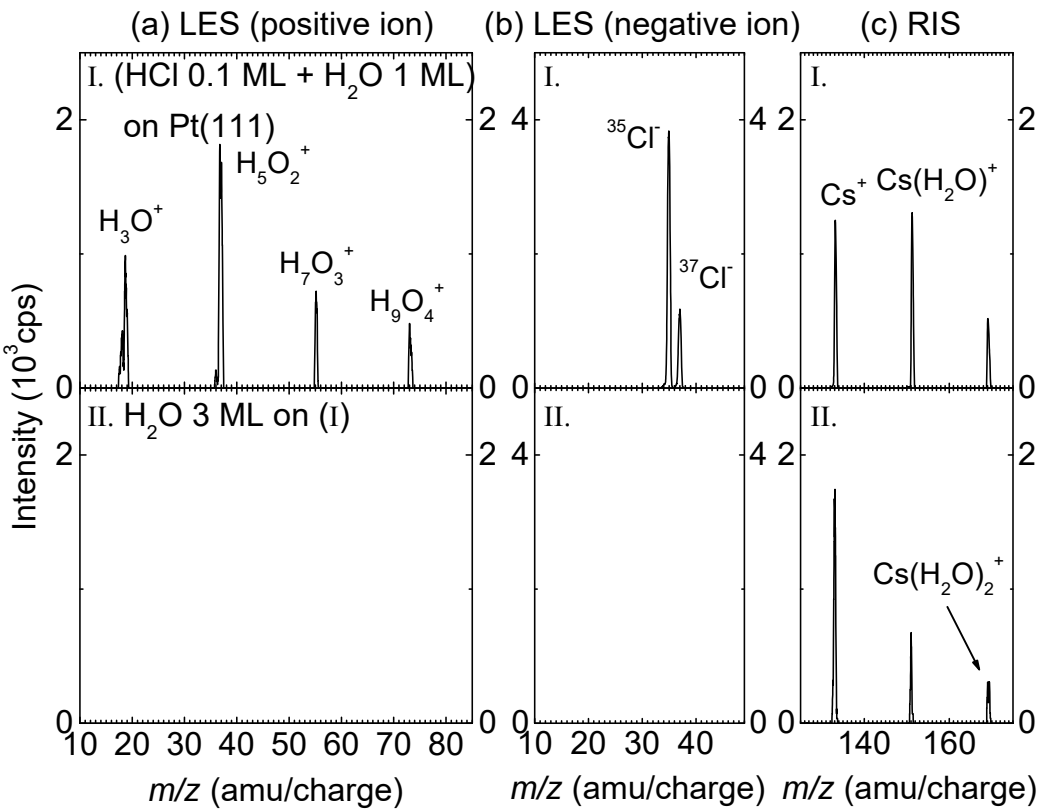

Figure 4-1. (a) Positive-ion LES , (b) negative-ion LES and (c) RIS spectra measured from the samples that were prepared under the following conditions: (I) adsorption of HCl for 0.1 ML on Pt(111) at 83 K and adsorption of H_2O for1 ML at 135 K, (II) addition of H_2O overlayer for 3 ML onto the sample (I) at 80 K. All the spectra were recorded below 90 K with Cs^+ beam energy of 32 eV.

The strong LES intensities of $H_5O_2^+$, $H_7O_3^+$, and $H_9O_4^+$ indicate that multiply hydrated protons are preferentially formed on the surface. This interpretation is strengthened by the fact that larger molecular ions are less efficiently desorbed by Cs^+ collisions on the surface. An interesting feature that differs from previous observation for H^+ ions formed by ionization of adsorbed hydrogen atoms on Pt(111) [35] is that the

monohydrated H_3O^+ signal has a substantial intensity in the present case. In a previous study [35], the H_3O^+ signal was almost absent, which was explained by the higher electron affinity (~6.11 eV) of H_3O^+ compared with the work function of a water-covered Pt surface (~5.5 eV) [36, 37]. In the present case with HCl adsorbate on the Pt surface, HCl did not drastically change the surface work function ($\Delta\Phi$ = -0.1 eV at HCl coverage of 0.1 ML) despite the strong interactions between Pt and Cl [6]. For this reason, the strong H_3O^+ signal might be attributed to the stabilization of this species by electrostatic interaction with Cl^- such as the formation of a H_3O^+–Cl^- ion pair, or by the change of the work function in a localized region [9, 38]. Apart from H_3O^+, the strong signals of multiply hydrated protons are clear evidence of their preferential formation in the water monolayer on Pt(111).

Figure 4-1II shows the result obtained after the deposition of the H_2O overlayer of 3 ML thickness onto the sample prepared in Figure 4-1I. Hydrated H^+ and Cl^- ion signals are absent from the spectra II(a) and II(b). This indicates that the water overlayer completely buried H^+ and Cl^- ions below the surface. In contrast, when hydrated protons are generated by ionizing HCl on an ASW film surface and a H_2O film of comparable thickness is then overlaid onto them, the protons migrate through the overlayer to populate the H_2O film surface [19]. Hydrated protons formed on a Pt surface behave differently from those on an ASW film surface. If protons have a certain mobility in ASW [21-23], this observation might indicate that protons are trapped at the water/Pt interface rather than migrate through the water film. In case of the Cl^- ion, this observation might be rationalized in terms of its strong binding affinity to the metal surface and low kinetic mobility through ASW at low temperature.

The transport behavior of hydrated protons and chloride ions from the Pt surface through the ASW overlayer is observed upon heating of the sample. Temperature-programmed LES (TPLES) experiments were used to measure the hydrated H^+ and Cl^-

signals at the ASW overlayer surface during increasing temperature as a linear function of time (0.5 K s^{-1}). The increase of the ion signals indicates their transport from the Pt/water interface to the sample surface. Figures 4-2I(a) and 4-2II(a) show the results of the TPLES measurements for hydrated protons migrating to the sample surface starting from the Pt/water interface [H_2O (28 ML)/H^+ (0.1 ML) + Cl^- (0.1 ML)/Pt(111)] and from the interior of the ASW film [H_2O (28 ML)/H^+ (0.1 ML) + Cl^- (0.1 ML)/H_2O (50 ML)/Pt(111)], respectively. The TPD experiments were also performed for separately prepared samples. The H_2O TPD curves, overlapped with TPLES results in the figure, indicate the amount of water desorption with increasing temperature, and thus the thickness of water film remaining in the sample.

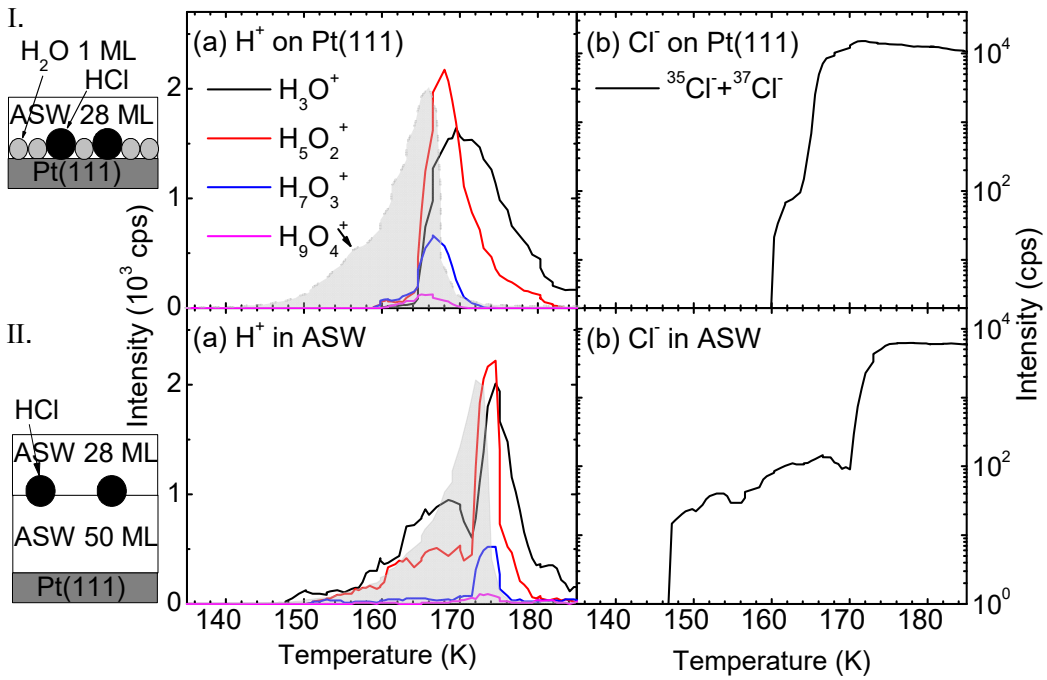

Figure 4-2. TPLES measurements of hydrated protons (H_3O^+, $H_5O_2^+$, $H_7O_3^+$, and $H_9O_4^+$) and chloride ions ($^{35}Cl^- + {}^{37}Cl^-$) reaching the sample surface via diffusion through an ASW overlayer with 28 ML thickness. Spectra I(a) and I(b) correspond to the ion diffusion from the water/Pt interface, measured for a sample structure: H_2O (28 ML)/H^+ (0.1 ML) + Cl^- (0.1 ML)/Pt(111). H^+ and Cl^- were generated by coadsorption of HCl (0.1 ML) and water (1 ML) on Pt. Spectra II(a) and II(b) measure the ion diffusion from ASW interior by preparing a sample structure: H_2O (28 ML)/H^+ (0.1 ML) + Cl^- (0.1 ML)/H_2O (50 ML)/Pt(111). The H_2O TPD spectra for corresponding samples are shaded and the height of the TPD curves are shown in an arbitrary scale. The chloride ion intensity is the summation of $^{35}Cl^-$ and $^{37}Cl^-$. The Cl^- curves are shown as log-scaled. All spectra were recorded at a temperature ramping rate of 0.5 K s^{-1}. The sample temperature was raised from 85 K, but the spectra are displayed for the region from 130 K. The Cs^+ beam energy for TPLES was 32 eV.

In spectrum I(a), hydrated proton signals start to appear at a temperature above ~159 K. At this temperature, the sample thickness reduced to ~10 ML due to the sublimation of ice surface, as estimated from the area under the water TPD curve. These signals have a low intensity before a dramatic increase occurs at 165 K. In contrast, the hydronium signal in spectrum II(a) is detected on the surface at a substantially lower temperature (~147 K). The desorption of water from the surface hardly occurs at this temperature, as shown by the TPD curve. The surface population of hydronium continually increases with increasing temperature, peaks at ~ 168 K, and then the signal decreases at a higher temperature. This result indicates that protons migrate from the ASW interior to the surface during the temperature increase, without evaporation of the surface water layer. Based on the comparison of the behavior of the two types of hydrated protons, hydrated protons produced on a Pt surface in spectrum I(a) do not migrate through the ASW overlayer in the 147–159 K region. They stay near the metal surface, until they are exposed at the surface due to desorption of the water overlayer.

The TPLES curves abruptly increase at ~165 K in spectrum I(a); the same behavior occurs at ~171 K in spectrum II(b). This behavior can be explained by a roughening transition of the samples, which produces patches of wetting water monolayer and small domains of ice crystals when the thickness of the ASW film is reduced below a critical value due to water sublimation. The roughening transition temperature is higher when the initial thickness of the film is higher. After the roughening transition, the LES intensities do not properly reflect the surface populations of ions because the LES efficiency of ions at the water monolayer is very large. It can be noted that the $H_5O_2^+$ signal is stronger than the H_3O^+ signal in spectra I(a) and II(a) in the narrow temperature region right after the roughening transition, again indicating the stability of multiply hydrated protons in the water monolayer on Pt. Larger protonated water clusters vanish more quickly with the

desorption of the water monolayer, and H_3O^+ persists to the highest temperature.

The weak signals of hydrated protons observed in the 159–165 K region in spectrum I(a) may be produced from water monolayer regions in the sample, rather than representing surfacing of these species via diffusion through the ASW film. This interpretation is based on the observation that multiply hydrated proton species have a relatively strong intensity compared with H_3O^+ in this region, although the H_3O^+ signal is the strongest on the surface of the ASW film with signals of more hydrated species decreasing rapidly with increasing hydration number [19, 26]. One possible scenario is an amorphous-to-crystalline phase transition of the sample, which is known to occur at a temperature near 156 K for a pure ASW film [39-42]. Because the present sample was very thin, reduced to a film thickness of ~10 ML at 159 K, the phase transition may have accompanied the formation of water monolayer in small local regions, even before the roughening transition of the whole sample occurred at ~165 K. This interpretation is consistent with the small absolute intensities of hydrated proton signals in spectrum I(a).

Figures 4-2I(b) and 4-2II(b) show the TPLES measurements of chloride anions on the surface. The Cl^- TPLES curves represent the summation of both $^{35}Cl^-$ and $^{37}Cl^-$ intensities; two isotopes show the same temperature dependency, as expected. In spectrum I(b), the Cl^- signal appears only above ~160 K, nearly the same temperature as for the appearance of hydrated protons. In spectrum II(b), the surfacing behavior of Cl^- from the ASW interior at a temperature above ~146 K closely follows the behavior of hydrated protons in the sample. These results indicate that Cl^- ions that initially formed on a Pt surface prefer to reside at the water/metal interface, similar to hydrated protons.

The observations discussed above indicate that H^+ and Cl^- ions that formed on a Pt surface have a thermodynamic tendency to reside near the metal surface rather than diffuse into the amorphous water film. An interesting question is the distribution of these ions near

the metal surface. To answer this question, the voltage (V_s) was measured resulting from different vertical distributions of H^+ and Cl^- ions within the sample. Figure 4-3(a) shows the ΔCPD curves measured as a function of the thickness of water film overlaid on H^+ and Cl^- ions on Pt(111). The ΔCPD corresponds to the difference of the CPD measured before and after the water overlayer adsorption. The results are shown for various concentrations (0.04–0.24 ML) of H^+ and Cl^-, which were produced by coadsorption of corresponding amounts of HCl and H_2O (1 ML) on the Pt surface. All curves show that ΔCPD increases toward a more positive voltage with increasing thickness of the water overlayer. The ΔCPD curves approach certain asymptotic voltages, and the voltage increases with increasing HCl coverage. This behavior is consistent with a capacitor model in which V_s is proportional to the surface charge density (Equation 4-1). The increment of ΔCPD with θ(HCl) is approximately linear when θ(HCl) is low, but the increment is no longer appreciable for θ(HCl) ≥ 0.12 ML.

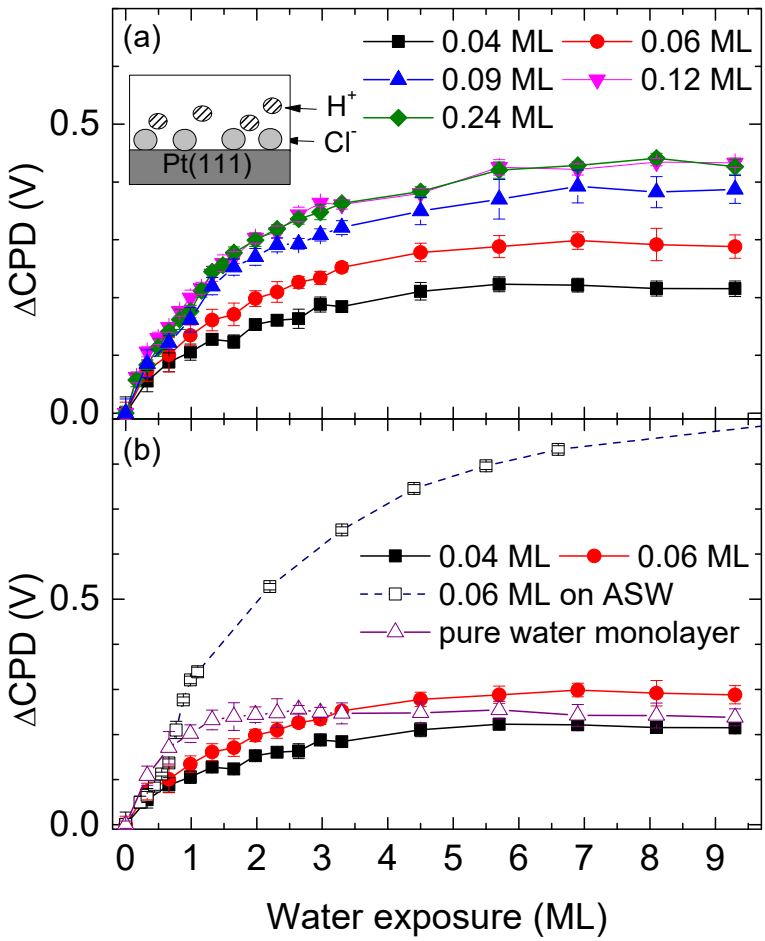

Figure 4-3. ΔCPD associated with the distributions of H^+ and Cl^- ions in ASW overlayer film with increasing exposure. (a) ΔCPD measurements for samples in which H^+ and Cl^- ions are initially formed on a Pt surface by coadsorption of HCl (0.04–0.24 ML) and H_2O (1 ML). (b) ΔCPD measurements for a sample in which H^+ and Cl^- ions are initially formed on the ASW surface by adsorption of 0.06 ML HCl (□). A sample initially only with pure water monolayer on Pt (△). A sample initially with H^+ and Cl^- ions (0.06 ML) on Pt (●), the same curve as that shown in (a). The sample temperature for the adsorption of ASW layer and CPD measurement was 83 K.

Figure 4-3(b) shows the result of the corresponding ΔCPD measurements (open squares) for H^+ and Cl^- ions (0.06 ML coverage) that were initially located on an ASW film surface. The ΔCPD increases continually as the thickness of the ASW overlayer increases, in contrast to the asymptotic saturation of ΔCPD in Figure 4-3(a). According to the capacitor model, the observation indicates that the vertical separation distance between H^+ and Cl^- ions continually increases with increasing overlayer thickness, which in turn, indicates that H^+ ions tend to float on the surface of the growing ASW film, while Cl^- ions are buried in position below the surface. The contrasting two ΔCPD curves in Figures 4-3(a) and 3(b) show that the vertical separation of H^+ and Cl^- ions via diffusion in the ASW films significantly differs depending on the initial location of the ions. The ion separation distance is significantly shorter when the ions are initially located at the water/Pt interface.

The ΔCPD originates not only from the separation of H^+ and Cl^- ions but also from water dipoles in the ASW film. To clarify the meaning of ΔCPD in Figure 4-3(a), the ΔCPD was measured resulting from the adsorbed water dipole on the Pt surface with the addition of ASW overlayer, shown in Figure 4-3(b). The ΔCPD value for the pure water monolayer increases faster with a thin water layer (< 2 ML) and reaches the asymptotic saturation earilier at certain voltage (~0.25 V) compared with the voltage of the samples that initially included H^+ and Cl^- ions on Pt. The CPD change of the pure water monolayer can be attributed the change of dipole direction of water adsorbed on the Pt surface. The first water monolayer on Pt(111) consists of H-down and flat-lying water molecules [43]. To grow an ice multilayer, which has dangling H on its surface, the water molecules in the first monolayer should be rearranged to allow H-bonding with water in the next layer. Recent studies showed that the H-down water molecules in the first monolayer can easily flip to H-up orientation without an energy barrier to bind to adsorbates [44, 45]. In addition, the work function change due to H-up orientation on Pt had a larger value than the change by

H-down molecules [46]. Therefore, a reasonable interpretation could be that the voltage change in the sample with a pure water monolayer is attributed to the change of the dipole orientation by flipping H-down water molecules to H-up orientation in the monolayer. No change of ΔCPD of crystalline ice, which has original dangling OH toward vacuum, supports the flipping adsorbed water on Pt (not shown). On the other hand, coadsorbed H^+ and Cl^- exert a strong electrostatic force on the water monolayer that results in reorientation of the water molecules in the structure of the pure water monolayer [47]. Extra water adsorbates on the monolayer will not change the water dipole orientation because ion–dipole attraction dominates rather than hydrogen bonding between water molecules. The smaller ΔCPD value for θ_{HCl} = 0.04 ML than that of the pure water layer is also a good indicator for the fact that the dipole orientation of water with H^+ and Cl^- ions on Pt might be less affected by extra adsorbates. Therefore, as a first approximation, it could be interpreted that the ΔCPD curve shape is determined primarily by the charge separation between H^+ and Cl^- ions, and the contribution of water dipole reorientation is insignificant.

The positive voltage produced by water adsorption is related to ion distribution on the metal surface. In the case of Cl^-, it is strongly bounded to the metal surface and hard to migrate at low temperature without molecular mixing because of the kinetic effect [23]. In contrast, H^+ ions can move via a unique proton hopping mechanism even at low temperatures. Positive voltage indicates that H^+ ions migrate along the water overlayer located above Cl^- ions and the vertical distribution of H^+ from the metal surface is larger.

To estimate the absolute distances between hydrated protons and chloride ions, the ΔCPD variations as a function of water exposure were analyzed by using a simple theoretical model. The ΔCPD in Figure 4-3(a) was converted to d/ε_r, using Equation (4-1), where d is the vertical distance and ε_r is the relative dielectric constant of the medium. Figure 4-4 shows the plot of d/ε_r for various HCl concentrations (0.04–0.12 ML). The d/ε_r was analyzed using a simple theoretical model to obtain the distance information. The model assumes that the distribution of H^+ will exponentially decay as function of distance from the metal surface to the water overlayer with a certain probability of proton migration, r, and both sides of this function were divided by unknown ε_r, which is regraded constant (see Supporting Information). In this model, water exposure is converted to water thickness using a random deposition model. The solid lines in Figure 4-4 show the model function of d/ε_r fitted to the experimental data, and the experimental d/ε_r for each HCl concentration is in reasonably good agreement with the model function. The value of r is calculated as ~0.39 for all HCl concentrations. Using only the value of r, the average distribution of H^+ from Cl^- ions is obtained from the distribution function (Equation 4-S1 in Supporting Information) and this value is saturated the value at $d(H^+) = (4.0 \pm 0.1) \times 10^{-10}\ m$. This estimated value can be interpreted that the distance of H^+ migration is close to 1ML of water ($= 4 \times 10^{-10}\ m$), regarded as second water layer from the metal surface.

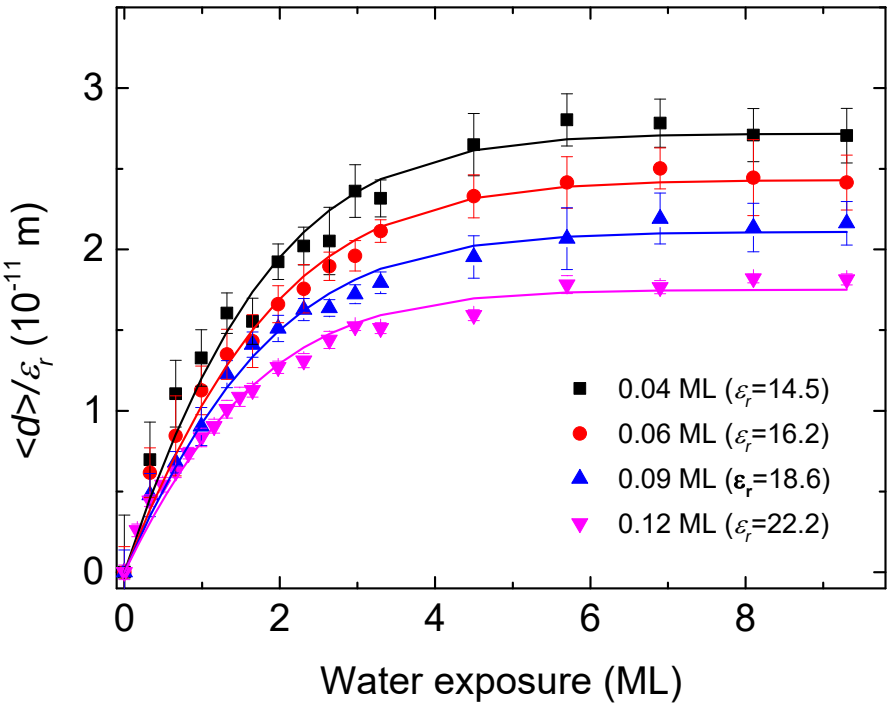

Figure 4-4. The vertical distance between H^+ and Cl^- divided by relative dielectric constant, d/ε_r, for various HCl concentration (0.04–0.12 ML). The d/ε_r values are obtained from ΔCPD in Figure 4-3(a) by converting Equation (4-1). The solid lines are the theoretical model fitted to the experimental data. ε_r values of each HCl coverage are calculated using a least-squares fit.

To investigate the nature of hydrated protons near the metal surface, hydrated protons on a Pt substrate were prepared by adsorption of HCl (0.1 ML) and H_2O (1.0 ML), and measured their intensity variation with LES as a function of water overlayer coverage. Figure 4-5(a) shows the intensity variation of different hydrated proton signals in the LES experiment. As the hydrated protons are covered by increasing amounts of the water overlayer, the total intensities of hydrated protons decrease because LES is sensitive to the outmost surface layer. Different protonated water clusters exhibit a somewhat different behavior during the addition of the water overlayer, although their intensities generally decrease with water coverage. To highlight the relative differences between the protonated water clusters, Figure 4-5(b) shows the normalized intensities of these species with respect to their intensities at zero overlayer thickness. This plot can remove the discriminating effect for larger protonated water clusters due to their lower detection sensitivity by LES.

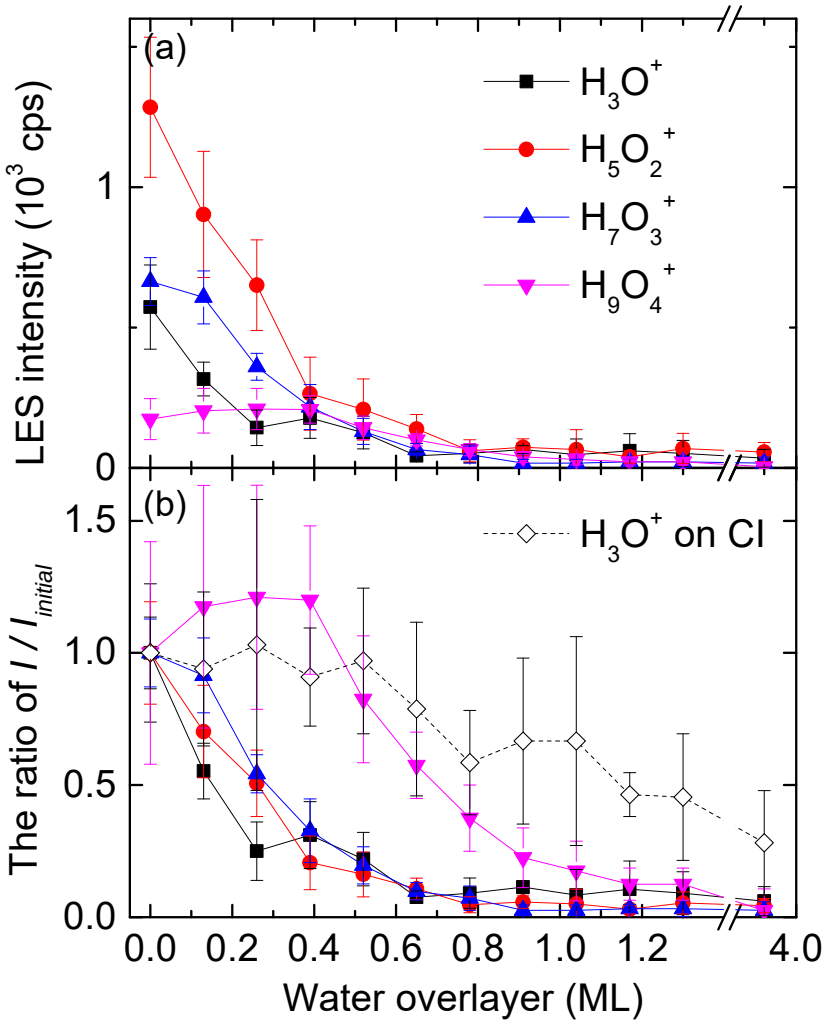

Figure 4-5. (a) LES intensities of hydrated protons as a function of water overlayer thickness measured for coadsorbed HCl (0.1 ML) and H_2O (1.0 ML) on Pt(111). The sample temperature was maintained at 80 K during the water adsorption and LES detection. (b) A display of the same data in the normalized intensity scale with respect to the intensity at zero thickness of water overlayer. The open circles (○) with the dotted line indicate H_3O^+ signal intensity measured for ionized HCl on a polycrystalline ice film (~50 ML). The Cs^+ beam was 32 eV.

In the region of 0–0.4 ML water coverage, only the relative ratio of $H_9O_4^+$ intensity compared with the initial intensity is higher than the H_3O^+ signals in the film of HCl adsorption on polycrystalline ice (~50 ML). The unique tendency of $H_9O_4^+$ suggests that the initial structure of hydrated protons in the monolayer evolves into a different structure. Hydrated protons formed by HCl ionization on metal are embedded in a two-dimensional H-bonding water network. The two-dimensional water structure will suppress the development of bulk-like hydrated protons (such as Eigen structure) and lead to the formation of a $H_5O_2^+$, $H_7O_3^+$, and $H_9O_4^+$ structure. After adsorption of the water overlayer which provides a bulk-like environment to hydrated protons, the two-dimensional $H_5O_2^+$, $H_7O_3^+$, and $H_9O_4^+$ structure can be transformed into the three-dimensional $H_9O_4^+$ structure.

Above a water coverage of 0.5 ML, $H_9O_4^+$ signal intensity sharply decreases, similar to the other hydrated protons, and disappears when the water overlayer is ~1 ML. These results suggest that two-dimensional hydrated protons immediately evolve into a three-dimensional structure with small coverage of the water overlayer, and these hydrated protons are totally covered by additional water exposure. According to the estimated distance in Figure 4-4, three-dimensional $H_9O_4^+$ may remain in the second water layer.

4. Discussion

In the previous section, several pieces of evidence were provided to show that hydrated protons and chlorides have a thermodynamic preference to reside at the water/metal interface. They include (i) complete burial of surface hydrated H^+ and Cl^- ions by a thin water overlayer (Figures 4-1 and 4-3) and (ii) detection of hydrated protons and chlorides only when local regions of the water monolayer are exposed by roughening transition (Figure 4-2). These observations indicate that the surface hydrated protons and chlorides on Pt were trapped inside the water film without migrating all the way to the film surface

in spite of their mobility along the H-bond chain in ASW film [19, 21, 22, 25]. The distribution of hydrated protons was estimated from the measurement of the film voltage. The results show that chlorides may remain on the Pt surface and hydrated protons migrate to the next layer from the first water monolayer (Figure 4-4). Hydrated protons become a fully solvated structure as they migrate to the hydration sphere in the bulk phase (Figure 4-5).

Figure 4-6 shows a conceptual drawing of the potential energy curve of an excess proton as it moves from the metal interface to the ice surface of the sample. According to a previous study [25], the proton can migrate over a long distance via successive proton hopping. Several results for the ASW film show that protons migrate from the interior to its surface and accumulate there [19, 22, 23]. This indicates that protons have a thermodynamic preference to reside at the ASW surface rather than migrate and destruct the bulk structure. These results could be explained with the shallow trapping site at the surface (Figure 4-6). In the case of the protons on a metal surface, the results shown in the previous section indicate that a trapping site also exists in the second water layer from the metal surface. The driving force for protons to migrate to the second water layer is the stability of the fully solvated structure rather than the two-dimensional structure on the metal surface. Moreover, it is possible that the potential well of the trapping site near the metal surface might be deeper than that of the ASW surface because no hydrated protons were detected on the ASW surface. When NH_3 molecules were adsorbed on top of the ASW surface, a NH_4^+ ion signal was observed [35]. This signal indicates the formation of NH_4^+ via protonation of NH_3 adsorbates by protons migrating from the water/metal interface. This suggests that NH_3 on the ASW surface forms a more stable trapping site so that protons can be stabilized in the ASW. This suggests that the protons may migrate back and forth in the ASW, but on average, they tend to stay near the metal surface.

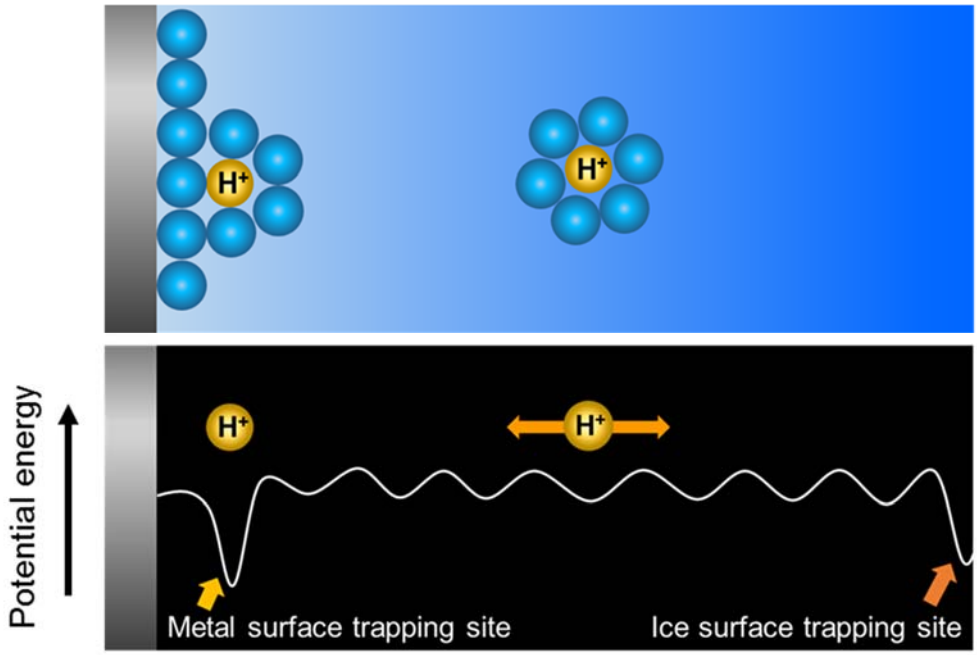

Figure 4-6. Schematic potential energy of hydrated protons from the metal surface to ASW surface.

It is interesting to discuss the present observation in view of the EDL model of the electrolyte/electrode interface. The observed ionic distributions help to understand the microscopic picture of the EDL, which consists of "specifically adsorbed ions" and "non-specifically adsorbed species." Compared with electrochemical studies, H^+ and Cl^- on the metal are regarded as non-specifically adsorbed ions and specifically adsorbed anion directly bounded on the metal surface, respectively. Moreover, the separation distance between the hydrated protons and chloride ion might be related to the location of outer Helmholtz plane (OHP) in the EDL model, which represents the locus of the electrical centers of the hydrated cations. The distance of OHP from the inner Helmholtz layer could be regarded as ~1 ML thickness of water. Although there is a fundamental difference between the UHV environment and electrochemistry, this experimental approach has

unique capabilities for the studies of electrochemical interfaces at the molecular scale.

5. Conclusion

The spatial distribution of hydrated protons and chloride ions at the solid water–metal interface was investigated using positive and negative LES. These ions are completely buried by a thin water overlayer. The buried hydrated protons and chloride ions are detected by LES only when the water monolayer is exposed at the sample surface, whether by a roughening transition or thermal desorption of the overlayer. In contrast to the hydrated protons and chloride ions that originally were in bulk ASW, which spontaneously migrate from the interior to the surface, these ionic species formed on Pt thermodynamically prefer to remain near the metal surface. This discovery may indicate the existence of shallow trapping sites at the water–metal interface as well as at the water surface. The CPD measurements of H^+ and Cl^- ions on the Pt surface show that hydrated protons migrate to a ~1ML of water from the first monolayer while chlorides are directly adsorbed on the metal surface at low temperature. The driving force of proton migration may be the thermodynamic stability of fully hydrated protons compared with two-dimensional structures.

The distribution of hydrated protons and chloride ions at the water–metal interface help to understand the microscopic picture of the EDL. The experimental results for H^+ and Cl^- at the water–metal interface show the consistence of specifically adsorbed (Cl^-) and non-specifically adsorbed (H^+) ions in the EDL and provide the location of the OHP in terms of the molecular–level. The present work demonstrates that the UHV modeling study in a bulk-like environment provides useful insight into fundamental understanding of electrochemical interfaces.

References

1. Thiel, P. A.; Madey, T. E. The Interaction of Water with Solid-Surfaces: Fundamental Aspects. *Surf. Sci. Rep.* **1987**, *7*, 211-385.
2. Wagner, F. *Structure of Electrified Interfaces*; VCH: New York, 1993.
3. Ito, M. Structures of water at electrified interfaces: Microscopic understanding of electrode potential in electric double layers on electrode surfaces. *Surf. Sci. Rep.* **2008**, *63*, 329-389.
4. Wagner, F. T.; Moylan, T. E. Identification of Surface Hydronium - Coadsorption of Hydrogen-Fluoride and Water on Platinum (111). *Surf. Sci.* **1987**, *182*, 125-149.
5. Wagner, F. T.; Moylan, T. E. Generation of Surface Hydronium from Water and Hydrogen Coadsorbed on Pt(111). *Surf. Sci.* **1988**, *206*, 187-202.
6. Wagner, F. T.; Moylan, T. E. Hydrogen-Chloride Adsorption and Coadsorption with Hydrogen or Water on Platinum(111). *Surf. Sci.* **1989**, *216*, 361-385.
7. Shingaya, Y.; Ito, M. Coordination number and molecular orientation of hydronium cation bisulfate anion adlayers on Pt(111). *Surf. Sci.* **1996**, *368*, 318-323.
8. Shingaya, Y.; Ito, M. Simulation of the electric double layers on Pt(111). *Surf. Sci.* **1997**, *386*, 34-47.
9. Fukushima, T.; Song, M. B.; Ito, M. Local work-function changes of Pt(111) studied by STM and IRAS: coadsorption of Cl^- with H_3O^+, NO, and CO molecules. *Surf. Sci.* **2000**, *464*, 193-199.
10. Jung, K. H.; Park, S. C.; Kim, J. H.; Kang, H. Vertical diffusion of water molecules near the surface of ice. *J. Chem. Phys.* **2004**, *121*, 2758-2764.

11. Park, S. C.; Moon, E. S.; Kang, H. Some fundamental properties and reactions of ice surfaces at low temperatures. *Phys. Chem. Chem. Phys.* **2010**, *12*, 12000-12011.

12. Collier, W. B.; Ritzhaupt, G.; Devlin, J. P. Spectroscopically Evaluated Rates and Energies for Proton-Transfer and Bjerrum Defect Migration in Cubic Ice. *J. Phys. Chem.* **1984**, *88*, 363-368.

13. Wooldridge, P. J.; Devlin, J. P. Proton Trapping and Defect Energetics in Ice from Ft-Ir Monitoring of Photoinduced Isotopic Exchange of Isolated D2o. *J. Chem. Phys.* **1988**, *88*, 3086-3091.

14. Uras-Aytemiz, N.; Joyce, C.; Devlin, J. P. Protonic and Bjerrum defect activity near the surface of ice at T < 145 K. *J. Chem. Phys.* **2001**, *115*, 9835-9842.

15. Devlin, J. P.; Buch, V. Evidence for the surface origin of point defects in ice: Control of interior proton activity by adsorbates. *J. Chem. Phys.* **2007**, *127*, 091101.

16. Vacha, R.; Buch, V.; Milet, A.; Devlin, P.; Jungwirth, P. Autoionization at the surface of neat water: is the top layer pH neutral, basic, or acidic? *Phys. Chem. Chem. Phys.* **2007**, *9*, 4736-4747.

17. Pursell, C. J.; Zaidi, M.; Thompson, A.; Fraser-Gaston, C.; Vela, E. Acid-base chemistry on crystalline ice: HCl+NH3. *J. Phys. Chem. A* **2000**, *104*, 552-556.

18. Geil, B.; Kirschgen, T. M.; Fujara, F. Mechanism of proton transport in hexagonal ice. *Phys. Rev. B* **2005**, *72*, 014304.

19. Lee, C. W.; Lee, P. R.; Kang, H. Protons at ice surfaces. *Angew. Chem. Int. Ed.* **2006**, *45*, 5529-5533.

20. Lilach, Y.; Iedema, M. J.; Cowin, J. P. Proton segregation on a growing ice interface. *Surf. Sci.* **2008**, *602*, 2886-2893.

21. Uritski, A.; Presiado, I.; Erez, Y.; Gepshtein, R.; Huppert, D. Temperature Dependence of Proton Diffusion in I(h) Ice. *J. Phys. Chem. C* **2009**, *113*, 10285-10296.

22. Moon, E. S.; Lee, C. W.; Kang, H. Proton mobility in thin ice films: a revisit. *Phys. Chem. Chem. Phys.* **2008**, *10*, 4814-4816.

23. Park, E.; Lee, D. H.; Kim, S.; Kang, H. Transport and Surface Accumulation of Hydroniums and Chlorides in an Ice Film. A High Temperature (140–180 K) Study. *J. Phys. Chem. C* **2012**, *116*, 21828-21835.

24. Lee, D. H.; Bang, J.; Kang, H. Surface Charge Layer of Amorphous Solid Water with Adsorbed Acid or Base: Asymmetric Depth Distributions of H^+ and OH^- Ions. *J. Phys. Chem. C* **2016**, *120*, 12051-12058.

25. Moon, E. S.; Kim, Y.; Shin, S.; Kang, H. Asymmetric Transport Efficiencies of Positive and Negative Ion Defects in Amorphous Ice. *Phys. Rev. Lett.* **2012**, *108*, 226103.

26. Park, S. C.; Maeng, K. W.; Pradeep, T.; Kang, H. Unique chemistry at ice surfaces: Incomplete proton transfer in the H_3O^+-NH_3 system. *Angew. Chem. Int. Ed.* **2001**, *40*, 1497-+.

27. Kang, H. Chemistry of ice surfaces. Elementary reaction steps on ice studied by reactive ion scattering. *Acc. Chem. Res.* **2005**, *38*, 893-900.

28. Kang, H. Reactive Ion Scattering of Low Energy Cs+ from Surfaces. A Technique for Surface Molecular Analysis. *Bull. Korean Chem. Soc.* **2011**, *32*, 389-398.

29. Zimbitas, G.; Haq, S.; Hodgson, A. The structure and crystallization of thin water films on Pt(111). *J. Chem. Phys.* **2005**, *123*.

30. Daschbach, J. L.; Kim, J.; Ayotte, P.; Smith, R. S.; Kay, B. D. Adsorption and desorption of HCl on Pt(111). *J. Phys. Chem. B* **2005**, *109*, 15506-15514.

31. Rabalais, J. W. Principles and Applications of Ion Scattering Spectrometry. Wiley-Interscience: New Jersey, 2003.

32. Hahn, J. R.; Lee, C. W.; Han, S. J.; Lahaye, R. J. W. E.; Kang, H. Low-energy Cs^+ scattering from water on Pt(111): A kinetic energy analysis of the Cs+ - Water clusters. *J. Phys. Chem. A* **2002**, *106*, 9827-9831.

33. Lahaye, R. J. W. E.; Kang, H. Reactive rideal ion surface scattering as an Eley-Rideal process: A molecular dynamics study into the abstraction reaction mechanism by low energy Cs+ from Pt(111). *ChemPhysChem* **2004**, *5*, 697-705.

34. Tsekouras, A. A.; Iedema, M. J.; Cowin, J. P. Amorphous water-ice relaxations measured with soft-landed ions. *Phys. Rev. Lett.* **1998**, *80*, 5798-5801.

35. Kim, Y.; Shin, S.; Kang, H. Zundel-like and Eigen-like Hydrated Protons on a Platinum Surface. *Angew. Chem. Int. Ed.* **2015**, *54*, 7626-7630.

36. Masel, R. I. *Principles of adsorption and reaction on solid surfaces*; Wiley: New York, 1996.

37. Salmeron, M.; Ferrer, S.; Jazzar, M.; Somorjai, G. A. Photoelectron-Spectroscopy Study of the Electronic-Structure of Au and Ag Overlayers on Pt(100), Pt(111), and Pt(997) Surfaces. *Phys. Rev. B* **1983**, *28*, 6758-6765.

38. Fulton, J. L.; Balasubramanian, M. Structure of Hydronium (H3O+)/Chloride (Cl-) Contact Ion Pairs in Aqueous Hydrochloric Acid Solution: A Zundel-like Local Configuration. *J. Am. Chem. Soc.* **2010**, *132*, 12597-12604.

39. Smith, R. S.; Huang, C.; Kay, B. D. Evidence for molecular translational diffusion during the crystallization of amorphous solid water. *J. Phys. Chem. B* **1997**, *101*, 6123-6126.

40. Smith, R. S.; Kay, B. D. The existence of supercooled liquid water at 150 K. *Nature* **1999**, *398*, 788-791.

41. Dohnalek, Z.; Ciolli, R. L.; Kimmel, G. A.; Stevenson, K. P.; Smith, R. S.; Kay, B. D. Substrate induced crystallization of amorphous solid water at low temperatures. *J. Chem. Phys.* **1999**, *110*, 5489-5492.

42. Smith, R. S.; Matthiesen, J.; Knox, J.; Kay, B. D. Crystallization Kinetics and Excess Free Energy of H_2O and D_2O Nanoscale Films of Amorphous Solid Water. *J. Phys. Chem. A* **2011**, *115*, 5908-5917.

43. Hodgson, A.; Haq, S. Water adsorption and the wetting of metal surfaces. *Surf. Sci. Rep.* **2009**, *64*, 381-451.

44. Kimmel, G. A.; Zubkov, T.; Smith, R. S.; Petrik, N. G.; Kay, B. D. Turning things downside up: Adsorbate induced water flipping on Pt(111). *J. Chem. Phys.* **2014**, *141*.

45. Lechner, B. A. J.; Kim, Y.; Feibelman, P. J.; Henkelman, G.; Kang, H.; Salmeron, M. Solvation and Reaction of Ammonia in Molecularly Thin Water Films. *J. Phys. Chem. C* **2015**, *119*, 23052-23058.

46. Meng, S.; Wang, E. G.; Frischkorn, C.; Wolf, M.; Gao, S. W. Consistent picture for the wetting structure of water/Ru(0001). *Chem. Phys. Lett.* **2005**, *402*, 384-388.

47. Nakamura, M.; Song, M. B.; Ito, M. Hydrogen bonding between a water molecule and electronegative additives (O or Cl^-) on a Pt(111) surface. *Chem. Phys. Lett.* **2000**, *320*, 381-386.

Supporting Information

Calculation of the Charge Separation Distance for Hydrated Protons and Chloride Ions on the Pt Surface

When water molecules are overlaid on the hydrated protons and chlorides that formed on the Pt surface, H^+ ions move upward through the growing water film by proton hopping. It is assumed that the distribution of H^+ ions can be described by an exponential function, $f(x) = r^x$, where r is the probability of proton migration across on a water layer and l is the distance from the Pt surface in units of water monolayer thickness (1 ML = 4×10^{-10} m). It is assumed that the Cl^- ions remain in their original positions because it is difficult to break the Pt–Cl bond and molecular diffusion is prohibited at low temperature. The average distance of vertical separation between H^+ and Cl^- ions is obtained by integrating $xf(x)$ over the distribution range of H^+ ions, as shown in the equation.

$$d(l) = \frac{\int_0^l x r^x dx}{\int_0^l r^x dx} \tag{4-S1}$$

Here, x is the vertical height from the initial position and l is the overlayer thickness. Because the value of d/ε_r can be only obtained from ΔCPD, Equation (4-S1) is divided by the value of ε_r.

$$\frac{d(l)}{\varepsilon_r} = \frac{1}{\varepsilon_r} \cdot \frac{\int_0^l x r^x dx}{\int_0^l r^x dx} \tag{4-S2}$$

Because the water molecules are randomly deposited at the surface, the thickness of the overlayer is not proportional to the exposure. The coverage of each layer, θ, can be described as,

$$d\theta_i(x) = \left(\theta_{i-1}(x) - \theta_i(x)\right)dx \quad \text{(4-S3)}$$

$$\theta_i(x) = 1 - e^{-x} \times \sum_{j=0}^{i-1}\left(\frac{x^j}{j!}\right) \quad \text{(4-S4)}$$

where x represents the water exposure. d and d/ε_r can be changed using Equation (4-S4).

$$d(l) = \frac{\left[\sum_{i=1}^{\infty}\left\{1 - e^{-x}\sum_{j=0}^{i-1}\left(\frac{x^j}{j!}\right)\right\}r^i\right]}{\sum_{i=1}^{\infty} r^i} \quad \text{(4-S5)}$$

$$\frac{d(l)}{\varepsilon_r} = \frac{1}{\varepsilon_r}\cdot\frac{\left[\sum_{i=1}^{\infty}\left\{1 - e^{-x}\sum_{j=0}^{i-1}\left(\frac{x^j}{j!}\right)\right\}r^i\right]}{\sum_{i=1}^{\infty} r^i} \quad \text{(4-S6)}$$

By fitting Equation (4-S6) to the experimental d/ε_r values in Figure 4-4, ε_r and r can be determined. To calculate the average distance between H^+ and Cl^-, the estimated r value is applied to Equation (4-S5). The average distance between H^+ and Cl^- ions is shown in Figure 4-S1 as a function of the water exposure. The infinite value of the distance is calculated as $d = (4.0 \pm 0.1) \times 10^{-10}$ m. The uncertainty of the distance was obtained from the standard deviation of r for all HCl coverages. The estimated distance from this fitting corresponds to the height of a single water monolayer (1 ML = 4×10^{-10} m).

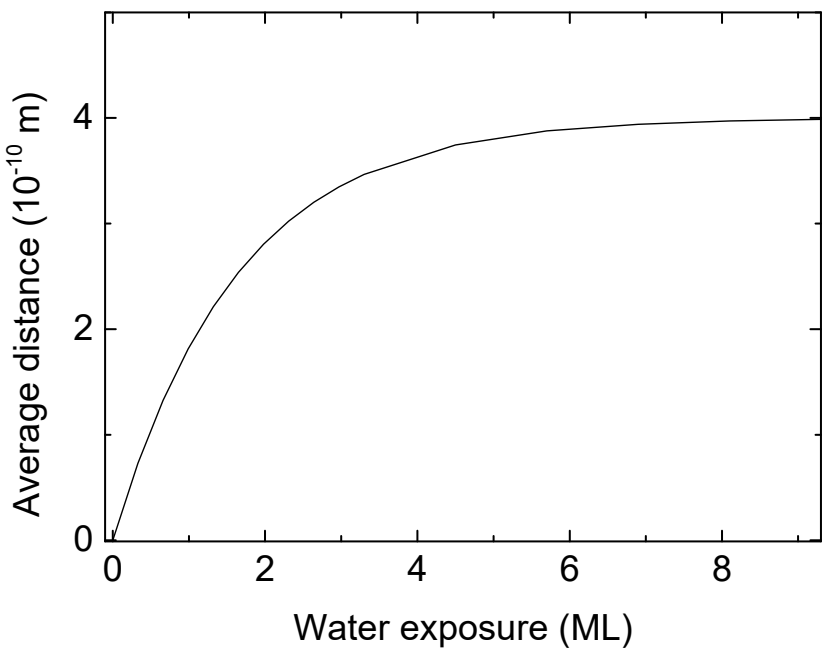

Figure 4-S1. Average distance of H^+ from Cl^- as a function of water exposure.

List of Publications

1. Moon, E. S.; **Kim, Y.**; Shin, S.; Kang, H. Asymmetric Transport Efficiencies of Positive and Negative Ion Defects in Amorphous Ice. *Phys. Rev. Lett.* **2012**, *108*, 226103.
2. **Kim, Y.**; Moon, E. S.; Shin, S.; Kang, H. Acidic Water Monolayer on Ruthenium(0001). *Angew. Chem. Int. Ed.* **2012**, *51*, 12806-12809.
3. Shin, S.; **Kim, Y.**; Moon, E.-S.; Lee, D. H.; Kang, H.; Kang, H. Generation of Strong Electric Fields in an Ice Film Capacitor. *J. Chem. Phys.* **2013**, *139*, 074201.
4. **Kim, Y.**; Shin, S.; Moon, E. S.; Kang, H. Spectroscopic Monitoring of the Acidity of Water Films on Ru(0001): Orientation-Specific Acidity of Adsorbed Water. *Chem. Euro. J.* **2014**, *20*, 3376-3383.
5. Shin, S.; **Kim, Y.**; Kang, H.; Kang, H. Effect of Electric Field on Condensed-Phase Molecular Systems. I. Dipolar Polarization of Amorphous Solid Acetone. *J. Phys. Chem. C* **2015**, *119*, 15588-15595.
6. **Kim, Y.**; Shin, S.; Kang, H. Zundel-like and Eigen-like Hydrated Protons on a Platinum Surface. *Angew. Chem. Int. Ed.* **2015**, *54*, 7626-7630.
7. Lechner, B. A. J.[+]; **Kim, Y.** [+]; Feibelman, P. J.; Henkelman, G.; Kang, H.; Salmeron, M. Solvation and Reaction of Ammonia in Molecularly Thin Water Films. *J. Phys. Chem. C* **2015**, *119*, 23052-23058. [+] **Co-first author**

8. Shin, S.; Park, Y.; **Kim, Y.**; Kang, H. Dissociation of Trifluoroacetic Acid in Amorphous Solid Water: Charge-Delocalized Hydroniums and Zundel Continuum Absorption. *J. Phys. Chem.* C **2017**, *121,* 12842-12848
9. **Kim, Y.**; Noh, C.; Jung, Y.; Kang, H. The Nature of Hydrated Protons on Platinum Surface. *To be submitted.*
10. **Kim, Y.**; Lee, D. H.; Shin, S.; Kang, H. Spatial Distributions of Hydrated Protons and Chloride Ions at Solid Water–Metal Interface. *To be submitted.*
11. Shin, S.; Park, Y.; **Kim, Y.**; Kang, H. Electric Field Effect on Condensed-Phase Molecular Systems. IV. Conformational Change of 1, 2-Dichloroethane. *To be submitted.*

요약(국문초록)

본 학위 논문은 물–금속 계면에서 수화된 양성자의 특성에 관한 연구 결과를 다루었다. 금속 표면에서 존재하는 양성자는 전기화학에서 수소 발생 반응과 밀접히 연과 되어 있다. 하지만 핵심적인 메커니즘을 규명하기 위해서는 전극 표면에서 일어나는 현상을 밝혀야 하는데 실제 전기화학 환경에서는 표면을 분자 수준에서 실험적으로 관찰하는 것에 제약이 있다. 이러한 한계를 극복하기 위해 본 연구에서는 전극과 수용액 환경을 극고진공상태에서 구현한 전기화학 계면 모형을 만든 후 표면 분석법을 이용하여 양성자 생성 및 전달 반응을 관찰하였다. 저 에너지 스퍼터링과 세슘 반응성 이온산란법을 통하여 얻은 질량 스펙트럼은 흡착된 물과 수소가 이온화하여 양성자를 생성할 수 있으며 이 양성자는 기존에 잘 알려진 단일 물 분자에 수화된 옥소늄 이온이 아닌 다중 물 분자에 수화된 형태의 양성자 화합물만 생성됨을 보여주었다. 반사–흡광 적외선 분광법을 통해서도 백금 표면에 존재하는 수소와 물의 반응으로 다중 물 분자에 수화된 양성자의 생성을 관찰하였다. 백금 표면에 생성된 양성자는 벌크에서 가장 안정하다고 알려진 삼차원 수화 구조가 아닌 금속 계면에 존재할 수 있는 특수한 이차원 구조를 갖는다는 것을 확인하였다. 금속 표면에 존재하는 양성자에 추가로 물 층을 흡착시키면 전기화학에서와 유사한 벌크와 같은 환경을 만들 수 있다. 이를 이용하여 이차원 수화 구조를 갖는 양성자에 물 층을 흡착시킨 결과 양성자가 물의 수소 결합을 따라 금속과 결합하지 않은 물 층으로 자발적 전달 현상이 일어나는 것을 관찰하였다. 이러한

전달 과정을 통해 이차원 양성자 구조가 삼차원 양성자 구조로 바뀜을 확인하였는데 이것은 표면에 흡착된 양성자는 벌크 물에 자발적으로 용해되며 최종적으로 기존에 알려진 수소 발생 반응의 생성물과 같음을 알 수 있다. 실험 결과를 통해 전기화학에서 금속 표면에 흡착하여 이차원적 구조를 가진 다중 물 분자에 수화된 양성자가 수소 발생 반응에서 알려지지 않은 핵심 중간체로 존재하는 새로운 메커니즘을 규명하였다.

물과 염화수소를 백금 표면에 흡착시켜 생성된 양성자와 염화 이온을 생성하여 전기화학 계면 모형을 만든 후 전극 표면에 존재하는 전기 이중층에 존재하는 양성자와 음이온의 분포를 연구하였다. 이를 위해 저 에너지 이온 스퍼터링과 켈빈 일함수 측정법을 기반으로 하여 양성자의 이동을 관찰하고 양성자와 음이온의 거리를 측정하였다. 그 결과 양성자와 염화 이온은 열역학적으로 금속 근처에 존재하는 것을 비결정성 물 내부로 확산하는 것 보다 선호함을 관찰하였다. 또한, 양성자와 음이온이 금속 근처에서 갖는 분포도를 연구하기 위해 양성자와 음이온의 거리를 측정하였다. 금속에 흡착된 염화 이온은 저온에서는 표면에서 이동하지 못하는데 이를 이용하여 양성자의 분포를 관찰할 수 있었다. 염화 이온으로부터 양성자의 평균 수직 거리는 두 이온이 분리되면서 생기는 전압을 측정하였고 그 결과 물 한 층 높이로 측정되었다. 양성자가 금속 근처에 존재하는 것을 선호하면서도 표면에서 물 한 층 높이 만큼 이동한 이유는 삼차원구조로 수화된 양성자가 금속표면에 존재하는 이차원 구조를 가지는 수화된 양성자 보다 안정하기 때문이다. 양성자와 염화 이온의 분포는 전기 이중층을 구성하는 특이 흡착된 음이온과 비특이성 흡착된 양이온과 연관 시킬 수 있다. 이를 통해 양성자가 평균적으로 존재하는 위치

는 전기이중층에서 비특이성 흡착이온이 존재하는 평면으로 알려진 외부 헬름홀츠 평면의 거리에 관한 정보를 제공한다.

주요어 : 양성자, 물–금속 계면, 백금, 수소 발생 반응, 전기이중층, 표면분석

학번 : 2011-20285